1-1-2013

Atmospheric Patterns and Asian Typhoon Landfalls

Ivetta Abramyan
University of South Carolina

Atmospheric Patterns and Asian Typhoon Landfalls

by

Ivetta Abramyan

Bachelor of Science
Florida State University, 2008

Submitted in Partial Fulfillment of the Requirements

For the Degree of Master of Science in

Marine Science

College of Arts and Sciences

University of South Carolina

2013

Accepted by:

Cary Mock, Major Professor

Alexander Yankovsky, Committee Member

John Grego, Committee Member

Lacey Ford, Vice Provost and Dean of Graduate Studies

ACKNOWLEDGEMENTS

First and foremost, I would like to thank my major professor, Dr. Cary Mock, for his steadfast guidance and expertise throughout this entire process, and for giving me the opportunity to work on a research topic that I truly enjoy. The valuable skills that I have developed and the knowledge I have gained during this research will benefit me indefinitely.

I would like to thank my committee members, Alexander Yankovsky and John Grego for taking the time to serve on my committee and provide feedback and assistance. I could not have done it without their brilliant insight.

I thank God for giving me the strength, patience, perseverance and wisdom needed to pursue my dreams. I am also extremely grateful to my parents for their continuous support and encouragement.

In addition, I would like to express sincere gratitude to all my friends and colleagues who have contributed to my progress, whether it was help with formulating a sentence or moral support with a cup of coffee. Special thanks to faculty and graduate students in the Climate Lab for providing an environment of such bright and generous people, the staff at the SC State Climatology Office, specifically Hope Mizzell, for her outstanding mentorship and encouraging words, and Matt Rodgers for spending countless

hours helping me with GIS and giving me advice to make my life easier. You are all very much appreciated.

Last but not least, this research would not have been possible without the NCEP/NCAR reanalysis data provided by the NOAA/ESRL Physical Sciences Division. I would also like to thank Jon Gottschalck at the NOAA Climate Prediction Center for helping me interpret MJO data and students in the USC Statistics Department for assisting me with my statistical analysis.

"An investment in knowledge always pays the best interest" - *Benjamin Franklin*

ABSTRACT

The Western North Pacific Ocean (WNP) produces more frequent and intense tropical cyclones (TC) than anywhere else in the world, and these storms greatly impact society. This study examines synoptic scale atmospheric patterns and their effects on landfalling typhoons in Japan, Taiwan and Vietnam using composite analysis at upper and mid-levels of the atmosphere, as well as analyzing teleconnection impacts on tropical cyclone frequency, duration and intensity.

Examined Best Track data (1946-2010) shows an increased likelihood of Taiwan landfalls earlier in the season, Japan landfalls mid-season, and Vietnam landfalls towards the end of the typhoon season. The formation locations also differed slightly, with storms that made landfall in Japan forming further east than those that hit Taiwan and Vietnam. Probabilities of landfall in a specific region increased with knowledge of this spatial and temporal information, and ENSO phase.

Synoptic composite anomaly maps show the presence of an upper-level anticyclone in each of the three landfall locations. All three landfall areas reveal that tracks mostly followed the periphery of the upper-level anticyclones toward their respective landfalls. Vector wind composites also supported the findings of the upper-air composites, clearly showing areas of little to no wind shear in the path of the typhoons, indicating a favorable environment for tropical systems. The vector wind analyses also depicted where the dominant steering mechanism was, usually areas of anticyclonic flow

surrounding the ridges. Analysis of the spatiotemporal evolution for selected typhoons shows the development of these synoptic features and how they evolve in relation to the typhoon, in particular affecting its intensity.

The effects of ENSO and MJO on tropical cyclone frequency and intensity were also investigated using a statistical and quantitative analysis. 83% of TC during El Nino conditions achieved typhoon strength, with 66% of those intensifying even further to 100 knots or greater. In comparison, about 57% of TC reached typhoon strength during La Nina, and 43% of those reached 100 knot winds. Although the total number of cyclones was equal for the selected El Nino and La Nina events, a Poisson regression showed that during El Nino, the number of typhoon days with winds of at least 100 knots increases by a factor of 3.22 over La Nina years, indicating that TC are more likely to intensify during an El Nino. The average storm activity significantly shows about one extra day of at least 100 knot winds during an El Nino than during a La Nina. TC activity during an MJO event is similar with that of La Nina conditions.

This research has many broad implications in the fields of atmospheric, oceanic and social sciences. Understanding synoptic-scale processes is critical for improving model simulations of short-term (3-5 day) typhoon forecasts, downscaling meteorological data to link with biological and geological marine processes, flood mitigation, disaster preparedness planning, etc. All types of coastal communities, from zooplankton populations to maritime forests to densely-packed resort towns, are affected by these inescapable forces of nature.

TABLE OF CONTENTS

LIST OF FIGURES

CHAPTER 1

INTRODUCTION

1.1 Background

More tropical cyclones are generated in the Western North Pacific Ocean (WNP) than anywhere else in the world. Approximately one-third of all tropical cyclones originate here (Elsner and Liu, 2003). This basin is located north of the equator between Asia and the International Date Line and spawns some of the strongest tropical cyclones on record. The typhoon season has no official boundaries because storms can form year-round, but the peak generally occurs in late August/early September. On average, the WNP produces about 26 tropical cyclones per year (Fig 1), 18 of which become typhoons. China has the highest frequency of land-falling tropical cyclones in the world, averaging about 8.8 per year (Weyman and Anderson-Berry, 2002). Both the Japan Meteorological Agency (JMA) and the Joint Typhoon Warning Center (JTWC) have tropical cyclone classification systems for the NW Pacific. All tropical cyclones that form from 180° to 100°E in the Northern Hemisphere are officially monitored by the Regional Specialized Meteorological Center (RSMC) in Tokyo, Japan, which is operated by the JMA. Typically, TC motion in the WNP is steered by the synoptic-scale flow pattern within which it is embedded, with mid-tropospheric winds (500-700 hPa). Therefore, the size

and position of major atmospheric features in the WNP, such as the monsoon trough and the subtropical high, strongly influence TC tracks (Terry and Feng, 2010).

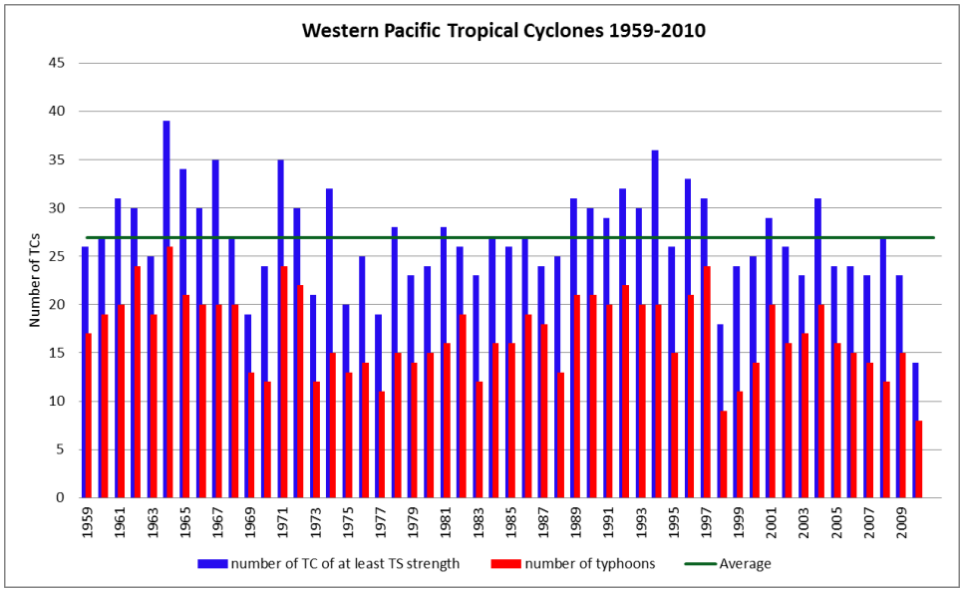

Figure 1.1. Tropical cyclones of tropical storm or greater intensity in the western North Pacific (1959-2005). Data source: JTWC

Typhoon paths are generally categorized into three groups, which reflect the directions they take from their location of origin (Elsner and Liu, 2003). Straight moving storms take a westward path and can pose a threat to the Philippines, Vietnam, and southern China, storms that curve to the northwest can affect Japan and northern China, and storms that move northward or recurve back toward the northeast usually do not affect land. This three-type classification is not always the case though, as with Tian and Li (2010) who divide tracks into five different groups: westward moving, northwestward moving, and three types of recurving tracks.

In order to better predict typhoon landfalls, it is necessary to understand the various atmospheric and oceanic components that govern large-scale steering flows,

which, in turn, control track patterns. Factors at different timescales along with their interactions must be evaluated to create reliable long-term forecasts. JTWC best track data shows a statistically significant (at the 5% level) increase in PDI (Power Dissipation Index), which is the sum of the cube of the maximum wind speed for all tropical systems (Emanuel, 2005) between two consecutive 15-year time periods (1975-1989 and 1990-2004). The correlation coefficient between the annual tropical cyclone-related damage in monetary terms and the annual PDIs is 0.47 for JTWC best track data, which is statistically significant (marginally at the 5% level) using the *t* test (Wu et al., 2006). This connection supports the case that forecasting improvements are needed to foretell where intense storms are going to land to better prepare people and reduce damage to life and property.

The study of typhoon climatology is also important for short-term seasonal and intraseasonal forecasts. Much recent discussion has questioned as to whether the trends found in tropical cyclone intensity and destruction are linked to anthropogenic warming, or to natural multidecadal oscillations. Furthermore, discussion has debated on whether climate change is causing a change in the frequency and/or intensity of tropical cyclones. For example, Webster et al. (2005) say that the number of category 4 and 5 hurricanes have increased since the 1970, while Emanuel (2005) says rising SST are associated with increasing TC wind speed since the 1970s. Landsea (2005), Pielke (2005), and Chan (2006) argue that Emanuel and Webster's findings are based on inappropriately small data sets.

1.2 Thesis Objectives

Improvements in the accuracy and reliability of monthly and seasonal forecasts of TC landfalls must be made in order to protect life and property. For long-term forecasts, it is essential to understand how tropical cyclone behavior is connected with atmospheric and oceanic low-frequency variability at subseasonal to interannual timescales (Kim et al., 2008). In order to improve our forecasting of Western Pacific typhoons we must first understand the various environmental factors and controls of tropical cyclone variability. This thesis describes the relationships between atmospheric patterns and typhoon landfalls in the Western North Pacific Ocean (WNP).

Results show a correlation between upper-air features present over China and typhoons landfalling in three locations on the East Asia coast -Taiwan, Japan, and Vietnam. Previous studies have focused mostly on teleconnections and their influence on seasonal typhoon activity as well as other large-scale climate variables and interseasonal oscillations (Wu et al., 2004; Chan, 1985; Briegel and Frank, 1997). Although these teleconnections do play a significant role in interannual variability, they do not explain variability on smaller time scales, such as at daily to monthly, which involve the synoptic methodological aspects in this research. Environmental factors must be evaluated on these smaller scales to gain a better understanding of when the seasonal patterns break down to assess the contribution of additional steering mechanisms in order to improve future forecasting.

The objectives of this thesis are:

- Understand the relationship between synoptic-scale atmospheric patterns over East Asia and typhoon landfalls for Japan, Taiwan, and Vietnam.
- Conduct a temporal and spatial scale analysis of upper-air anticyclones and their interaction with typhoon landfalls, including track and intensity, and investigate the timeframe, in relation to landfall, where the anticyclone signal is the most pronounced.
- Statistically analyze the influence of the ENSO and MJO on TC frequency, intensity and duration in the WNP.
- Explore the impacts of other variables at mid-levels of the atmosphere, such as vector winds at the 500 hPa steering level, to help determine and understand the dominant intraseasonal steering pattern for WNP typhoons.

CHAPTER 2

LITERATURE REVIEW

Typhoon climate studies focus on various factors associated with typhoon activity on a broad range of scales. A combination of these approaches is important to paint a comprehensive picture of all the factors involved and their respective magnitude of contribution toward the environment surrounding each storm. Tropical cyclone tracks are generally controlled by large-scale atmospheric circulation patterns, and their variability is affected by many factors including but not limited to ENSO, the subtropical high, MJO, PDO and wind shear. These factors have a high spatial and temporal variability, which makes tracks extremely difficult to quantify and standardize. We do not have a system to quantify track shape based on measured parameters, nor consistent nomenclature for different track types as of yet (Terry and Feng, 2010). A change in the storm direction can occur from an internal wobble caused by TC dynamics, or from something as large as planetary-scale teleconnection interactions, although the latter generally serves more as a seasonal predictor and has a less pronounced influence on smaller scales. Localized effects also yield high uncertainty with respect to TC tracks. For example, the interaction of a typhoon's circulation with the topography of Taiwan's central mountain range can lead to track deflection and changes in intensity (Wu and Kuo, 1999). TC activity is also strongly linked to local oceanic conditions. Not only do warm sea surface temperatures (SST) provide a favorable environment for tropical

cyclogenesis, but subsurface properties are also important, especially for strong typhoons, because a deep warm water layer can weaken the typhoon-induced cooling effect (Lin et al., 2008; Lynn and Brewster, 2010).

2.1 El Nino-Southern Oscillation

The El Nino/La Nina Southern Oscillation (ENSO) is a 3 to 7 year climatic pattern in the tropical Pacific Ocean characterized by a warming/cooling of sea surface temperatures in the Eastern Pacific coupled with atmospheric pressure changes over the Western Pacific. El Nino occurs when surface ocean temperatures in the tropical Pacific warm by at least 0.5°C and a higher than average pressure pattern sets up in the Western Pacific. La Nina conditions occur with at least a 0.5°C cooling of ocean temperatures with a below average atmospheric surface pressure over the Western Pacific.

The influence of the El Niño-Southern Oscillation (ENSO) on interannual tropical cyclone activity and variability in the Western North Pacific has been extensively studied (Chan, 1985, 2000; Chen et al., 1998; Wang and Chan, 2002; Chia and Ropelewski, 2002; Elsner and Liu, 2003; Camargo and Sobel, 2005). It is widely accepted that ENSO is the planetary-scale phenomenon with the greatest influence on tropical cyclone activity (Kim et al., 2008), and it affects the genesis location, track, intensity, duration, and landfall location of tropical cyclones in the WNP. During El Nino years, more tropical cyclones form in the southeast region of the WNP basin while La Nina conditions result in an increase of tropical cyclogenesis over the northwestern part of the WNP (Chan, 1985; Wang and Chan, 2002). These interannual spatial variations in genesis locations can be attributed mainly to an increased expanse of warmer sea surface temperatures, but

also to vertical wind shear, the monsoon trough extension, and relative vorticity anomalies in the lower troposphere (Chen et al., 1998; Chan, 2000; Wang and Chan, 2002; Wu et al., 2004; Kim et al., 2005). Tropical cyclones in El Nino conditions are also more likely to reach typhoon intensities than those in La Nina conditions due to the southeastward displacement of their formation regions, which gives them a greater area of favorable warm water to travel across (Thompson et al., 1992; Sinclair, 2002; Camargo and Sobel, 2005).

Elsner and Liu (2003) conducted a study that provided a detailed analysis of three general TC track directions – straight-moving, north-oriented, and recurving. They also concluded that straight moving storms are significantly correlated with ENSO cycle, and that the frequency of straight-moving storms has an inverse relationship with the number of recurving storms (Liu et al., 2001; Elsner and Liu, 2003). Storms that form further east during an El Nino have a greater likelihood of recurving northward and thus, staying to the east of China. On the other hand, during a La Nina, storms form further west and the landfall frequency over China is increased (Elsner and Liu, 2003; Camargo et al., 2007b). Some studies have also indicated a relationship between WNP TC frequency and ENSO, but the majority do not (Sobel and Maloney, 2000). Understanding these and other behaviors of TCs with respect to ENSO phase allows it to be a reliable seasonal forecasting tool.

2.2 Northwest Pacific Subtropical High

The Northwestern or North Pacific Subtropical High (NPSH), also known as the Western Pacific Subtropical High (WPSH), is a ridge of high pressure situated around

30° latitude in the Western Pacific Ocean. In summer, the NPSH exhibits significant 2–3 year and 3–5 year oscillations with interdecadal variability (Sui et al., 2007). It is difficult to forecast due to its nonlinear, complex and variable characteristics (Hong et al., 2011). The NPSH shifts north (poleward) in the summer and south (equatorward) in the winter. This migration is a result of an increasing temperature gradient between higher and lower latitudes and also corresponds to the seasonal shift of the Intertropical Convergence Zone (ITCZ), an area near the equator where winds from both hemispheres converge.

The position of the NPSH also varies with respect to ENSO phase. During El Nino years, the NPSH is slightly flatter and displaced eastward with a more southerly ridge axis. La Nina years are associated with a more northerly ridge axis and a westward displacement of the NPSH. This change in location causes TC tracks during an El Niño to take a more northerly track or one that recurves, and a more straight-moving path during a La Niña. Also, locations west of Japan and Korea usually see much fewer TC impacts during the months of September, October, and November in El Nino years. This decrease in landfalls is thought to be related to a break in the NPSH around 130°E, which pulls storms in the direction of Japan, along with the eastward shift of the mean formation region. During La Nina years, the NPSH remains connected and shifts westward along with the mean TC formation region. This scenario causes China to have the highest predictability of landfalling TCs late in the season of anywhere else in the WNP (Wu et al., 2004).

Ten typhoons struck Japan in 2004, which is the all-time high (Kim et al., 2005). The average number for Japan landfalling storms is 2.6 per year (Nakazawa, 2006). According to Kim et al. (2005), the mean seasonal large-scale circulation that year was

characterized by a break in the NPSH east of Taiwan and persistent anticyclonic anomalies to the southeast of Japan, which enabled typhoons to penetrate the weakened NPSH and travel toward Japan. As mentioned before, this is typical of an El Nino, but usually to a lesser extent than what was seen in the 2004 season. Kim et al. (2005) suggested two possible causes for maintaining the persistent anticyclonic anomalies near Japan. One cause was a positive feedback between typhoons moving northward and midlatitude circulation near Japan, and the other was a response to the broad-scale tropical deep convection. Another study on interdecadal track variability by Chang-Hoi et al. (2004) stated that interdecadal changes in typhoon tracks were affected by the westward expansion of the NPSH and that the expansion of the NPSH to the southeast coast of Asia may result in a larger elliptic pathway of typhoon migration.

2.3 Pacific Decadal Oscillation

The Pacific Decadal Oscillation (PDO) is a climate variability pattern similar to El Nino that has two phases, the warm or positive phase, and the cold or negative phase. The PDO has an interdecadal variability and changes phase approximately every 20-30 years (Mantua, 2002). A positive PDO phase produces climate and circulation patterns that are similar to El Niño and a negative PDO phase produces climate and circulation patterns similar to La Niña (Gershunov and Barnett, 1998). Gershunov and Barnett (1998) also found that the climate signal of El Niño is likely to be stronger when the PDO is highly positive while the climate signal of La Niña will be stronger when the PDO is highly negative. This does not indicate that ENSO is controlled by the PDO, but rather that the resulting climate patterns interact. The PDO also has a significant influence on the NPSH and the midlevel steering flow during the WNP TC season. It generates a

north-south dipole of geopotential height anomalies which alters zonal winds and also affects the strength and extension of the NPSH (Liu and Chan, 2008). The PDO was in a cool phase from 1946 -1976. It then entered a warm phase, coincidentally right around the start of the satellite era. Scientists who believe that climate change is mostly natural and that climate is fairly insensitive to anthropogenic input tend to agree that the PDO has a significant impact on global climate (Spencer et al., 2007). The pattern subsequently returned to the warm phase after a brief cool phase from 1998-1999. The transition years 1946, 1976, and 1998 had a minimal number of tropical cyclones (Folland et al., 2002).

Kubota and Chan (2009) conducted a study on the interdecadal variability of tropical cyclone landfall in the Philippines in which they found that the landfall numbers are associated with different ENSO phases as well as the PDO. During the negative PDO phase, the annual number decreased significantly in El Niño years and increased in La Niña years. During the positive PDO phase, the results were inconclusive (Kubota and Chan, 2009). Liu and Chan (2008) also believe that decal variability may be partly attributed to the PDO signal.

2.4 Madden-Julian Oscillation

The Madden-Julian Oscillation (MJO) is an intraseasonal planetary-scale oscillation that originates over the Indian Ocean and propagates eastward at 5 ms^{-1} with a period of 30-60 days (Madden and Julian, 1971, 1972; Zhang, 2005). It is the dominant component of interseasonal variability in the tropics and is characterized by quasiperiodic large-scale coupled patterns in atmospheric circulation and deep convection (Madden and

Julian, 1971; Zhang, 2005). Along with eastward propagating regions of enhanced and suppressed convection, there are also distinct patterns of lower and upper level atmospheric circulation anomalies. Convectively-coupled westward propagating Rossby and eastward propagating Kelvin waves accompany the MJO. Observational studies (e.g. Hendon and Salby, 1994) have found that while the MJO propagates as a coupled Kelvin-Rossby system early on, it eventually breaks up with the Kelvin wave propagating away from the convection region at greater phase speeds. The role of the Kelvin waves that are embedded in the MJO in tropical cyclogenesis remains unknown (Schreck and Molinari, 2011).

Plentiful scientific evidence shows that there exists a link between MJO and ENSO. Although MJO does not directly cause an El Nino onset, it can contribute to the development and intensity of El Nino episodes (Kessler and Kleeman, 2000; Zhang and Gottschalck, 2002). In the WNP, stronger MJO activity is observed about 6 to 12 months prior to an El Nino onset, but is essentially absent during and after its peak (Zhang, 2005; Gottschalck and Higgins, 2008). Also, the MJO signal is generally greater during a La Nina event.

The MJO significantly influences tropical cyclogenesis in each basin by modulating convection, low-level vorticity, and vertical wind shear within each TC season (Schreck and Molinari, 2011). It provides a large-scale favorable or unfavorable environment for TC formation. For example, the strongest tropical cyclones usually develop when the MJO is in the enhanced/convective phase. WNP TCs have been found to be more frequent during the active MJO phase because of the existence of more pre-existing depressions rather than any increase in the percentage which undergo

cyclogenesis (Liebmann et al., 1994). Gray (1979) first detected the connection between MJO and TC activity. He discovered that the active TC genesis period tends to be clustered over a period of 2-3 weeks, followed by a similar period of inactivity. These intraseasonal patterns were thought to be attributed to the MJO. Liebmann et al. (1994) stated that TC genesis tends to be common during the MJO convective period, however, the ratio of tropical storms and typhoons to tropical depressions seems to be relatively constant regardless of the MJO phase. Some recent studies have tried to explain the enhanced TC genesis during the MJO convective phase by analyzing the genesis mechanism by means of low-level barotropic wave dynamics over monsoon confluence regions where the monsoon westerlies impinge on the trade easterlies (Sobel and Maloney, 2000; Maloney and Hartmann, 2001; Aiyyer and Molinari, 2003). This phenomenon can also be explained as a barotropic wave accumulation associated with zonal wind variations. The 850 hPa barotropic wave activity flux was also found to increase during an MJO convective phase in the WNP (Sobel and Maloney, 2000).

Kim et al. (2008) examined WNP TC variability (i.e., genesis, track, and landfall) in relation to various categories of the MJO during June–September for the period 1979–2004, which are defined based on the empirical orthogonal function analysis of outgoing longwave radiation data. The number of TCs increases when the MJO-related convection center is located in the WNP. The genesis region axis methodically fluctuates in response to changes in the large-scale environments associated with both the eastward and northward propagation of the MJO and the intraseasonal variability of the NPSH. When the MJO-related convection center is found in the tropical WNP, a dense area of TC

tracks migrates westward. At that time, studies of spatial variations of WNP TC activity in connection with MJO evolution have not been conducted (Kim et al., 2008).

TC genesis patterns over the Fiji, Samoa, and Tonga (FST) region are significantly altered with approximately 5 times more TCs forming in the active phase than in the inactive phase of the MJO. This is even further strengthened during El Niño periods. Genesis-related environmental conditions (i.e., low-level relative vorticity, upper-level divergence, and vertical wind shear) show a distinct pattern of variability for both MJO phases. The MJO also has a substantial effect on TC intensity in the FST region (Chand and Walsh, 2010). Hall et al. (2001) determined that the MJO strongly affects TC genesis around Australia, with a stronger MJO-TC relationship during El Nino. They also found that changes in TC genesis patterns associated with MJO are strongly correlated to the 850-hPa cyclonic relative vorticity anomalies. A study by Bessafi and Wheeler (2006) for the South Indian Ocean also showed significant MJO modulation of TC genesis which was attributed to changes in low-level cyclonic relative vorticity, vertical wind shear, and deep convection. Camargo et al. (2009) studied MJO modulation of TC genesis on a global scale using an empirical genesis potential index developed by Emanuel and Nolan (2004), and found that this modulation is caused primarily by changes in mid-level relative humidity and low-level absolute vorticity with slight contribution from vertical wind shear and potential intensity.

Extensive efforts have been made to understand the origin and dynamical/physical characteristics of the MJO and its impact on global and regional climate (Zhang, 2005). The MJO is often analyzed in time-longitude format to show the propagation of the

features over time. Most time-longitude plots are produced for outgoing longwave radiation (OLR), velocity potential, wind anomalies, and 500-hPa height anomalies (Gottschalck and Higgins, 2008). MJO observations are still full of difficulties. The description of the MJO as sinusoidal perturbations with equal amplitudes in its enhanced and suppressed phases is inadequate. MJO properties could be better described if each episode were treated as a distinct, pulse-like event (Salby and Hendon, 1994; Yano et al., 2004). New satellite data containing high-resolution vertical water vapor and temperature profiles are necessary to validate global model reanalysis data, which is what the vertical structure of the MJO as we know it is mostly based on (Zhang, 2005). In addition, the prediction skill of the MJO is limited to about 15-20 days, so it is virtually unpredictable on interannual timescales (Slingo et al., 1999; Waliser et al., 2003).

2.5 Recent Changes in Tropical Cyclone Activity

Long-term changes in TC activity have been actively studied in the past few years. Emanuel (2005) found an increase in TC power dissipation, which is related to duration and intensity, in the WNP over the past 30 years. Webster et al. (2005) indicated that there has been a large increase in the quantity of Category 4 and 5 typhoons and associated typhoon days over the past 35 years. However, other studies show a small or nonexistent trend (Klotzbach, 2006; Kossin et al. 2007). This inconsistency may be due to the quality, or lack thereof, of TC datasets (Landsea et al., 2006). Data homogeneity among TC datasets has become a major challenge. Three historical datasets for the WNP were analyzed (from the Joint Typhoon Warning Center (JTWC), Japan Meteorological Agency (JMA) and China Meteorological Administration (CMA)) and significant

discrepancies were found among them, primarily regarding intensity estimates (Ren et al., 2011). Song et al. (2010) looked at best track data sets from 1945-2007 of the JTWC, the Regional Specialized Meteorological Center (RSMC) Tokyo, and the Shanghai Typhoon Institute (STI). They found the variation in tracks to be negligible, but typhoon classification differences between datasets resulted in a misleading upward trend in the amount of stronger typhoons. The differences in TC center position were less than 30 km, which is very small. However, greater differences were discovered in TC intensity measurements, with the JTWC showing higher intensity estimates for typhoons but lower intensity estimates for tropical depressions. The authors believe this is due to different algorithms that are used to calculate TC intensity for each data set. The JTWC measures maximum sustained winds over an interval of 1 minute while the RSMC measures wind speed based on maximum sustained winds averaged over a 10-minute interval. Atkinson (1974) noted that the 10-minute averaged wind speed is approximately 88% of the 1-minute averaged speed, which is something to keep in mind when comparing datasets.

An unprecedented 10 typhoons hit Japan in 2004, while South China experienced widespread drought associated with the lack of moisture from TC landfalls (Wu et al., 2005). A decrease of the seasonal mean frequency of tropical cyclone occurrences near South China decreased over the past four decades. The cause of the track shift is a primary result of changes in the large-scale steering flow, and Wu et al., (2005) suggested tropospheric cooling as the culprit. The East Asian tropospheric cooling is associated with the lowering of the upper tropospheric geopotential height and the enhancement of the anomalous surface anticyclone, which is associated with the westward expansion of

the strengthening NPSH. However, causes of enhanced cyclonic steering flows are still not fully known (Wu et al., 2005).

Tu et al. (2011) found that since 2000, intense typhoons in the WNP have generally occurred earlier in the season than before. They examined the frequency of intense typhoons in the month of May and saw that prior to 2000, intense May typhoons only occurred about once a decade. After 2000, that number increased to almost once per year. The factors responsible could be a combination of variables that support a higher TC genesis index, such as an increase in tropospheric water vapor and mid-tropospheric relative humidity (Tu et al., 2011). Tian et al. (2010) found that typhoon tracks over the WNP are closely related to the atmospheric intraseasonal oscillation (ISO) activity. The low-frequency (30-60 days) circulation pattern is a good indicator of typhoon tracks. However, the tracks are associated with the low-frequency wind-field patterns of the ISO, particularly to the maximum value lines (belts) of low-frequency cyclonic vorticity at 850 hPa (Tian and Li, 2010).

Recent studies have shown that the NPSH has expanded to the west since the late 1970s (Gong and Ho, 2002; Zhou et al., 2009). The reason for this is not clear, but Zhou et al. (2009) suggests that this significant change is partly due to the atmosphere's response to the observed Indian Ocean–western Pacific (IWP) warming. The relative percentage of TCs in the regions south of 20°N has been decreasing since the 1980s, but in the regions north of 20°N, it has been increasing (Gong and He, 2002). This is evident in the recent increase of tropical cyclone landfalls in Japan. Although the NPSH does play an important role in the general steering of tropical cyclones, it may not be sufficient enough to describe the overall pattern within a season. Thus, to get a more thorough

understanding of tropical climatology, it is important to look at smaller timeframes, as well as other synoptic and mesoscale climate features in conjunction with basin-scale and planetary-scale interseasonal oscillations.

2.6 Upper-level anticyclones

Upper-level high pressure areas are usually superimposed over tropical cyclones. TCs, which are warm core in nature, release latent heat aloft by cloud formation. Motion is forced horizontally outward, usually between the 300 hPa and 150 hPa levels. For this reason, high pressure aloft is associated with upper-level divergence, which is an important process in TC intensification. The warm core of a TC is crucial to its growth because it intensifies the upper-level anticyclone. For intensification to occur, the outflow must be strong enough to advect air away from the storm's center so that it is not circulated back in at lower levels. Further intensification may occur if the jet stream or a large area of cold air passes over at around 200 hPa. This would enhance the exhaust of the TC and accelerate its circulation. Upper-level anticyclones can have a major impact on the weather at the surface. Because air tends to sink on the east side of the ridge, clear, dry conditions usually prevail to the east of the upper-level ridge axis. On the other hand, air tends to rise on the west side of the ridge so cloudy, wet weather usually occurs to the west of the ridge axis.

2.7 Typhoon-trough interaction

Harr and Elsberry (1995) demonstrated that WNP active (inactive) monsoon regimes seemed to be associated with active (inactive) periods of TC activity. Therefore, significant intraseasonal TC variability may be related to large-scale monsoon

circulations. Most of the TCs in the WNP originate from within the monsoon trough, a feature that usually lies across the South China and Philippine Seas. Its presence contributes to dynamic conditions that are favorable for tropical cyclone activity. Some disagreement concerns as to the exact mechanism which leads to TC formation here, but Chen and Weng (1998) found a strong association between the monsoon trough and synoptic-scale disturbances in the WNP. When the monsoon trough extends (retreats) eastward (westward), the synoptic-scale disturbances also follow suit. The main source of interannual variability in monsoon-TC influence is ENSO, while over intraseasonal timescales, the MJO plays more of a role. (Harr and Chan, 2004). Harr and Elsberry (1991) showed that the mechanism responsible for an enhanced monsoon trough also determines the track that the developing cyclone will take. If the monsoon trough is enhanced by easterlies along the southern edge of the subtropical ridge, the developing cyclone will most likely follow a straight path. On the other hand, if a monsoon surge is responsible for the monsoon trough enhancement, the cyclone will often recurve.

Another mechanism for TC formation is the Tropical Upper Tropospheric Trough (TUTT). The TUTT is a dominant climatological feature of the upper troposphere throughout the summer in the Pacific (Sadler, 1976), and extends from the mid-latitudes of the eastern North Pacific to the tropical western North Pacific. They are elongated troughs that appear in summer monthly averaged maps of the upper-tropospheric flow over the oceans (Ferreira and Schubert, 1999). When the western end of this trough lies to the north of the monsoon trough it helps in TC development. There are cases that TUTTs assist the genesis and intensification of tropical cyclones by providing more

forced ascent near the TC's center and a well-organized outflow channel in the upper troposphere, most likely near its most westward periphery (Sadler, 1976).

Hanley et al. (2001) found that tropical cyclones over warm water and away from land are more likely to intensify than weaken after an interaction with an upper-level trough. For conditions to be favorable for development, the trough has to be of proper horizontal scale (one that matches that of the TC) and strength so it does not shear the storm apart. Favorable trough interactions are not very common because the troughs are typically much larger than the TC. However, if a sufficiently strong upper-level ridge or some other blocking mechanism is present near the TC the trough can narrow until it resembles a similar scale.

An upper-level low can also constructively interact with a TC and stimulate development. Unlike trough interactions, these upper-level low interactions occur in the area of the tropics/subtropics and away from mid-latitude troughs. The distance of the upper-level low to the TC is critical because if they are too close, the TC will be sheared apart, and if they are too far, the low will not have a significant impact on the TC. The strength of the upper-level low also plays an important role since a weak or moderate upper-level low is more conducive than an intense low. It is not known for sure whether the upper-level low and the TC have a mutual interaction or if one steers the other, but there seems to be a positive feedback. Outflow is enhanced as the TC develops, which is feeding into the low that is being further aided by wind shear vorticity, allowing further enhancement of the outflow.

Forecasting the intensity change of tropical cyclones remains one of the biggest challenges facing operational meteorologists (Elsberry et al. 1992; Avila 1998). The high percentage of superposition cases (when a TC intensifies with an upper-tropospheric potential vorticity (PV) maximum within 400 km of the tropical cyclone center) that intensify could be used as a forecast tool for intensity change during trough interactions. The results suggest that if a numerical model shows the approach of an upper PV maximum of a scale similar to that of a TC, the tropical cyclone is likely to intensify as superposition begins to occur (Hanley et al., 2001).

2.8 Forecast Models

The JTWC develops a TC motion forecast in three phases: field analysis, objective technique analysis, and forecasting (Guard et al., 1992). During the field analysis using The Navy Operational Global Atmospheric Prediction System (NOGAPS), some of the key synoptic features that are evaluated are subtropical ridges, mid-latitude troughs and associated subtropical ridge weaknesses, cyclonic cells in the TUTT, and the presence of other TCs. The models used by the JTWC, including the GSM (global spectral model) and TYM (typhoon model), are comparable to those of the NHC, and guidance from NHC models is often used. One of the main differences between procedures at the two forecast centers, NHC and JTWC, is that NHC frequently communicates with civil defense and news agencies. Also, aircraft reconnaissance is utilized for tropical cyclones threatening populated areas. The JTWC and other forecasters can incorporate multi-variable synoptic analyses at different atmospheric levels, and on various scales, including climate indices, into model simulations. In conjunction with numerical algorithms for short term forecasting, the model scenarios

can be used for research purposes in a field where access to in situ and satellite data is fairly limited.

It is well known that track and intensity predictability depends largely on larger-scale environmental conditions, such as moisture, stability and wind shear (Gray, 1979; Liu et al., 1997). It is possible to realistically predict the track, intensity, and inner-core structures of TC from synoptic conditions if high grid resolution, appropriate model physics, and proper initial vortices in relation to these larger-scale conditions are incorporated. TC interaction with its large-scale environment affects its characteristics just as internal dynamics and thermodynamics do (Liu et al., 1997).

CHAPTER 3

DATA AND METHODOLOGY

Interpreting signals in synoptic climatology patterns is pertinent to assess the factors that influence tropical systems in the Western Pacific, where studies are sparse in comparison to the North Atlantic basin. This study examined variables that adequately show these atmospheric interactions at different scales, both temporal and spatial. It utilized data and statistical methods that are conventional in synoptic climatology and meteorology.

3.1 Data

3.1 a. Geopotential Height Data

Geopotential height anomalies are the departures of the geopotential height, which is the actual height of a pressure surface from the mean at a given level. They were plotted at 200 hPa, where the height composites indicate dominant upper level cyclones and anticyclones, which are the main synoptic steering patterns in the upper atmosphere over eastern Asia and the Western Pacific Ocean. Geopotential height anomaly composites were created using the National Centers for Environmental Prediction/National Center for Atmospheric Research (NCEP/NCAR) reanalysis data provided by the NOAA/OAR/ESRL Physical Sciences Division, Boulder, Colorado, from their website at http://www.esrl.noaa.gov/psd. The goal of the reanalysis project was to produce new atmospheric analyses using historical data (from 1948 on) as well as

analyses of the current atmospheric state (Climate Data Assimilation System, CDAS) in support of the needs of the research and climate monitoring communities. This project involved accessing, quality controlling and assimilating land surface, ship, rawinsonde, pibal, aircraft, satellite and other sources of data. The horizontal resolution of the data is 2.5^{o} x 2.5^{o} and it is available for various atmospheric variables (Kalnay et al., 2006).

3.1 b. Typhoon Track Data

The source of the Tropical Cyclone (TC) tracking data is JTWC best track data (1945-present), which records the position (latitude and longitude) of the surface cyclone's center and 1-minute averaged maximum sustained surface winds at 6-hour intervals, obtained and analyzed at http://weather.unisys.com/hurricane/w_pacific/ (data obtained from the Joint Typhoon Warning Center). These positions were derived by a combined analysis from aircraft, satellites, radar and synoptic weather charts. They were determined after each TC has dissipated, and can differ from "working best track" positions provided in TC warnings by as much as 120 nm. Post-storm analysis is beneficial because more raw data is generally available, as well as more time and a complete storm history to produce best tracks for the JTWC Archive.

Although the Best Track dataset provides a reliable continuity of storm positions, on average, they varied up to about 25 km from the actual surface center positions measured from aircraft. This is likely attributed to different analysis levels, navigational errors, and small scale variations in the movement and path of the cyclone which are normally smoothed out in the Best Track analysis. Therefore, when doing a more detailed analysis on the wind field, structure, or precise track of each storm, researchers should

combine Best Track data with aircraft data or some other form of raw observations (Weatherford and Gray, 1988). In the case of the broad scope of this study at the synoptic scale, the smoothed Best Track dataset is suffice.

3.1 c. Typhoon Data Quality

The Western Pacific TC data is far less robust and reliable than the Atlantic Basin data. It contains many inconsistencies in observations spanning the spectrum from speed to intensity and gets sparse even as we get outside the realm of the last thirty years or so (Chu et al., 2002). The JTWS has Annual Tropical Cyclone Reports (ATCRs) that go back to 1959, which are detailed reports for each season, including the number of typhoons, the area of formation and development, size and intensity, and movement. They also include discussion of each storm and detection and forecasting techniques. Despite these reports being some of our more reliable sources for the pre-satellite era, they are riddled with discrepancies. When compared with reanalysis data, there are quite a few years that differ in the number of total TCs. This is clearly not a minor incongruity, such as a difference in a wind speed of a few knots or a track that was off by several kilometers would be. Storm size and forward speed data are also very difficult to evaluate from the Western Pacific data. Forward speed must be calculated based on the storm's position and the radii to be able to infer size are difficult to obtain.

Advancements in technology increased our understanding of tropical cyclones and the introduction of satellite observations in the 1960s greatly improved the quality and quantity of TC data. The data quality and supporting documentation are less reliable for older storms, and the report designed to address and resolve discrepancies associated

with the best track dataset states that the 1985-2000 tracks are of highest quality, while older data should be utilized with caution (Chu et al., 2002). More recent best track data utilize near-surface wind measurements from GPS dropwindsondes as well as flight-level to surface wind reduction factors developed using GPS dropwindsonde data (Franklin et al. 2003), which have been used since 2002. A brief inspection of the older, undocumented best-tracks was conducted, but the tracks were not cross-validated due to lack of documentation.

Recent best track data also contains intensity estimates, but confidence in the quality of these estimates is low. The primary source starting in the satellite era of these estimates is the Dvorak model (Dvorak, 1975, 1984, 1995), which is considered to be less accurate than in-situ measurements, such as aircraft reconnaissance, dropsondes and surface reports. Perhaps the most reliable measure of TC intensity is the minimum sea level pressure (MSLP) although the TC's destructive potential is better described by the maximum wind speed at/near the surface (Knaff and Zehr, 2007). Because the maximum surface wind speed (MSWS) is a difficult quantity to measure, "wind-pressure relationships" between the MSLP and the MSWS were developed in attempts to better understand TC intensity. Knaff and Zehr (2007) took five factors into account when calculating these wind-pressure relationships: environmental pressure, storm motion, latitude, storm size and intensification trend. Reanalyzing western Pacific best tracks during the period when reliable MSLP measurements were available would likely increase the number of strong typhoons (1974-1987) and therefore, reduce the increased intensity trends in the best track (1970-2004) as discussed in Webster et al (2005) and Emanuel (2005).

One discrepancy with the JTWC intensity estimates is that they are based on 1-minute mean sustained wind speeds, while other forecast agencies in the JTWC Area of Responsibility base their estimates on 10-minute mean winds. These 1-minute mean wind speeds are generally higher than 10-minute mean wind speeds by 14%. As a result of this, caution should be used when comparing JTWC best tracks with those of other agencies (Chu et al., 2002). To correct the JTWC archive data, differences from other sources, such as the Hurricane Risk Assessment database (Neumann, 1987, 1999) and the Hong-Kong Observatory charts (Chin, 1972) were compared and documented Differences between JTWC's archive data and their Annual Tropical Cyclone Reports were also assessed and necessary corrections were posted in the updated JTWC archive.

Historical best track data is prone to issues with intensity, especially in the pre-satellite era. Prior research has generally used a small subset of available best track data, but Kruk et al (2010) proposed a technique to combine best track data from regional forecast centers into one single point for distribution, named the International Best Track Archive for Climate Stewardship (IBTrACS). Prior to IBTrACS, there has been no publicly available nonproprietary data that incorporates documented TC best track data for all basins from all available agencies. Before the MSWS can be compared between agencies, it must be converted to a common averaging period. For IBTrACS, MSWS values were converted to a 10-min period (Knapp et al., 2010).

3.1 d. MJO

The MJO is directly monitored using several different variables. These analyses are frequently displayed in time-longitude format to show the propagation, amplitude and

location of the MJO-related features. Typically, these time-longitude plots include: outgoing longwave radiation, velocity potential (a derived quantity isolating the divergent wind component at upper levels), wind anomalies at various levels, and 500 hPa height anomalies to represent how the atmosphere responds in midlatitudes.

Since convective instability requires a large extent of warm sea surface temperatures, these MJO signals are typically confined to the Indian and Western Pacific oceans. During an El Nino event, as the eastern edge of the warm pool extends eastward (Picaut et al., 1996), MJO activity follows suit (Fink and Speth, 1997; Hendon et al., 1999; Bergman et al., 2001). A relationship between the level of global MJO activity and sea surface temperature indices symbolizing ENSO has been found to be quite weak (Slingo et al., 1999; Hendon et al., 1999) suggesting that the interannual variability of the MJO might be more influenced by the internal dynamics of the atmosphere than surface conditions.

For this study, MJO analysis data was obtained from the NOAA Climate Prediction Center (CPC) at http://www.cpc.ncep.noaa.gov/products/precip/CWlink/MJO/mjo.shtml. This data consists of overlapping five-day (pentad) means for 200-hPa velocity potential, 200-hPa zonal wind and 500-hPa geopotential height derived from the NCEP/NCAR CDAS/Reanalysis data (Kalnay et al. 1996). In addition, pentad outgoing longwave radiation (OLR) data, used as a proxy for deep tropical convection, was derived from measurements made by the NOAA operational polar-orbiting satellites for the period 1979-2000 (Xue et al., 2002). The CPC created MJO indices by the following method: First, an Extended Empirical Orthogonal Function (EEOF) analysis was applied to pentad

200-hPa velocity potential (CHI200) anomalies southward of 30°N for 15 ENSO-neutral and weak ENSO winters (November-April) in 1979-2000. The ENSO-neutral and weak ENSO winters during 1979-2000 are selected according to the CPC ENSO classification (http://www.cpc.ncep.noaa.gov/research_papers/ncep_cpc_atlas/8/ensoyrs.txt). Subsequently, ten MJO indices were constructed by regressing pentad CHI200 anomalies onto the ten time-lagged patterns of the first EEOF of pentad CHI200 anomalies. Anomalies are based on the 1979-1995 time period, and indices are normalized by each of their standard deviations during ENSO-neutral and weak winters.

3.2 Methodology

3.2 a. Composite Anomaly Approach

Studying modern synoptic climatology provides a basis for understanding the hierarchy of climatic controls that operate at different spatial and temporal scales (Mock et al., 1998). Composites are a very valuable tool to synoptic climatologists, often complementing and even replacing other more complicated climatological techniques. Compositing is a common approach that averages a set of selected maps satisfying certain environmental criteria, representing the key synoptic features of a specific situation (Yarnal, 1993). It is a simple and flexible method which can summarize complex criteria and various physical aspects of weather and climate that includes hazards such as tropical cyclones, and is not restricted to pressure surfaces (Barry and Perry, 1973; Hirschboeck et al., 1996). The method is also useful because when averaging data fields from different time periods, standardized anomaly composites from the long-term mean provide a helpful tool for viewing synoptic patterns that govern selected atmospheric events. Because of the way they are calculated, composites are

insensitive to problems such as measurement of variables being at incompatible time steps or encountering too much missing data (Yarnal, 1993). Compositing is an environmental-to-circulation approach to synoptic climatology. The classification criteria are independent of the atmospheric circulation, so the choice of synoptic types is unbiased (Winkler, 1988). Composites are often used in conjunction with correlation fields to test if the correlation coefficients produced by a correlation-field analysis resemble patterns on actual plotted pressure fields. Another benefit is that compositing allows one to identify nonlinear responses than are not apparent in correlation mapping (Stidd 1954; Hirschboeck et al., 1996). One of the issues with composites is that they can average dissimilar atmospheric settings, thus inducing a false impression of the situation usually associated with a certain criteria. Also, atmospheric circulation composites are neither independent of the surface environment nor continuous in time; therefore, model-comparison statistics cannot be used with composites (Yarnal, 1993).

The composites were created from the geopotential height anomalies for each of the selected landfall dates, from NCEP/NCAR reanalysis data (Kalnay et al., 1996) at 200 hPa, which were plotted on a grid of 0º-60º N latitude 90°-180º E longitude encompassing the WNP. This spatial area was chosen because it encloses all three groups of typhoon tracks, as well as the prevailing atmospheric patterns analyzed. 200 hPa is one of the most common layers at which to analyze broad scale circulation patterns. The average height of the 200 hPa level is about 12,000 meters depending on time of year and latitude, and the distance from the surface allows us to neglect the influence of friction.

Based on traditional NCEP reanalysis composite mapping, shades of blue/purple on the plots indicate negative height anomalies and shades of yellow/red indicated

positive height anomalies. Interpretation is anomalous clockwise (anticyclonic) flow around positive centers and counterclockwise (cyclonic) around negative centers. Although the negative height anomalies usually indicate an upper level trough or cyclone and the positive height anomalies indicate an upper level ridge or anticyclone, this is not necessarily true in terms of actual conditions. For example, since anomalies are departures from normal, you can have a slightly higher pressure without having a closed anticyclone. The same is true for lower pressure. Therefore, in addition to the anomaly composites, mean geopotential height composites were created (c.f., Birkeland and Mock, 1996). They were then compared to the anomaly composites to provide a better understanding of the variations in the broad scale synoptic circulation.

Although the large-scale upper-level flow in this thesis is the primary steering pattern for typhoons, I acknowledge the fact that the opposite could also be true where the TC itself can influence atmospheric circulation patterns. Tropical cyclones consist of a warm-core vortex, where the strongest cyclonic circulation lies near the surface and gradually weakens with height. As rising air reaches approximately 200 hPa, high pressure is formed near the tropopause, and flow diverges away from the center. This convective anticyclonic outflow (or anticyclonic jet) creates a positive feedback effect, intensifies the TC and impacts surrounding structure dynamics. The outflow has a spatial scale much larger than that of the TC's cyclonic circulation, and can have long-lasting effects on the upper-level large-scale circulation. Furthermore, if the outflow from a TC reaches a mid-latitude potential vorticity gradient, downstream Rossby waves may be stimulated. If the outflow potential vorticity differs from that of the ambient upper-tropospheric potential vorticity, an outflow jet forms along the PV gradient (Lazear,

2007). Convective outflow modifies the jet as a TC evolves resulting in less shear and more rapid intensification of the TC–jet couplet. As the TC outflow expands into the area of weak inertial stability on the anticyclonic shear side of the jet stream, an outflow channel is thought to be generated minimizing the energy expended and allowing radiational cooling to decrease the work of subsidence. It is also hypothesized that evolving conditions in the outflow layer modulate the TC core structure in such a way that TC outflow can penetrate weak inertial stability in the environment (Rappin et al., 2011).

3.2 b. Study Area

Typhoon landfalls analyzed were hand-selected from the best track dataset based on the following criteria: each storm had a wind speed of at least100 knots at landfall and made a direct landfall in each study area – Vietnam, Japan and Taiwan. These three regions were selected because they experience multiple typhoon landfalls per season (on average), and are located in three distinct geographic locations. They are spatially far enough apart where they are affected by storms paths of different directions. For example, Vietnam gets mostly straight-moving storms while Japan gets storm tracks that recurve to the N/NE. The number of selected dates varies between locations due to differing sample sizes, and the ones chosen for this study range from 1964-2007. Japan and Taiwan both had more typhoon landfalls of $\geq$ 100 knots than Vietnam. Although only 10 storms were selected from Vietnam, that is sufficient for this study because the TCs are not being analyzed individually, but instead are contributing to their respective composite for a physical climatological interpretation. The greater sample size does yield a more precise picture of strength and position of synoptic features and is stronger

statistically significant, but only of the storms chosen to create the composites. The plot will shift based on what is input, regardless of the quantity of landfalls. Because the purpose of this analysis is to deduce the general atmospheric pattern associated with certain landfalls, the difference in sample size is sufficient statistically.

3.2 c. Additional Composite Analysis

Typhoon tracks corresponding to the landfall dates, were generated in ArcGIS (Geographic Information Systems) after obtaining a complete dataset from IBTRaCS, an integrated global best track database (Knapp et al., 2010), and filtering out the selected storms. Storm tracks were geo-referenced and accurately superimposed onto the composite plots using ArcMap, the primary component of ArcGIS (Figure 3.1). This was repeated separately for each landfall location. The position and strength of the anticyclone was then analyzed with respect to the storm tracks. Due to the state of the data, it was not feasible to perform rigorous mathematical calculations to assess the intensity of the height anomalies, so the strength of the patterns was largely based on the value in the centers of action. Vector winds at 200 hPa and 500 hPa were also analyzed (Figure 3.2). The 500 hPa level represents conditions near the middle of the atmosphere where low pressure features are easily identified and lies at an altitude of about 5500 meters. The 200 hPa vector wind layer was chosen to supplement the 200 hPa geopotential height composites and the 500 hPa vector wind layer is widely used as the mean steering later for tropical cyclones. Ideally, one would want to conduct a mean wind analysis on a vertically averaged pressure layer since we are dealing with TC of different intensities, and stronger storms are going extending further up into the

atmosphere. Therefore, in addition to vector winds being analyzed on a case-by-case basis, composites of mean vector winds for the 200 hPa – 800 hPa level were also created. By analyzing winds over a vertically-averaged pressure column, we gain a more comprehensive perspective on the steering flow in the levels of the atmosphere where tropical cyclones exist and where their climatic influence is more evident. In addition to just the landfall dates, geopotential height anomaly composites were created for specific storms at different time frames: 1 week before landfall, 5 days before landfall and 3 days before landfall to better understand the spatial progression and variations in strength of the anticyclone as the storm draws nearer to landfall. This is also necessary to deduce whether the upper level atmospheric patterns developed independently of the typhoons or if they were a contribution of the typhoon itself, since strong typhoons have anticyclones aloft that can easily reach 200 hPa levels.

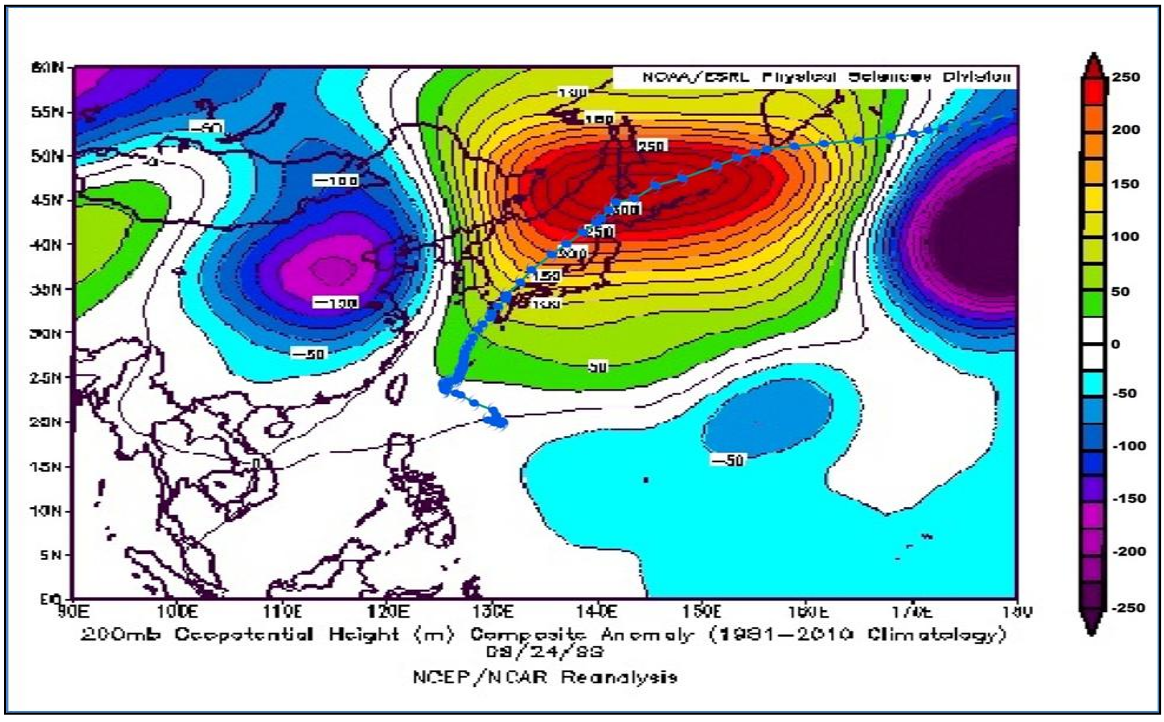

Figure 3.1. Typhoon Bart making landfall in Japan on 9/24/1999. The storm's track (blue line) is superimposed onto the 200 hPa geopotential height anomaly composite for that day.

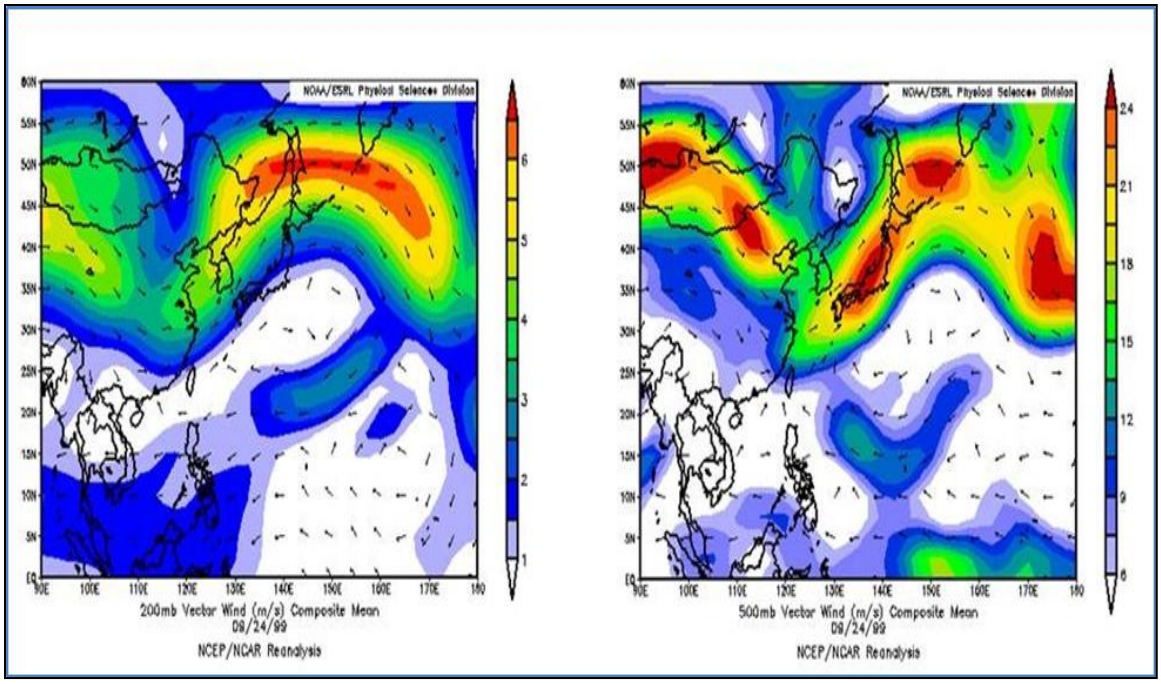

Figure 3.2. The left (right) image shows mean vector winds on 9/24/1999 at 200 hPa (500 hPa).

3.2 d. MJO and ENSO Analysis

Simulating a realistic Madden-Julian Oscillation continues to be a challenge for atmospheric modeling community. Dynamic models do not outperform statistical models in MJO forecasts (Waliser et al., 1999a; Lo and Hendon, 2000). They are generally not good predictors of the MJO, in part because of the fundamental difficulties regarding the correct mathematical treatment of tropical convective processes. Early model simulations appeared to be promising, with eastward propagating signals in both large-scale circulation and precipitation (Hayashi and Golder, 1986; Hayashi and Sumi, 1986; Lau and Lau, 1986) but their eastward propagation speeds were often closer to that of the observed Kelvin waves than to the speed of the MJO itself (Zhang, 2005). Even when sophisticated models try to reproduce the MJO's eastward propagating signals, they are too weak, their propagation speeds are too high, their spatial distributions and seasonal

cycles are unrealistic, and their convection and wind is decoupled (Slingo et al., 1996; Sperber et al., 1997).

Pentad MJO index plots since 1978 were analyzed for characteristic features of the MJO signal, indicated by alternating patterns of blues representing the enhanced phase and reds indicating the suppressed phase. The centers of enhanced convection for the ten indices, which are determined from the ten time-lagged patterns of the first EEOF of CHI200, are labeled on the x-axis (20°E, 70°E, 80°E, 100°E, 120°E, 140°E, 160°E, 120°W, 40°W and 10°W). From these labels, we can pinpoint the geographic region of the WNP by locating its latitude/longitude range. Since time increases from top to bottom, contours that are slanted down to the right signify eastward propagation (Figure 3.3). Figure 3.4 shows what an ENSO feature would look like on these plots. Notice the contours do not extend the entire width of the plot, meaning the feature is mostly stationary and the colors are not alternating, which is always true with the MJO since an enhanced phase is always followed by a suppressed phase.

After five three-month MJO events were selected, counts were done for TCs during that timeframe, as well as during three five-month El Nino and La Nina events. These included total number of TCs, number of typhoons over certain wind speed thresholds (65 and 100 knots), and the number of typhoon days per ENSO or MJO event, as well as percentages of TCs that intensified into both typhoon (65 knots) and supertyphoon (100 knots) strength. The purpose of this analysis is to determine whether ENSO or the MJO shows any effects on intensity or lifespan of TCs. Subsequently, box-and-whisker plots were created using SigmaPlot version 9 for number of typhoon days greater than 65 knots and number of typhoon days greater than 100 knots for the three

five-months ENSO events (both El Nino and La Nina) and five three-month MJO events. This was done by calculating the number of TC days per storm (adding all observations that satisfied the wind speed threshold and diving by four—since there were four observations per day—and then plotting number of days per storm as a single point). If the data did not contain at least three points, that set of points was not illustrated. Outliers were also plotted where applicable.

A statistical analysis was performed in SAS Version 9.2 using a Generalized Linear Mixed Model (GLMM) (specifically PROC GLIMMIX) with canonical parameter log (μ), where μ is the mean of the Poisson random variables, which in this case is the mean number of TCs or TC days. The distribution applicable here, the Poisson distribution, is a discrete probability distribution expressing the probability of a given number of events occurring in a fixed interval of time if the events occur with a known average rate and independently of the time since the last event (Haight, 1967). The appropriate method for this analysis is a Poisson regression to estimate the natural logarithm of the means of our response variable while accounting for random effects of the year and ENSO phase. A GLMM is used since we are outside the realm of normally distributed error terms, which is necessary for linear regression using ordinary least squares. It also prevents the violation of constant error variance.

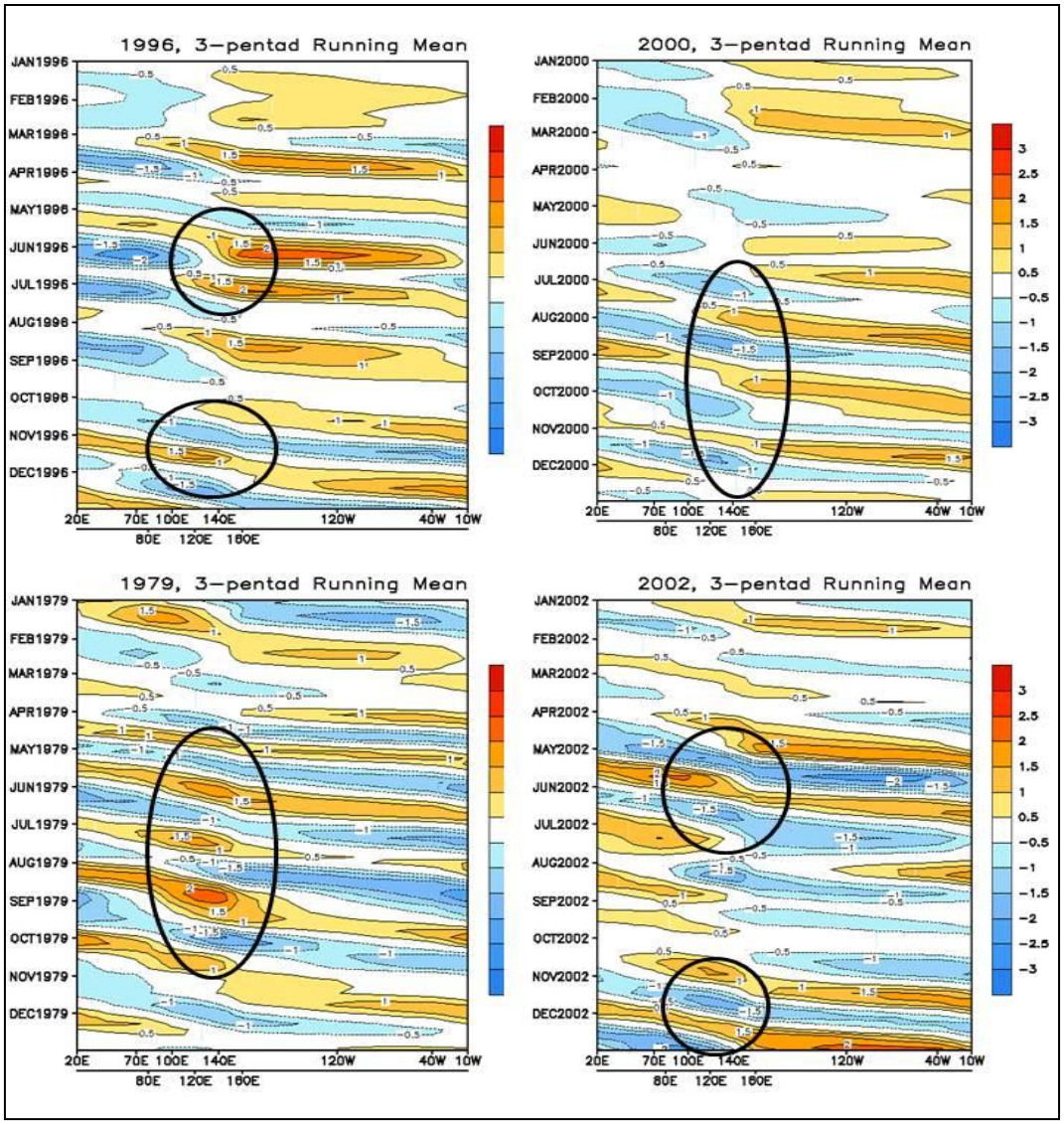

Figure 3.3. Selected MJO events (encircled in black) from 3-Pentad Running Mean MJO index plots (NOAA-CPC).

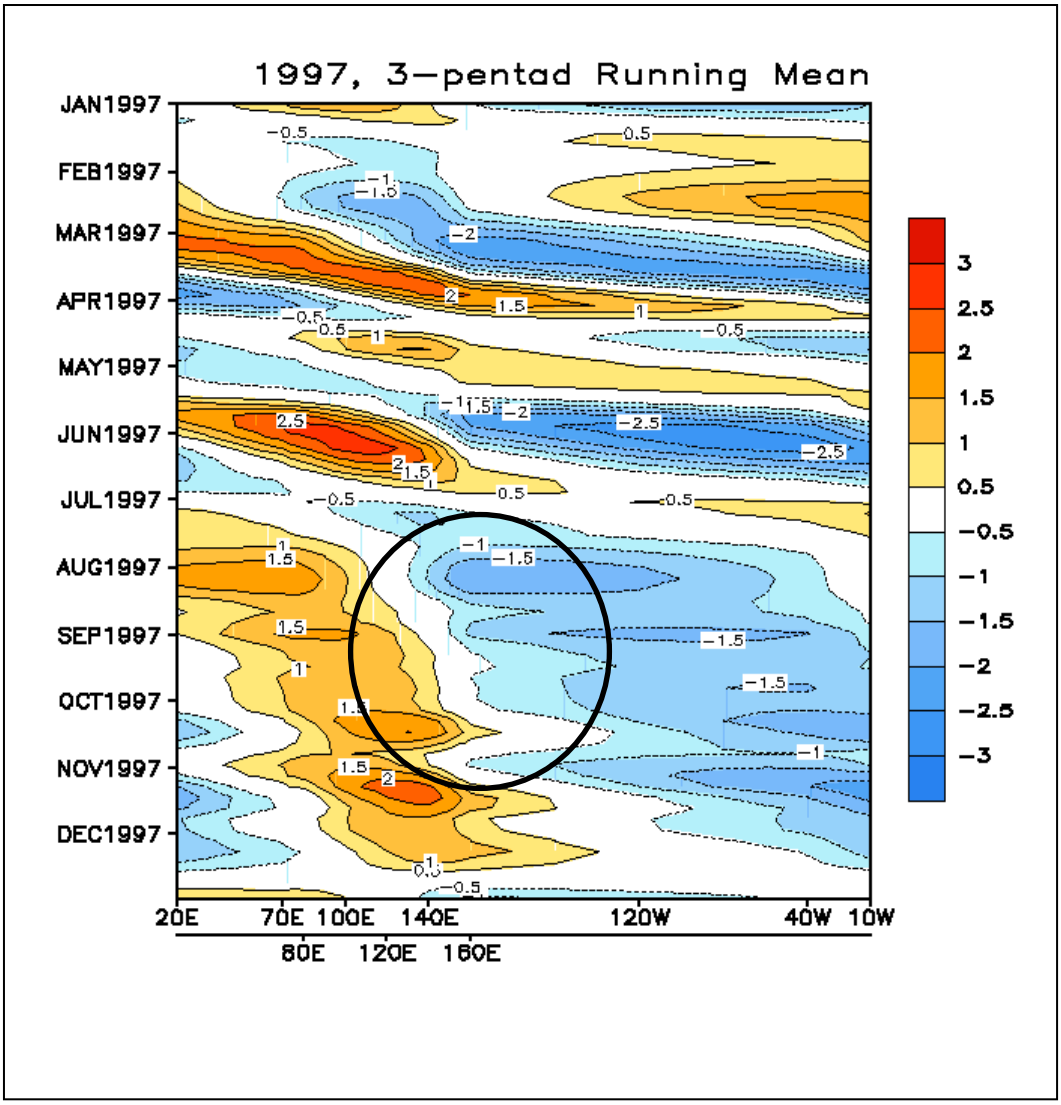

Figure 3.4. The presence of ENSO (black circle) is also distinguishable on the 3-Pentad Running Mean MJO Index Plots (NOAA-CPC).

CHAPTER 4

RESULTS AND DISCUSSION

4.1 Synoptic Circulation Features

4.1 a) *General upper-level geopotential height analysis*

The atmospheric circulation features that govern some of the strongest storms on Earth are not extensively studied like their counterparts in the Atlantic basin. Upper-air maps that depict conditions in the upper troposphere and lower stratosphere (altitudes of 9 to 14 km) are useful for viewing the upper-tropospheric flow pattern, locating the position of troughs and ridges, and jetstreams or jetstreaks (Lackmann, 2011). Studying these composites is important to better understand the dynamics and atmospheric interactions of circulation patterns over the Western Pacific Ocean. In assessing the risks of Asian typhoon impacts, it is critical to understand the interannual variability of not only the annual frequency of Western Pacific typhoons but also the spatial and temporal characteristics of their tracks (Xie and Yan, 2007).

The 200 hPa mean geopotential height composites for the months of August, September and October were plotted to see how the circulation pattern evolves throughout the WNP tropical season and whether there is consistency with the spatial orientation of geopotential height anomalies. The three consecutive months were chosen because out of the selected typhoons, most Taiwan landfalls occurred in August, most Japan landfalls occurred in September and most Vietnam landfalls occurred in October

and November (equally). The time period 1964-2007 was chosen to span the entire range of landfall dates chosen for this study.

The 200 hPa geopotential height mean composite for the month of August (Figure 4.1) shows higher pressure from 20°N to35°N and 90°E to 130°E with a zonal pattern to the north. For the month of September (Figure 4.2), the extent of higher pressure broadens to about 160°E. In October (Figure 4.3), the area of increased geopotential heights expands and increases across the basin spanning the entire study area. The 3 figures suggest that the area of increased geopotential heights broadens as the tropical season progresses. Warmer air temperatures also yield higher pressure surfaces.

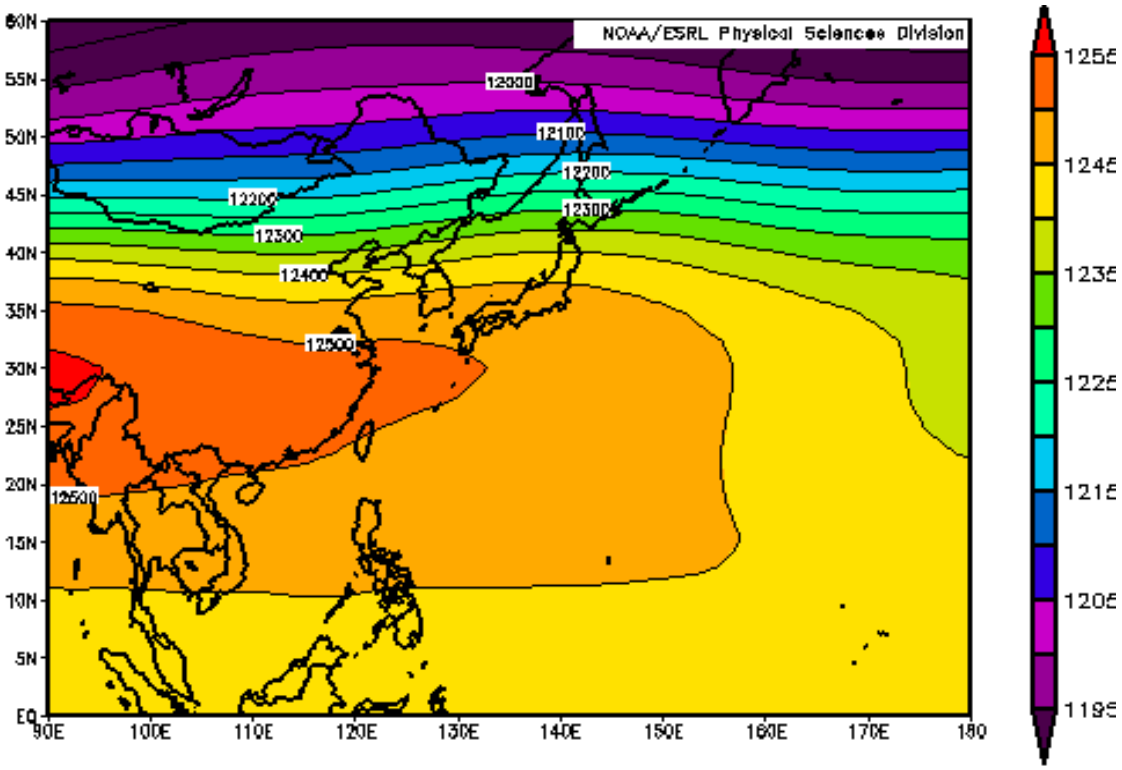

Figure 4.1. NCEP/NCAR Reanalysis 200-hPa geopotential height composite mean for August from 1964-2007.

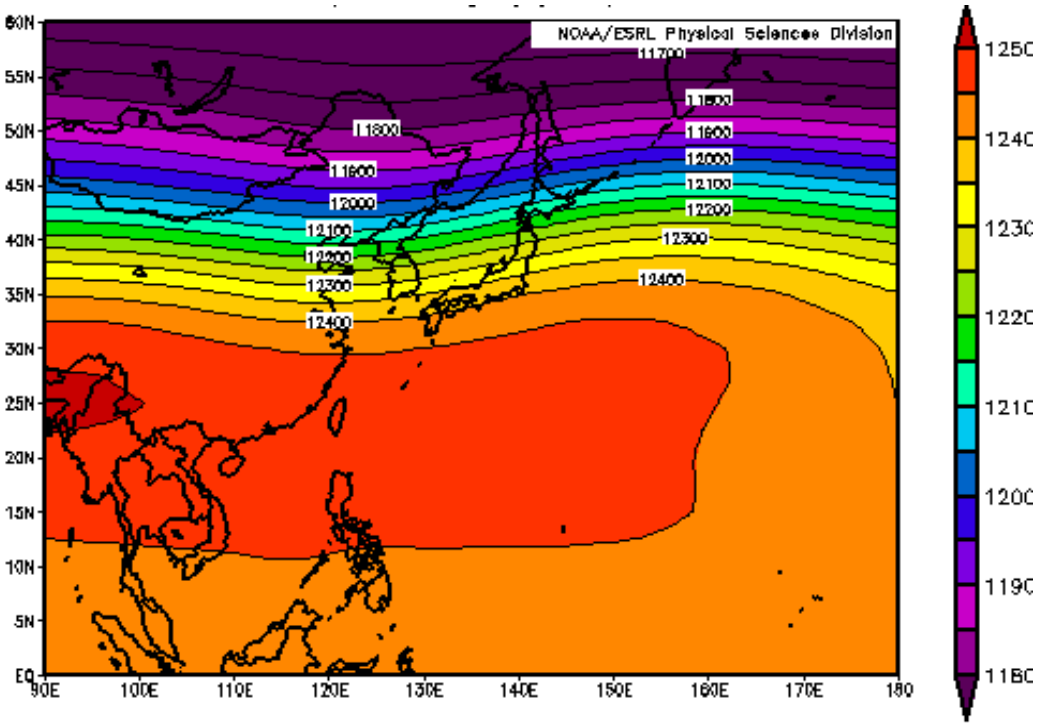

Figure 4.2. NCEP/NCAR Reanalysis 200-hPa geopotential height composite mean for September from 1964-2007

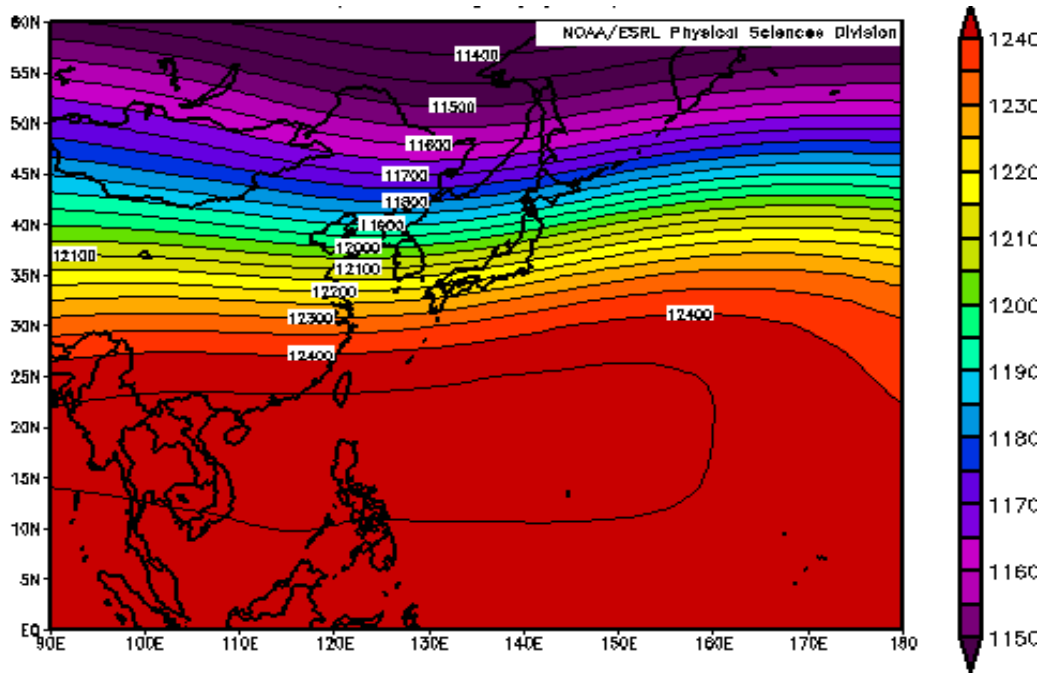

Figure 4.3. NCEP/NCAR Reanalysis 200-hPa geopotential height composite mean for October from 1964-2007

4.1 b) *200-hPa geopotential height anomalies for landfall dates*

Landfall Dates Used in Composites		
Japan	Taiwan	Vietnam
09/24/1964 *	09/22/1971 *	07/06/1971 *
09/24/1966	08/03/1975 *	12/09/1972 *
09/16/1972 *	08/09/1976 *	11/07/1984
09/19/1990	07/31/1977 *	10/15/1985
08/07/1992 *	07/29/1982 *	10/21/1985
09/29/1994	07/10/1994 *	08/16/1987 *
09/16/1997 *	09/01/1994 *	12/08/1993 *
10/17/1998 *	07/31/1996	11/01/1995
09/24/1999 *	08/28/1997 *	11/11/2001
08/08/2003	08/04/1998	10/01/2006 *
08/30/2004 *	08/22/2000	
09/07/2004 *	10/25/2004 *	
10/09/2004	08/31/2005	
09/06/2005	10/02/2005	
08/02/2007	08/18/2007 *	
	10/06/2007 *	
red = JUL-SEP | green = OCT-DEC | * denotes La Nina and * denotes El Nino		

Figure 4.4. Selected landfall dates for Japan, Taiwan and Vietnam for composite analysis. Dates in red (green) indicate landfall from July-September (October-December). Note that Vietnam landfalls typically occur later in the season. Blue (red) asterisks indicate typhoon landfalls during a La Nina (El Nino).

The 200 hPa geopotential height mean composite for Japan landfalls (Fig. 4.5) shows that there are two areas of higher geopotential height means. A ridge is present to the southeast of Japan and another ridge over Southeast Asia, from 20°N to 30°N and 90°E to 110°E. The ridge to the southeast of Japan, when overlaid on top of the typhoon tracks, has a strong influence on steering the storms toward the island. The bands of

relatively zonal decreasing geopotential heights poleward is a result of differential tropospheric heating.

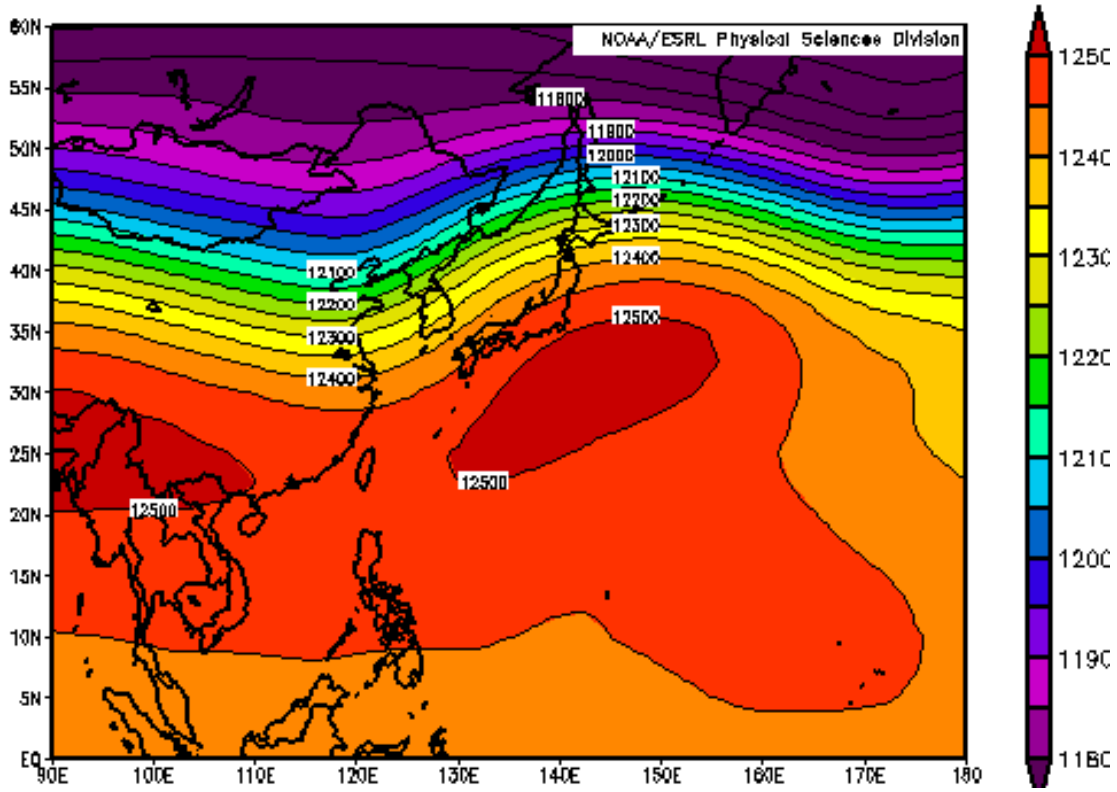

Figure 4.5. 200 hPa mean geopotential height composite for all Japan landfall dates (NCEP/NCAR)

The geopotential height mean composite for Taiwan landfalls (Fig. 4.6) shows a predominantly zonal pattern from about 35°N to 60°N with an area of increased geopotential heights from 20°N to 35°N. The southernmost edge of the eastern 12,500 meter geopotential height contour lies just above the island of Taiwan, signifying a blocking ridge.

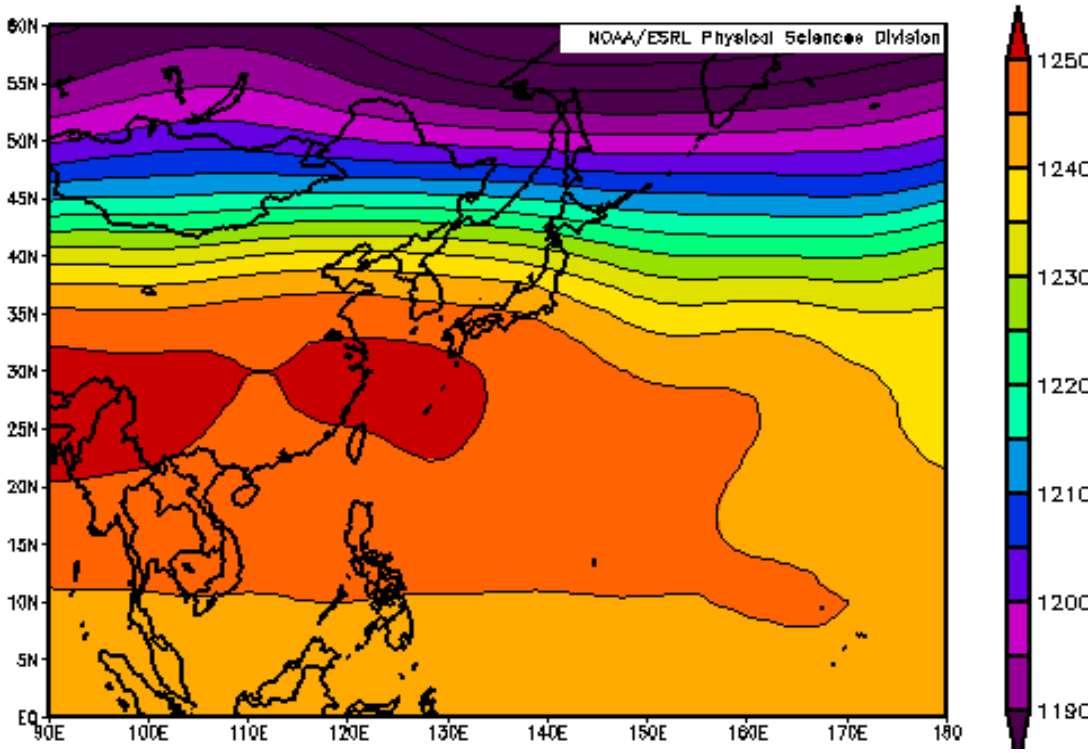

Figure 4.6. 200 hPa mean geopotential height composite for all Taiwan landfall dates (NECP/NCAR)

In comparison to the mean geopotential height pattern in Taiwan landfalls, the zonal pattern in Vietnam landfalls (Fig. 4.7) extends further south to approximately the 30°N line. South of that latitude, there is a broad area of increased geopotential height anomalies. It is evident that the SST are also cooler during Vietnam landfalls than Japan and Taiwan, as they do typically occur later in the season, by comparing the heights of the 35° latitude.

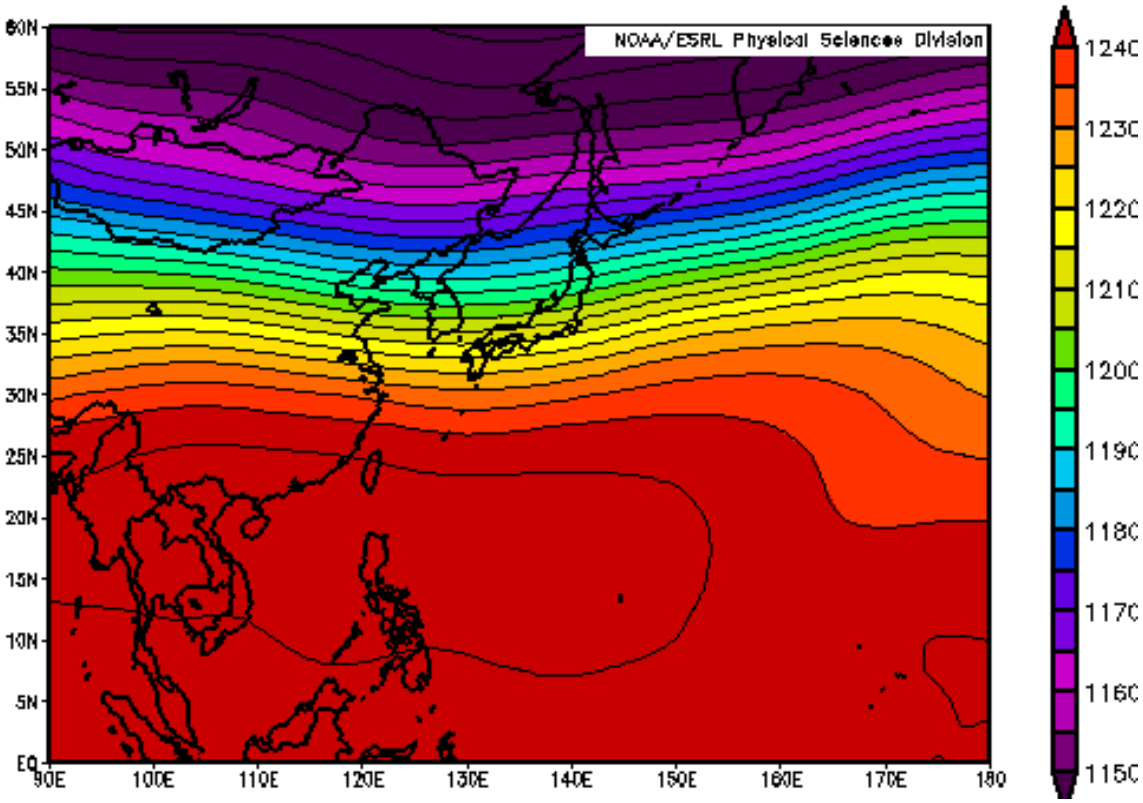

Figure 4.7. 200 hPa mean geopotential height composite for all Vietnam landfall dates (NECP/NCAR)

The 200 hPa geopotential height anomalies for July-Dec 1964-2007 were plotted to analyze the anomaly patterns for the entire time frame containing all the typhoons chosen for this thesis, in all three landfall areas (Fig. 4.8). The most prominent feature is an anomalous trough centered right over the Bohai Sea. Note that these are still negative anomalies, but because the magnitude of the anomalies is so small (only a range of about 10 meters), the color scale had to be adjusted accordingly to make it more apparent. When comparing this figure for the entire tropical season with those of the Japan, Taiwan and Vietnam landfalls (Figs 4.9 – 4.11) only Fig. 4.9 (Japan landfalls) has negative height anomalies over the same region. The general pattern for July through December shows

only a slight negative departure from normal, possibly meaning that the circulation pattern seen on Japan landfall dates appears more frequently during July-December than the circulation patterns seen on Taiwan and Vietnam landfall dates with an upper-level ridge over China. Further investigation is needed to determine if this also indicates that there were more total Japan landfalls than Taiwan/Vietnam landfalls for the same time period.

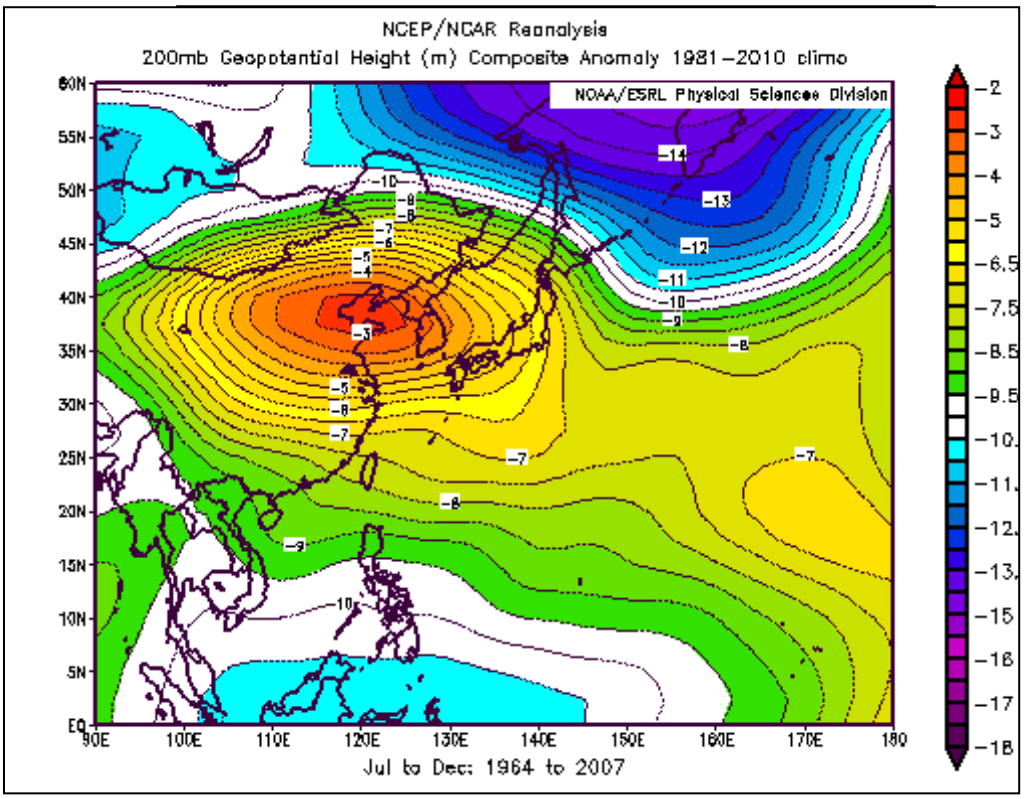

Figure 4.8. 200-hPa Geopotential Height (m) Composite Anomalies (using climatology 1981-2010) for July through December, 1964-2007 (from NCEP/NCAR Reanalysis)

The positive and negative geopotential height anomaly centers indicated in figures 4.9-4.11 are different from the strengths and positions of actual upper-level cyclones and anticyclones. The anomaly troughs and ridges are usually spatially offset from the "actual" highs and lows and indicate whether -- at the time incorporated into the composite -- the geopotential heights were higher or lower than their mean or "normal" values. Because this value is a departure, a positive (negative) geopotential height anomaly doesn't necessarily signify that there is a ridge (trough) in that location, but only that the pressure is higher (lower) than normal. For this reason, a weak upper-level trough (ridge) on a composite map can be denoted by positive (negative) geopotential height anomaly values.

The geopotential height anomaly composite map of Japan landfalls (Figure 4.9) shows a prominent area of positive anomalies, which likely represented the center of strong upper-level anticyclone at the 200 hPa level, indicative of the landfall dates seen in Figure 4.4. The center of the anomalous upper-level ridge lies over the northeastern part of Japan, near the island of Hokkaido, around 43°N and 143°E. The ridge is sandwiched between two anomalous upper-level lows, and the ensemble resembles a typical atmospheric long-wave pattern. The low to the east of the anticyclone, positioned over the North Pacific Ocean is much more intense than the low to the west, positioned over Northeast China. The anticyclone extends from about 20°N to 55°N and 125°E to 170°E.

The typhoon tracks for Japan curve around the southwestern periphery of the ridge and follow a path right through the anomalous anticyclone's center, northward along the length of Japan, which is right around the edge of the actual anticyclone shown in the mean composite image (Fig 4.5). They all recurve before they reach China and

none take a direct northwesterly path from their location of origin, indicating the consistent presence of the ridge and its dominant role in steering the storms. Further in this chapter, a daily evolution/progression of the anticyclone is examined with respect to typhoon position and intensity to help assess the contribution of the typhoon itself to the existing upper-level anticyclone.

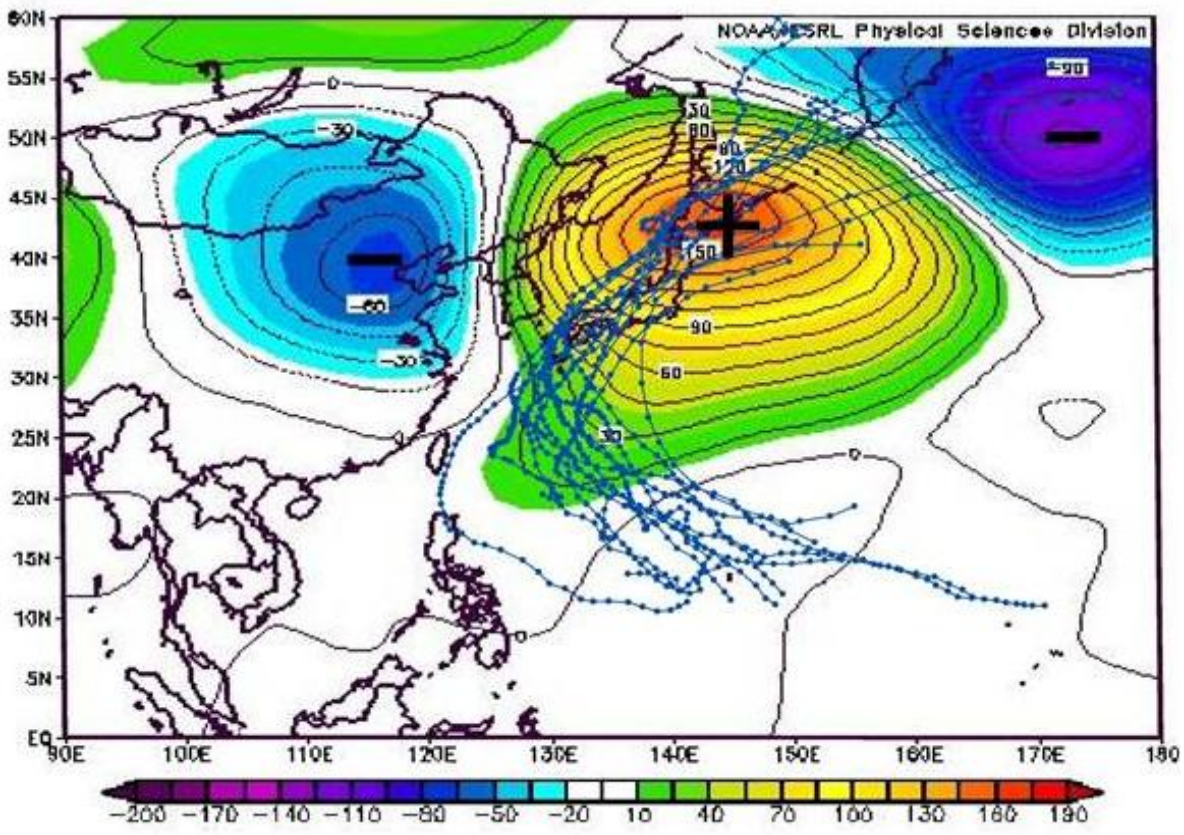

Figure 4.9. 200-hPa geopotential height anomaly composites for selected Japan landfall dates superimposed with official storm tracks. Composites from NCEP/NCAR reanalysis data and tracks are from JTWC best track data. The centers of positive (negative) anomalies are denoted with a black + (-).

The geopotential height anomaly composite map of Taiwan landfalls (Figure 4.10) shows only two dominant circulation features at the 200 hPa level. The anomalous upper-level anticyclone is not as strong as the one during the Japan landfalls and it is

shifted further west than in the Japan landfalls composite (Fig. 4.9), centered almost directly over Beijing, China. A weak to moderate anomalous cyclone borders the anomalous anticyclone to the east of Japan, which extends almost to the edge of the study area (180°) and it is bordered to the east (off the map) by another anomalous anticyclone. The anticyclone over China extends from approximately 90°E to140°E and 20°N to 60°N. To the southwest of the ridge is a small area of lower pressure lying over Burma, Thailand and Vietnam, as well as southernmost China. The anticyclone is not perfectly symmetrical, but unlike the Japan ridge in Figure 4.9, which is positively tilted, the ridge in Figure 4.10 is negatively tilted.

The tracks of the typhoons that made landfall in Taiwan tend to "ride" around the southern edge of the anticyclone, which consequently borders the northern tip of Taiwan. After landfall, many of the storms made a second landfall in southeast China and continued on a westward/northwestward path, but some recurved to the north/northeast. Also, most of the typhoons that hit Japan formed east of the 140° parallel, while only about half of the typhoons that hit Taiwan did so. This more westerly formation location is indicative perhaps of a La Niña pattern, while the more easterly forming storms are more characteristic of an El Niño pattern.

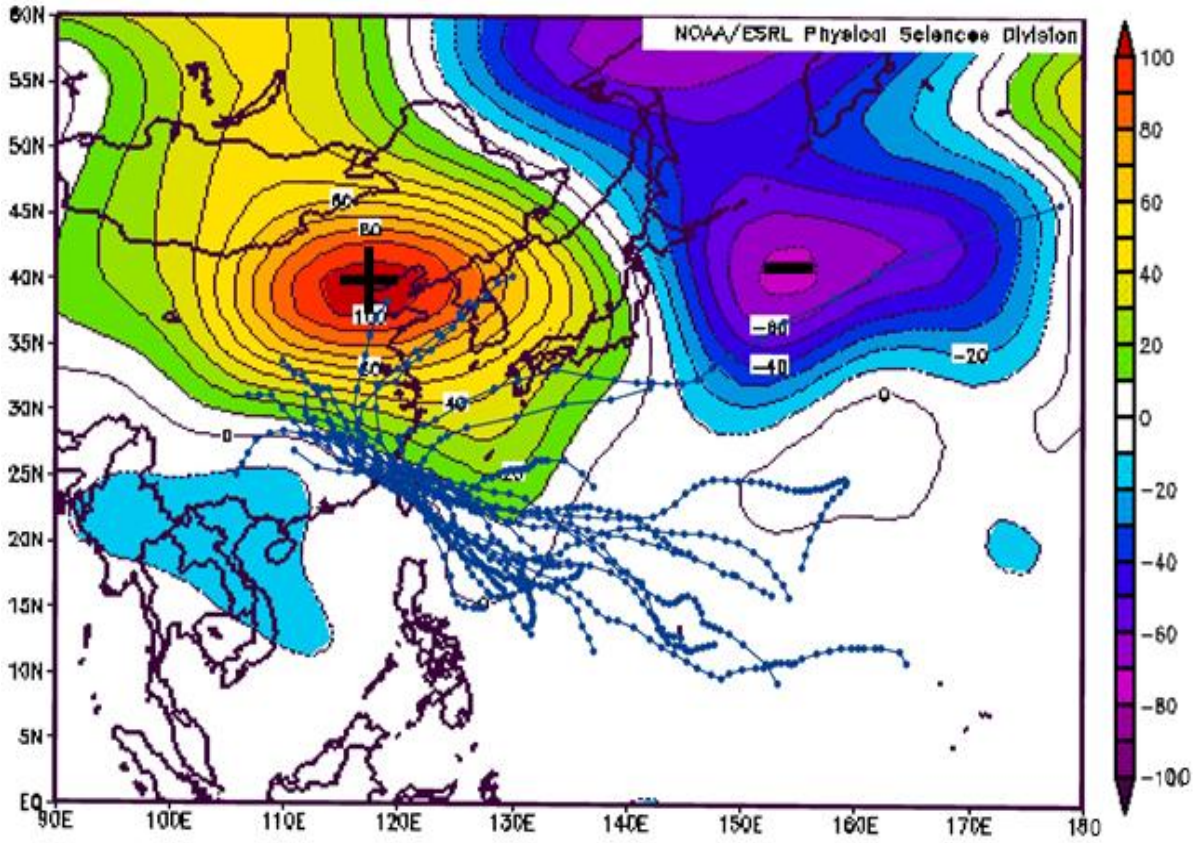

Figure 4.10. 200-hPa geopotential height anomaly composites for selected Taiwan landfall dates superimposed with official storm tracks. Composites from NCEP/NCAR reanalysis data and tracks are from JTWC best track data. The centers of positive (negative) anomalies are denoted with a black + (-).

The geopotential height anomaly composite map of Vietnam landfalls (Figure 4.11) shows an anomalous anticyclone that is both weaker and further west than the ones in both Figure 4.9 (Japan) and Figure 4.10 (Taiwan). It is also not the strongest feature on the map. A more intense anomalous anticyclone resides on the eastern edge of the study area, centered at about 180°. Underneath that anticyclone is a weak anomalous upper-level low that extends from 5°N to 30°N and westward to about 50°E. In addition, a small area of low pressure is over southeastern Japan. The westernmost anticyclone, or the one of interest in this case, is more symmetrical than the ones in the Japan and Taiwan landfall maps. It is positioned over central China and extends from about 20°N to 45°N

and from beyond the western edge of the map to about 130°E. There is also low pressure to its north over Mongolia and Russia.

The Vietnam typhoon tracks, once again, seem to "ride" the southern periphery of the anomalous anticyclone. In contrast to the Japan and Taiwan landfall scenarios (Figures 4.9 and 4.10), the tracks are more uni-directional taking a general west to west-northwest path across the Philippines into Vietnam and Thailand. All the tracks stay south of the ridge and none of them intercept or recurve through it like the Japan and Taiwan tracks. The tracks are also less erratic and much smoother overall than the Japan and Taiwan tracks. Only three of the storms form east of the 140° parallel, which is only about 1/3 of the total sampled. Again, this confirms what one would expect to during a La Niña with storms forming further west and tracking further south. By looking at the example of the typhoon that formed at around 155°E (easternmost track), it follows the curvature of the upper-level low, which possibly aided its development, and then follows the curvature of the high once it reaches about 130°E.

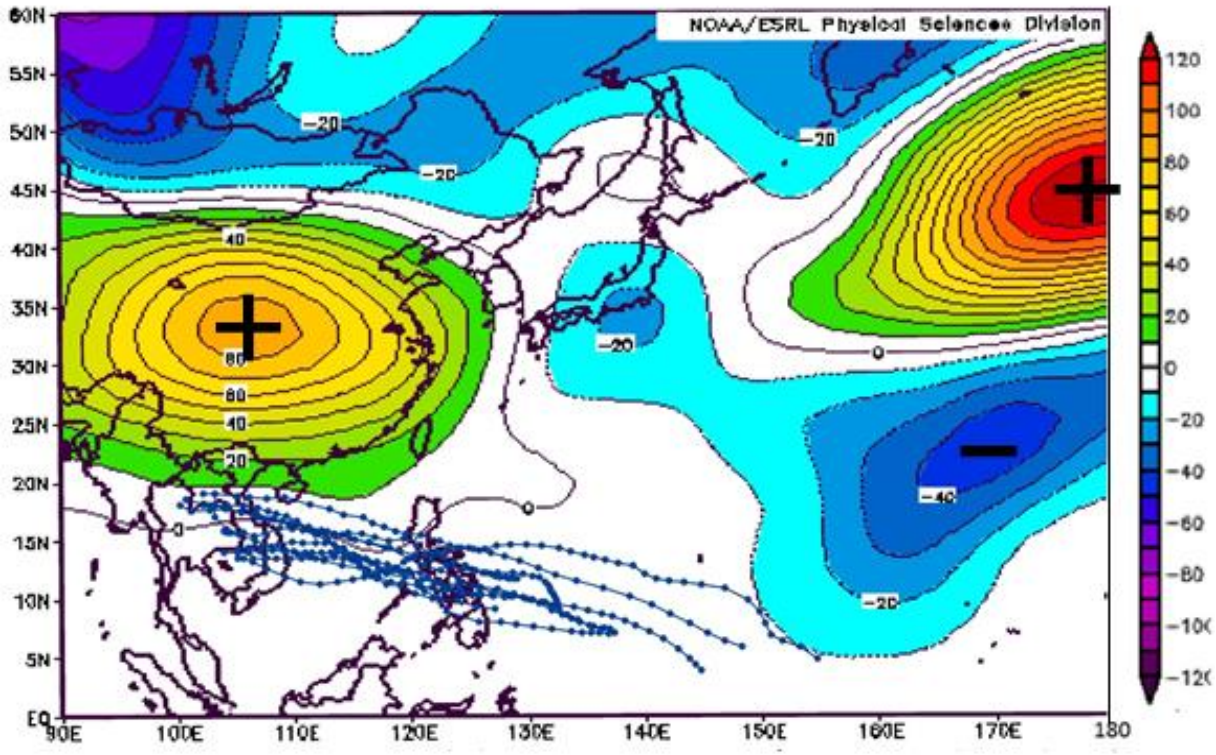

Figure 4.11. 200-hPa geopotential height anomaly composites for selected Vietnam landfall dates superimposed with official storm tracks. Composites from NCEP/NCAR reanalysis data and tracks are from JTWC best track data. The centers of positive (negative) anomalies are denoted with a black + (-).

4.1 c) *Vector Wind Analysis*

Analyzing vector wind composites can be very useful in determining steering controls for tropical cyclones and assisting in forecasting. For example, the position of a jet streak on an upper-level trough can help predict whether the trough will strengthen or weaken. Knowing the magnitude and direction of the wind helps identify cyclones and anticyclones and reveals regions of strong wind shear, which hinders TC development. All three mean vector wind composites for Japan landfall dates show anticyclonic flow around Japan (Fig 4.12). Figure 4.12a shows that the strongest upper level winds are concentrated in an area from 130°E to 170°E and about 40°N to 50°N, which is probably a jet streak, and the center of anticyclonic circulation is located around 145°E and 32°N,

just east of the southern part of Japan. The 500 hPa level (Fig 4.12b) also shows an anticyclonic pattern, with the center and area of highest winds offset slightly to the east. Figure 4.12c shows the mean vector winds across the entire layer from 850 to 200 hPa, which is important to look at because the vertical extent of a typhoon lies somewhere in this range, depending on the strength and structure of the individual storm. Anticyclonic winds to the south of Japan are centered around 30°N, along with a stream of southerly winds just to the east of Taiwan in between Japan and China. This area of southerly winds on the western edge of the anticyclone the most likely the culprit in recurving the typhoons toward Japan from their original northwestward path. The lower wind speeds allow the storms to keep their form and not get sheared apart.

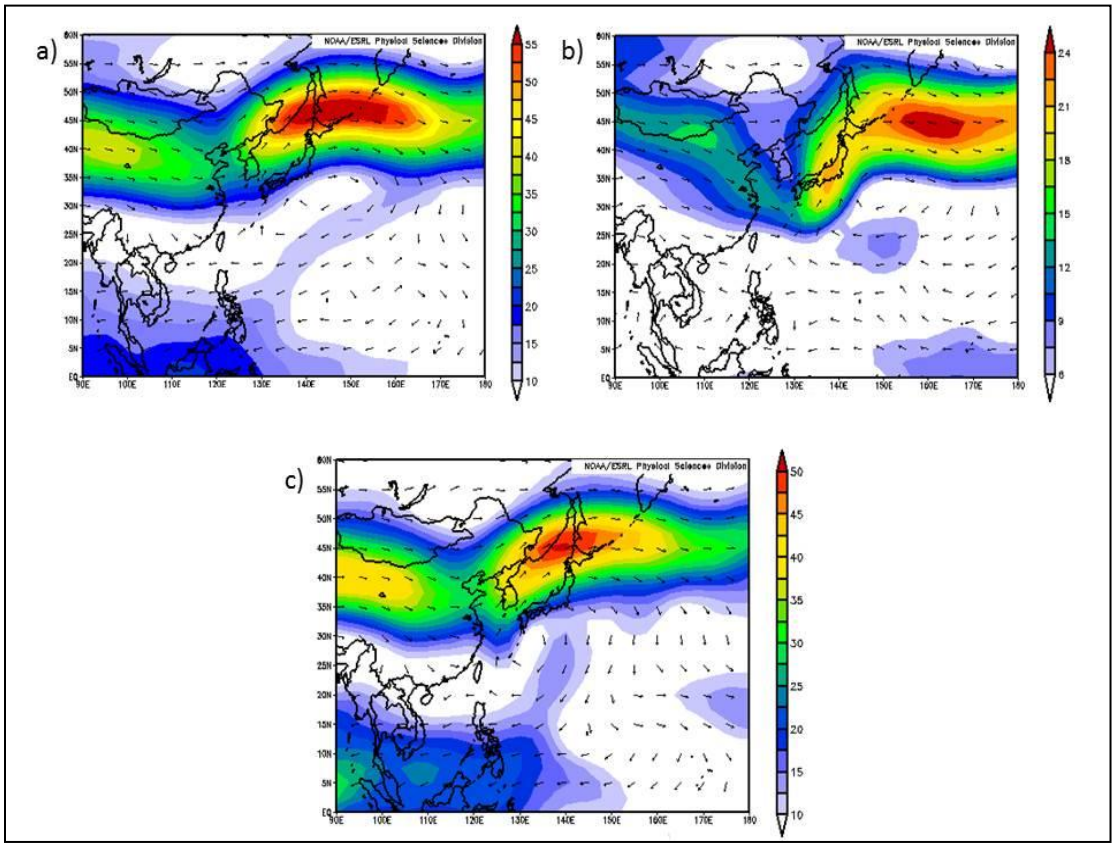

Figure 4.12 - Mean Vector Wind Composites (m/s) for Japan Landfalls (from NCEP/NCAR reanalysis) a) 200 hPa b) 500 hPa c) 850-200 hPa

Figure 4.13 shows vector wind anomalies for Japan landfalls at the 200-hPa, 500-hPa, and 850-200-hPa levels. The 200 hPa composite (Fig. 4.13a) shows a similar pattern to the 200 hPa mean vector winds (Fig 4.12a), with the exception of a more closed-off anticyclone due to the zonal mean wind being omitted from the composite, and the position of the entire anticyclone being further north, with the center at around 40°N, just off the coast of northern Japan. There is also upper-level anomalous cyclonic flow over China. When looking at the anomalies for the 500-hPa level (Fig 4.13b), there are two dominant features near Japan. There is a cyclonic wind anomaly centered just to the west of Japan and extending over eastern China, with the highest winds centered directly over the islands of Japan. Just to the east of that feature there is anomalous anticyclonic flow centered at about 38°N and 147°E. The southerly winds on the western edge of this anomaly wind anticyclone feed into the eastern edge of the cyclone creating an area of convergence as winds advect in from the east and the west. Figure 4.13c shows the vector wind anomalies for the 850-200 hPa layer. There is a definite area of anomalous anticyclonic flow around Japan with a crescent-shaped area of highest wind anomalies to the west of Japan. The wind direction is southerly at about 25°N, shifts to southwesterly at about 45°N and then westerly at 50°N. Again, this is useful to explain the direction of storm tracks as they approach Japan from the southeast. When comparing to Fig 4.12c (the 850-200 hPa mean vector winds), the center of anticyclonic flow is offset about 10 degrees to the northeast in Figure 4.13c, which is because anomaly centers often differ from actual conditions. However, the area of highest wind speeds only shifted slightly to the southwest in Figure 4.13c. Wind shear anomalies were also plotted, but the resulting

figures were identical to vector wind anomalies, perhaps due to a glitch in the program, so they were not included in the results.

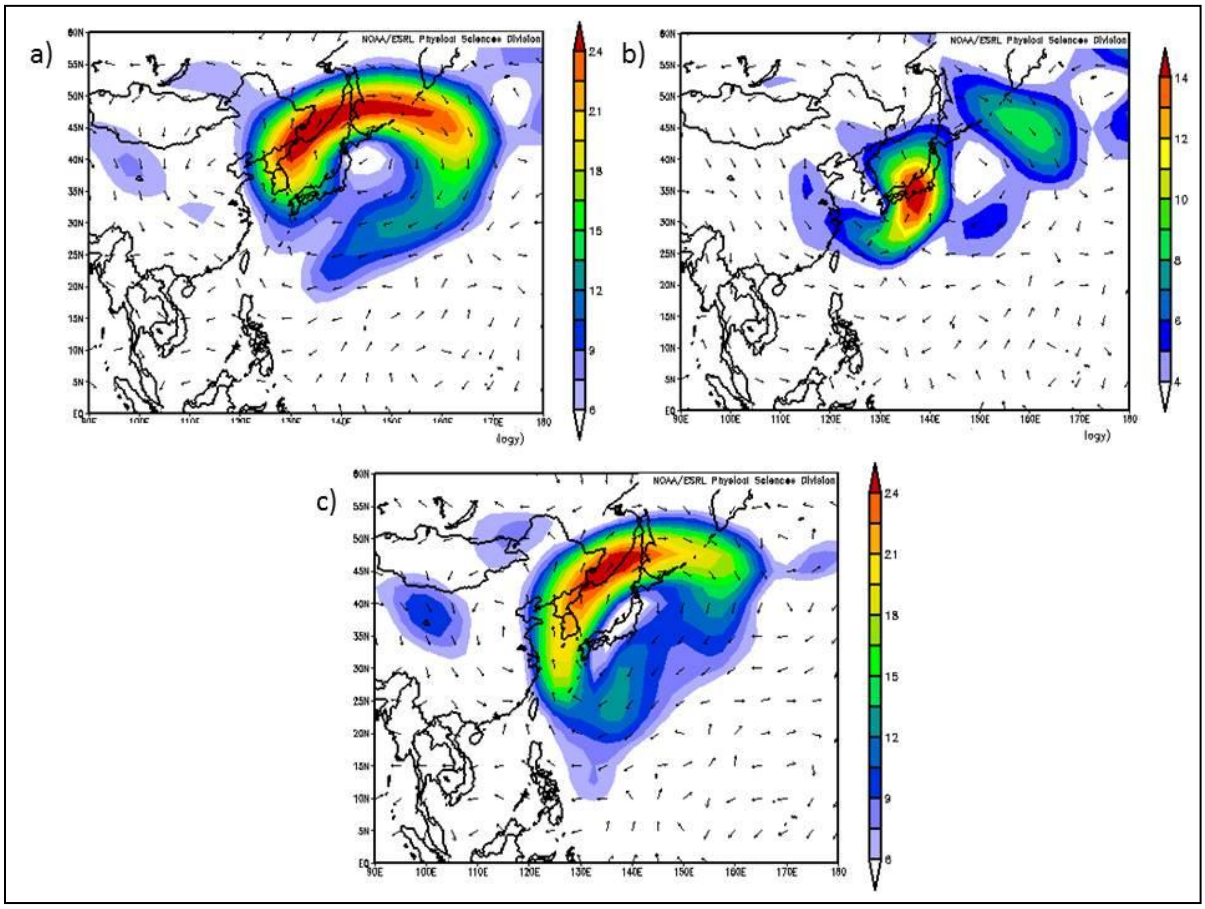

Figure 4.13 - Anomaly Vector Wind Composites (m/s) for Japan Landfalls (from NCEP/NCAR reanalysis) a) 200 hPa b) 500 hPa c) 850-200 hPa

The 200 hPa mean vector wind composite for Taiwan landfalls (Fig 4.14a) shows zonal westerly wind flow to the north of 30°N with the highest winds extending from about 40°N-45°N and 115°E-135°E. There are east and southeast winds around Taiwan with an area of northeast winds further eastward. Figure 4.14b shows a similar zonal wind pattern to the north of the 30°N latitude with an area of highest winds positioned over the Sea of Japan. An area of cyclonic flow lies centered around Taiwan with highest

winds just to the northeast of the island. There is an area of converging winds from the east and west at just to the northeast of the Philippines over the Ryukyu Islands of Japan, creating southerly flow into the east side of the cyclone surrounding Taiwan. The entire 850 – 200 hPa layer for Taiwan landfall dates (Fig. 4.14c) shows anticyclonic flow around Taiwan and zonal winds above 35°N. There is also an area of higher northeasterly winds to the south of Taiwan over the Philippines, Vietnam, Thailand and Malaysia, implying a large area of shear. When comparing to the Taiwan tracks in Figure 10, it is evident that most of the Taiwan-bound typhoons traverse the edge of this shear region, where wind shear is not much of a factor. A storm headed in the direction of Vietnam would probably not last in these conditions.

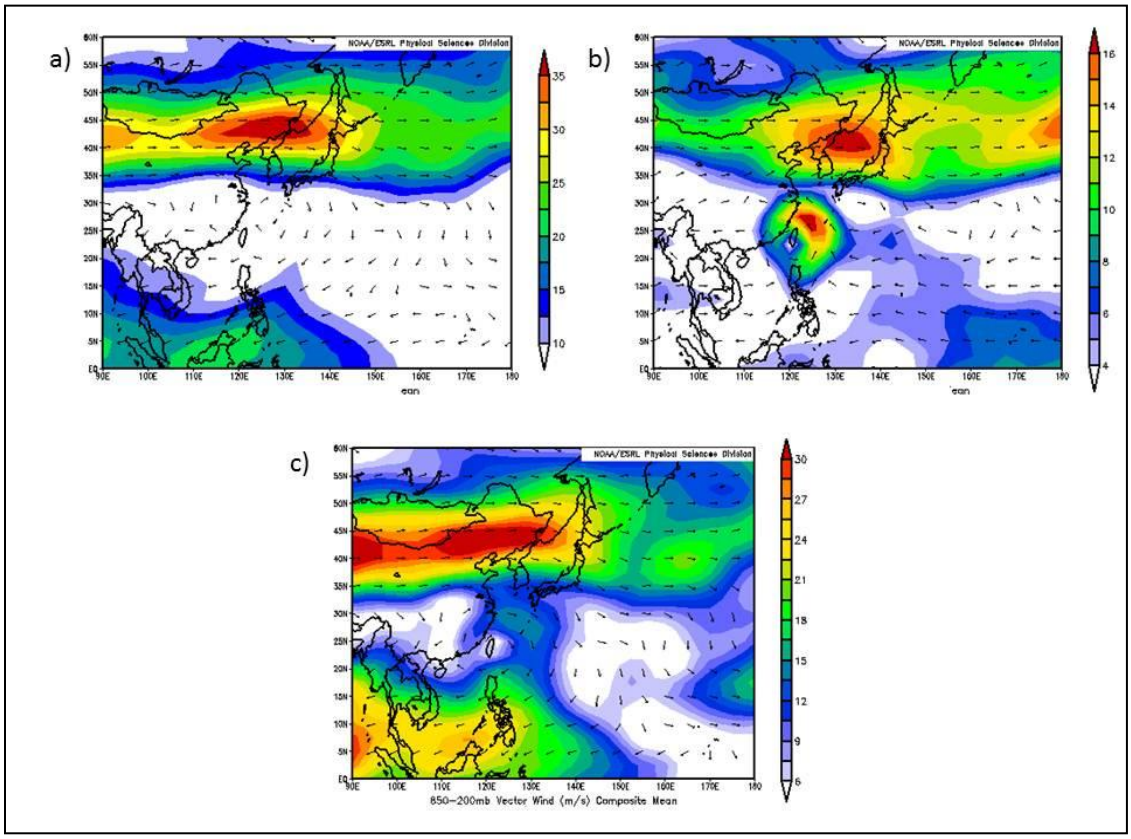

Figure 4.14 - Mean Vector Wind Composites (m/s) for Taiwan Landfalls (from NCEP/NCAR reanalysis) a) 200 hPa b) 500 hPa c) 850-200 hPa

Vector wind anomalies for Taiwan landfalls at 200 hPa (Fig. 4.15a) show anticyclonic flow across China and Japan with a stream of northerly winds extending from the southeastern edge of the anticyclone across the southern Philippines terminating around the equator. The center of this large area of anomalous anticyclonic flow is centered over the Bohai Sea. The areas with the highest winds are along the southwest and northeast edges of the anticyclone, over east-central China and Vladivostok. Taiwan is located at the base of the anticyclone, being influenced by the upper-level southeasterly winds. Figure 4.15b, vector wind anomalies at 500 hPa, shows anomalous cyclonic flow around Taiwan with maximum winds directly to the north/northeast of the island. This is expected, as the 500 hPa level shows a good depiction of the atmospheric signatures from the storms themselves. Vector wind anomalies across the 850 – 200 hPa layer (Fig. 4.15c) show anomalous anticyclonic flow around Taiwan with highest winds just to the west of the island over southeast China. There is another area of anticyclonic winds over northeast China centered at about 39°N and 120°E, which yields in northerly winds over Japan.

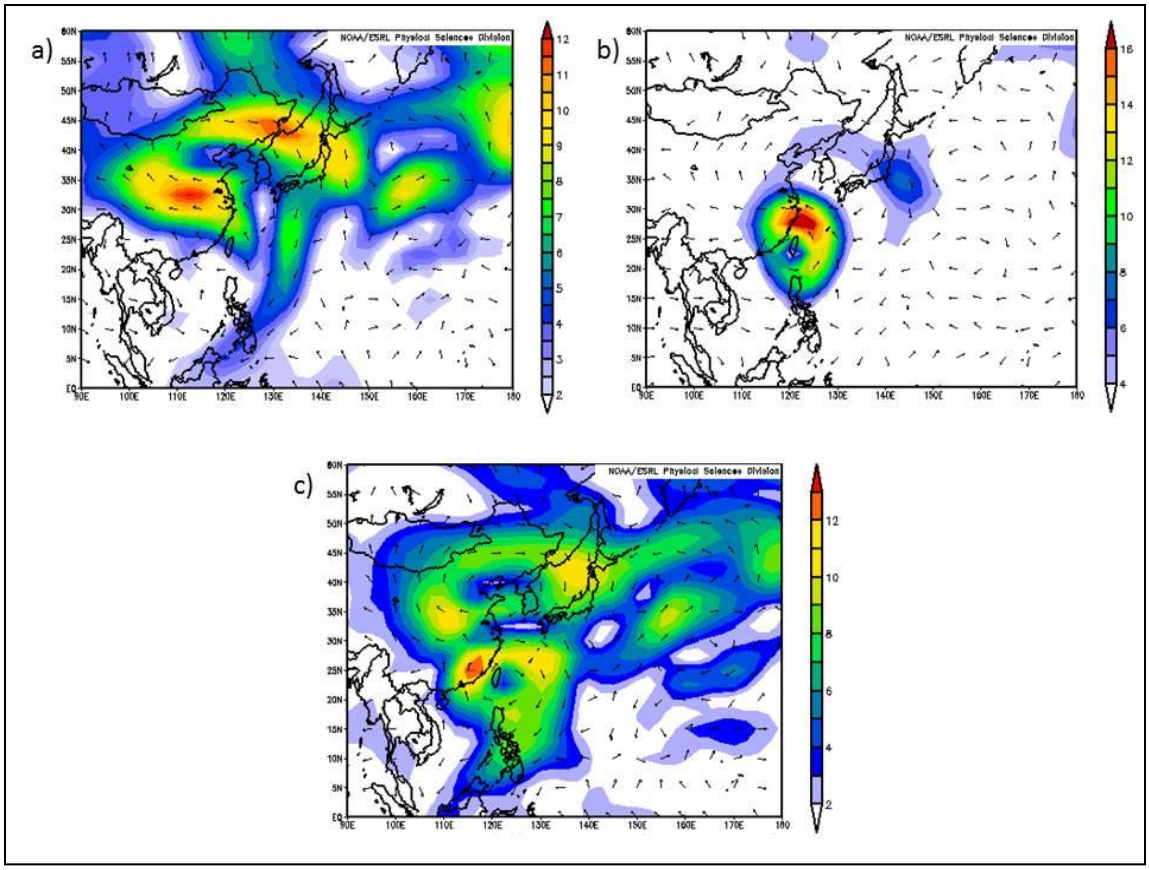

Figure 4.15 - Anomaly Vector Wind Composites (m/s) for Taiwan Landfalls (from NCEP/NCAR reanalysis) a) 200 hPa b) 500 hPa c) 850-200 hPa

The 200-hPa mean vector wind composite for Vietnam landfalls (Fig. 4.16a) shows strong zonal flow north of 25°N with two areas of maximum winds (jet streaks). One is located over north-central China approximately between 34°N-40°N and 100°E-120°E, while the other is east of Japan at approximately 35°N-45°N and 150°E-165°E. There is also a region of anticyclonic flow to the east of the Philippines over the Philippine Sea and easterly flow between the Philippines and Vietnam over the South China Sea. The wind speeds in this area are low, creating a sheltered path for typhoons to follow and not be affected by shear. The 500-hPa mean vector winds (Fig. 4.16b) also show zonal westerly winds north of about 25°N with the area of highest wind speeds

contained between about 37°N to 47°N and 155°E-175°E. Just to the east of Vietnam, there is a small area of southerly winds that are slightly stronger than the surrounding winds, at about 8 to 12 m/s. These southerly winds make up the eastern edge of a cyclonic circulation that is part of the typhoons. From here eastward to about 170°E is an area of light easterly winds. Figure 4.16c also shows the zonal flow at about 25°N and the two jet streaks shown in Figure 4.16a, with the westernmost jet streak being the stronger of the two. The stronger of the two jet streaks is located over China at approximately 35°N and 105°E and the second jet streak is located to the west of Japan at about 40°N and 155°E. There seems to be an anticyclonic circulation to the east of the Philippines and wind speeds are low across this region.

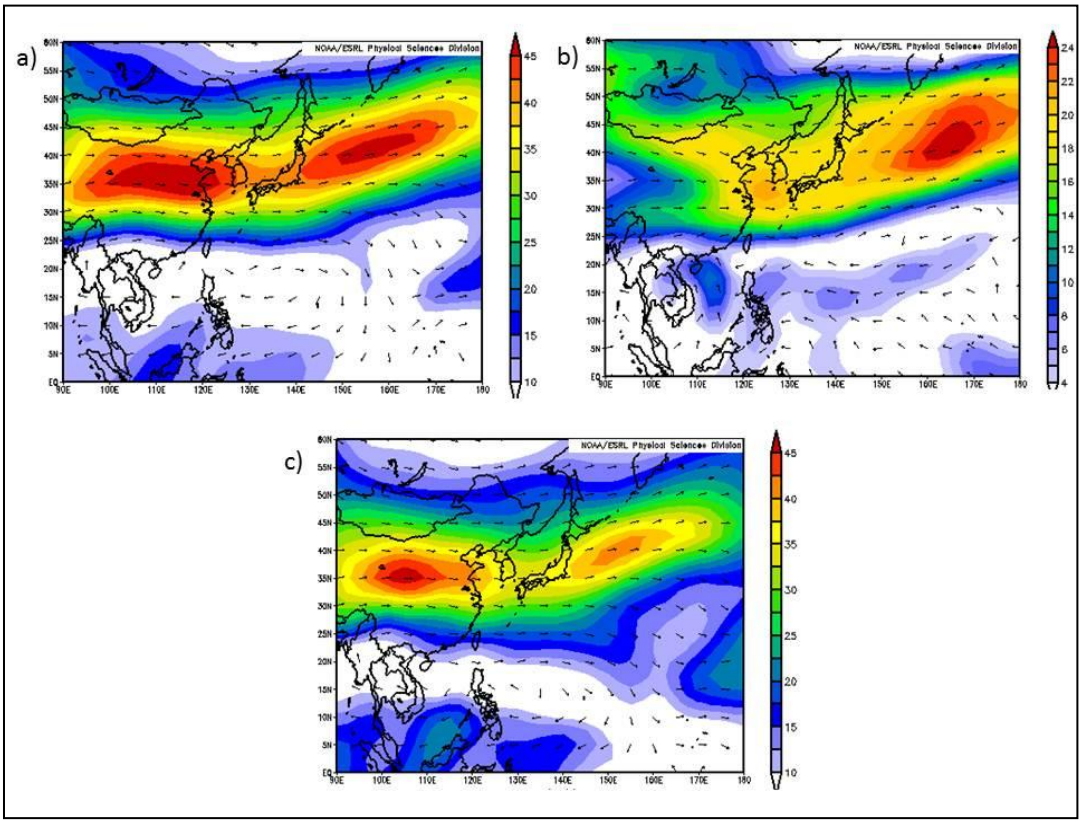

Figure 4.16 - Mean Vector Wind Composites (m/s) for Vietnam Landfalls (from NCEP/NCAR reanalysis) a) 200 hPa b) 500 hPa c) 850-200 hPa

Figure 4.17a shows anticyclonic flow over China centered at around 32°N and 105°E, indicating an anomalous upper-level ridge there. It looks like there is another anomalous anticyclone from about 155°E eastward that seems to be centered at about 180°, but only half of it is enclosed in the study area. To the east of the Philippines, there is another area of anomalous anticyclonic flow and an area of northerly winds sandwiched in between the Philippines and Vietnam. The typhoon structure is visible in Figure 4.17b as an area of strong cyclonic flow over Vietnam. The highest winds are on the northeastern side of the cyclone centered over the island of Hainan. The feature itself almost looks like a typhoon with the center of circulation resembling an eye-like structure. Figure 4.17c shows the blocking anticyclone over China and northeasterly winds (~6-10 m/s) near southeast Vietnam.

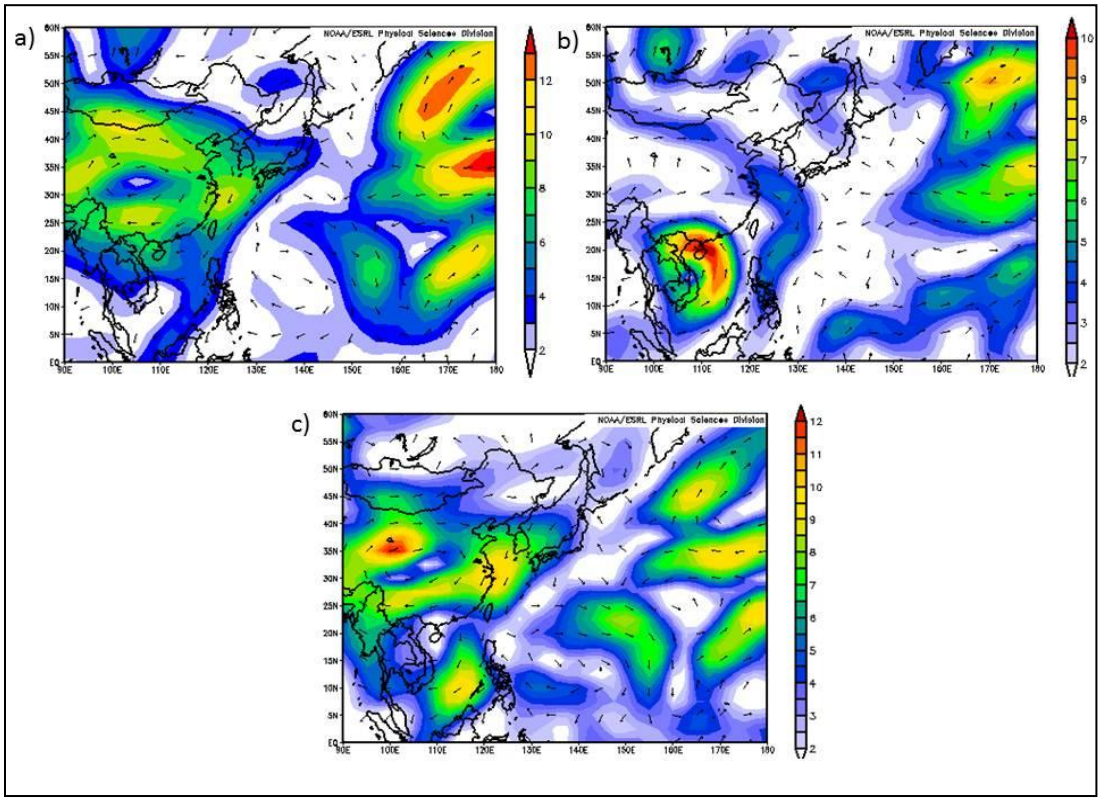

Figure 4.17 - Anomaly Vector Wind Composites (m/s) for Vietnam Landfalls (from NCEP/NCAR reanalysis) a) 200 hPa b) 500 hPa c) 850-200 hPa

4.1 d) *500 hPa level analysis*

The 500-hPa level represents conditions in the middle of the atmosphere and low pressure features (such as typhoons) are easily identifiable at this level. This region is also important to assess vorticity, shortwaves, and for predicting the development of highs and lows based on increasing/decreasing geopotential heights. Figure 4.18a shows anomalous omega values at 500 hPa for Japan landfall dates. Since pressure decreases downward, negative omega values indicate upward motion and positive values indicate downward motion (subsidence). There are negative omega anomalies centered over the typhoon landfall area of Japan, and positive omega anomalies adjacent to the west over eastern China. Figure 4.18b shows precipitable water at 500 hPa, which is the liquid water equivalent resulting after precipitating all the water vapor in a vertical column over a certain location. As expected, the precipitable water anomaly is highest at the landfall location, reaching as high as 18 kg/m² at over southern Japan. There are negative precipitable water anomalies, signifying drier air, extending from Taiwan to the Bohai Sea, encompassing part of the east coast of China. The 500-hPa geopotential height anomalies for Japan landfalls (Fig. 4.18c) show a positive pressure anomaly centered just to the east of Japan, including most of Japan except the southern tip, which is under a negative pressure anomaly that extends from about 25°N to 50°N and about 100°E to 139°E. This area of negative pressure anomalies emanates from the typhoons themselves. The overlap in the area of negative height anomalies with the region of drier air over eastern China (and knowledge of an upper-level cyclone over China during Japan landfalls) suggests the storms also have an effect on the east coast of China, despite land-falling in Japan.

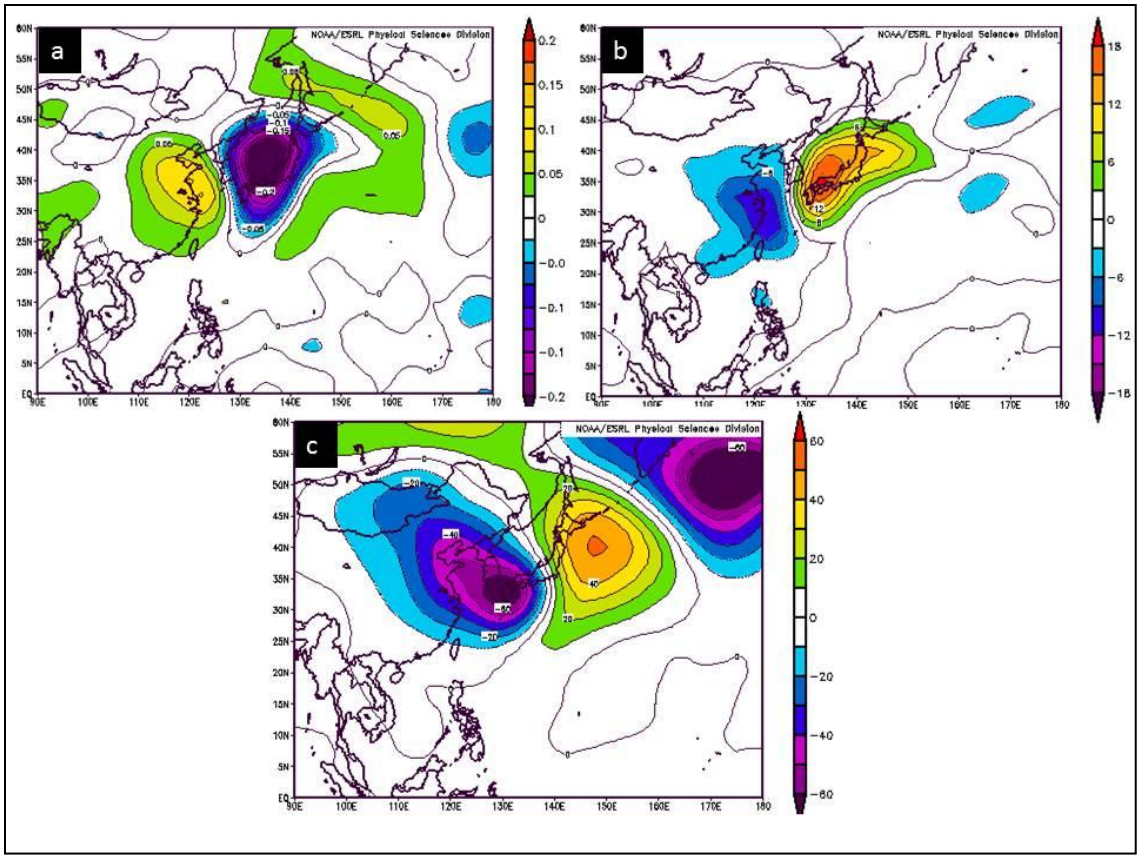

Figure 4.18. a) 500 hPa Omega (Pa/s) Composite Anomaly for Japan Landfalls (NCEP/NCAR Reanalysis) b) 500 hPa Columnar Precipitable Water (kg/m²) Composite Anomaly for Japan Landfalls (NCEP/NCAR Reanalysis) c) 500 hPa Geopotential Height (m) Composite Anomaly for Japan Landfalls (NCEP/NCAR Reanalysis)

Figure 4.19a shows negative anomalous omega values over Taiwan, as expected with the rising air in the typhoons. There are small regions of positive omega anomalies surrounding the landfall area perhaps signifying sinking air that has advected out from the storms' outflows. Negative omega values over northeastern China, located between 30°N to 40°N and 100°E to 125°E, indicate another area of increased moisture. This area also shows up as having a high precipitable water content on Figure 4.19b. The greatest positive precipitable water anomaly is at the landfall location, over Taiwan, and it is adjacent to an area of negative precipitable water anomalies extending laterally from Hainan to Hong Kong and up into the Guangdong province of southern China. There is a

strong negative geopotential height anomaly over Taiwan (Fig. 4.19c) which lies right below an area of positive geopotential height anomalies extending over eastern China and Japan from about 30°N to 46°N and 105°E to 145°E. This conflicts with the findings of Figure 4.19a and Figure 4.19b which suggests there may be an area of low pressure in that region due to an anomalous area of moisture and rising air, but this can simply mean that actual height patterns may elucidate a weaker than normal 500-hPa low there.

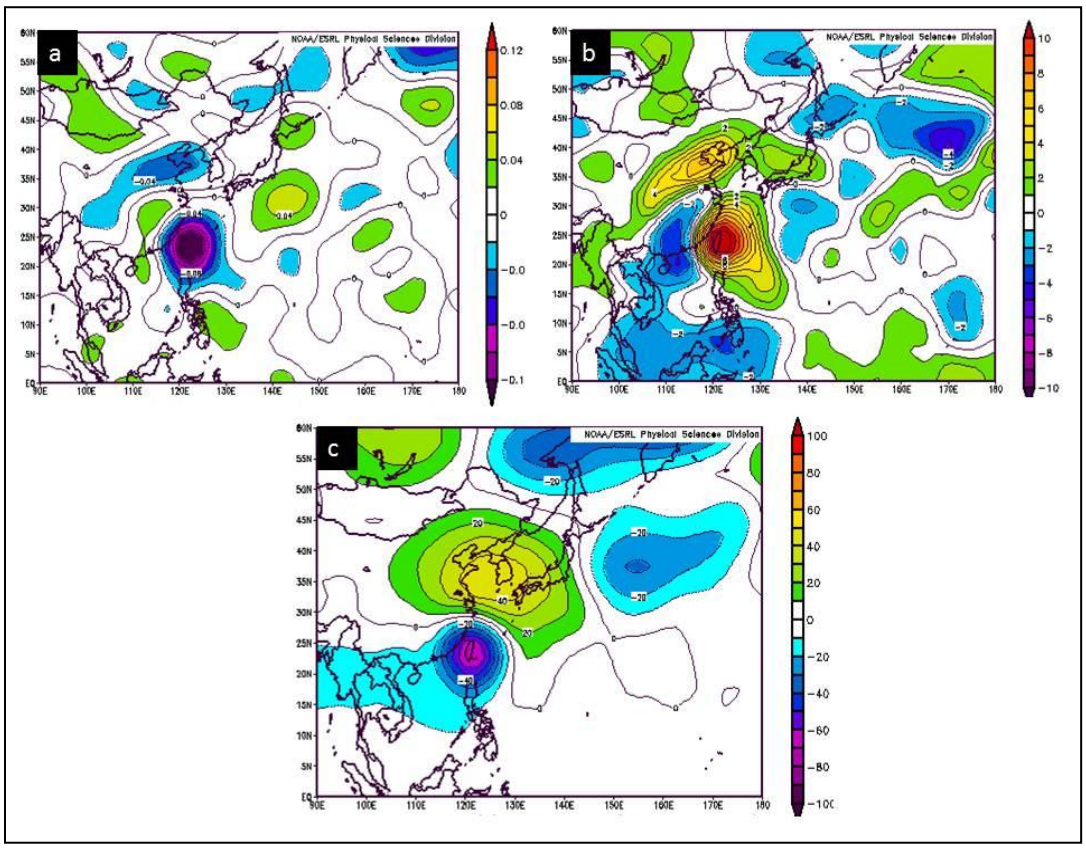

Figure 4.19. a) 500 hPa Omega (Pa/s) Composite Anomaly for Taiwan Landfalls (NCEP/NCAR Reanalysis) b) 500 hPa Columnar Precipitable Water (kg/m^2) Composite Anomaly for Taiwan Landfalls (NCEP/NCAR Reanalysis) c) 500 hPa Geopotential Height (m) Composite Anomaly for Taiwan Landfalls (NCEP/NCAR Reanalysis)

Omega anomalies for Vietnam landfalls (Figure 4.20a) show negative anomalous omega values over the landfall region with positive anomalous omega values directly to the north. There is also an area of rising air over the Philippine Sea and an area of

alternating strong negative and strong positive omega anomalies in the northwest of the study area, north of about 30°N. This same region also has coinciding alternating precipitable water anomaly areas (Figure 4.20b). There is an area of positive anomalous precipitable water just to the east of Vietnam over the landfall areas and one east of the Philippines. There are also negative precipitable water anomalies to the southwest of Vietnam. Figure 4.20c shows negative geopotential height anomalies over the landfall location and an area of slightly positive geopotential height anomalies just to the north over China and Taiwan (from about 25°N to 35°N and 100°E to 125°E). This suggests higher than normal pressure in that region and Figures 4.20a and 4.20b support this idea.

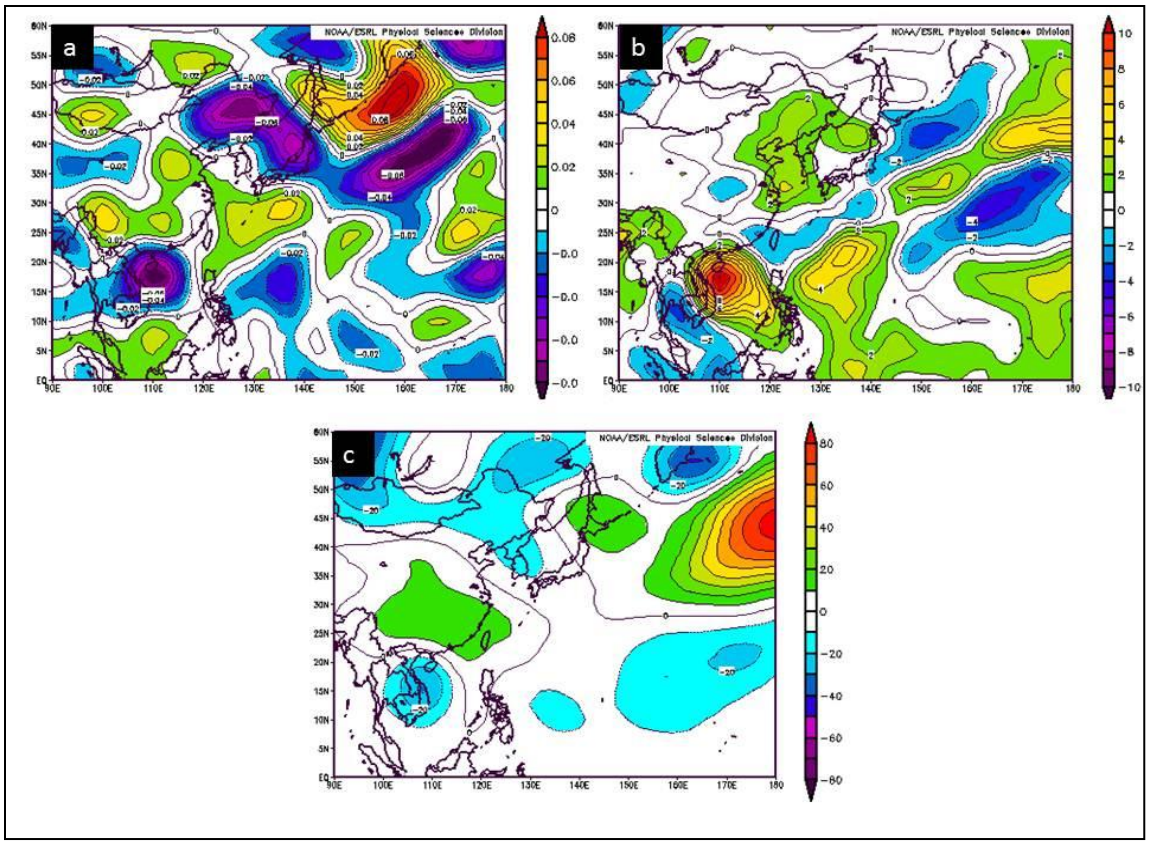

Figure 4.20. a) 500 hPa Omega (Pa/s) Composite Anomaly for Vietnam Landfalls (NCEP/NCAR Reanalysis) b) 500 hPa Columnar Precipitable Water (kg/m^2) Composite Anomaly for Vietnam Landfalls (NCEP/NCAR Reanalysis) c) 500 hPa Geopotential Height (m) Composite Anomaly for Vietnam Landfalls (NCEP/NCAR Reanalysis)

4.1 e) *200 hPa spatiotemporal evolution*

The purpose of these sets of figures is to analyze the chronological and spatial progression of the upper-air circulation patterns from a week before landfall to the day before landfall of a specific storm (Figures 4.21, 4.22 and 4.23). Seven days before the August 2, 2007 typhoon made landfall in Japan, there was a deep upper-level anomalous trough extending northward from about 35°N and approximately 125°E to 175°E (Fig. 4.21a). To the southwest of the trough, is an anomalous ridge centered at about 52°N and 105°E extending down into northwest China. Underneath that ridge is another area of negative height anomalies centered over north-central China. Two days later (Fig. 4.21b.), the anomalous ridge centered over northern Mongolia and Russia, retreats to the north and strengthens in magnitude. The strong anomalous trough to the east weakens, as does the one over central China. At three days before landfall (Fig. 4.21c), the trough breaks up into three negatively anomalous features all part of one triangular region extending from 25°N to 60°N and 120°E to 175°E with the southern (and strongest) part lying over Japan. The ridge undergoes some change in orientation, but remains mostly unchanged, and the anomaly trough over China virtually disappears. The day before landfall (Fig. 4.21d), an area of positive height anomalies moves in toward Japan from the east, and the anomalous trough over Japan weakens and substantially shrinks in size. The anomalous upper-level ridge that was sitting in the northwest corner of the map retreated further north and an area of slightly negative height anomalies popped up over central China. The area of negative geopotential heights anomalies to the southeast of Japan is likely part of the landfalling typhoon.

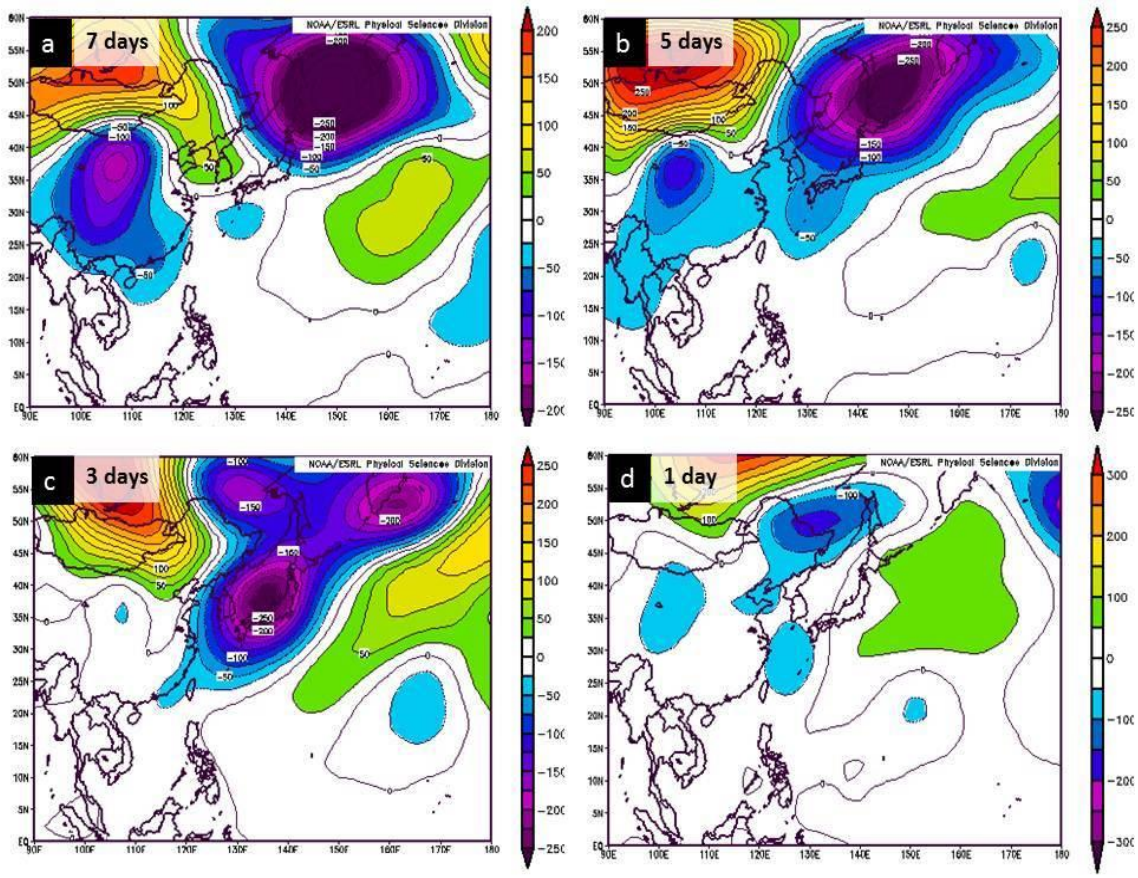

Figure 4.21. 200-hPa Geopotential Height Anomaly evolution through time for the 8-2-2007 Japan landfall. a) 7 days before landfall b) 5 days before landfall c) 3 days before landfall d) 1 day before landfall

Figure 4.22a shows an area of negative geopotential height anomalies over north-central China nestled between two positive-anomaly areas, one centered over western Mongolia and the other between China and Japan. To the east of the anomalous ridge west of Japan lies another region of negative height anomalies. This resembles a classic longwave pattern with alternating troughs and ridges. Two days later (Fig. 4.22b), the area of negative height anomalies over China weakens while the area of positive height anomalies in between Japan and China strengthens. Three days before landfall (Fig. 4.22c), positive height anomalies dominate the study area with the exception of an area of strong negative height anomalies from about 35°N to 55°N and 150°E to 180°. The day

before the typhoon hits Taiwan (Fig. 4.16d), an upper-level anomalous ridge is centered over eastern Mongolia and extends northward from about 34°N. The area of lower-than-normal geopotential heights has extended westward to about 140°E and the pattern now somewhat resembles that which is seen in Figure 4.3, comprising of all the Taiwan landfalls.

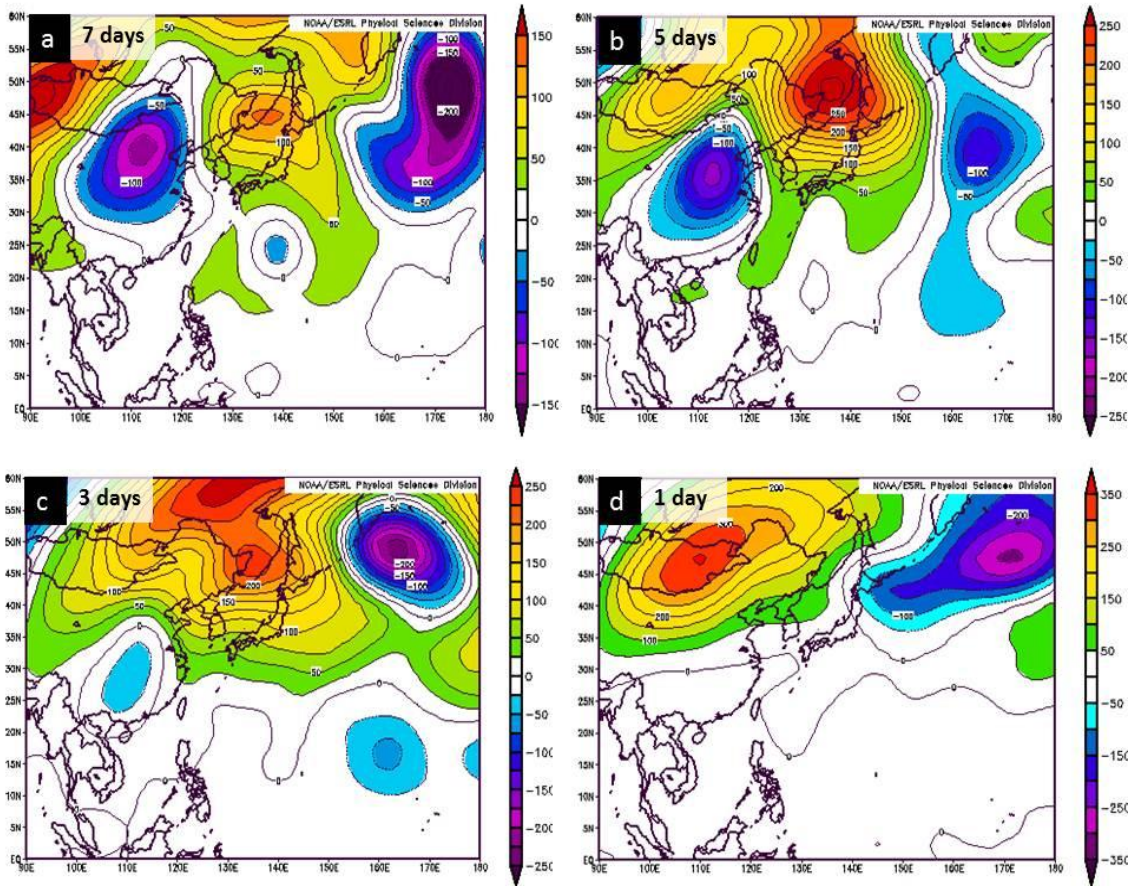

Figure 4.22. 200-hPa Geopotential Height Anomaly evolution through time for the 8-18-2007 Taiwan landfall. a) 7 days before landfall b) 5 days before landfall c) 3 days before landfall d) 1 day before landfall

Seven days before landfall, the dominant feature in Figure 4.23a is an anomalous ridge in the northeast corner of the map extending from about 33°N to 60°N and eastward from 150°E. There is also a region of negative geopotential height anomalies over eastern

Mongolia and northern China and one to the southeast of Japan. Five days before landfall (Fig. 4.23b), we now see an expanded area of negative height anomalies in between China and Japan, and positive height anomalies over Mongolia and northern China. Those positive height anomalies strengthen significantly over the next two days (Fig. 4.23c) and extend further down in to central China. Meanwhile, an area of negative height anomalies has formed over southern Japan while the anomalous ridge to the east of Japan extends further west. Figure 4.23d shows a broad area of slightly positive height anomalies from 20°N to 40°N and eastward to about 132°E. The negative height anomalies over southeast Japan are now bordered to the northwest and northeast by positive height anomalies, with the feature to the northeast being slightly stronger and more extensive.

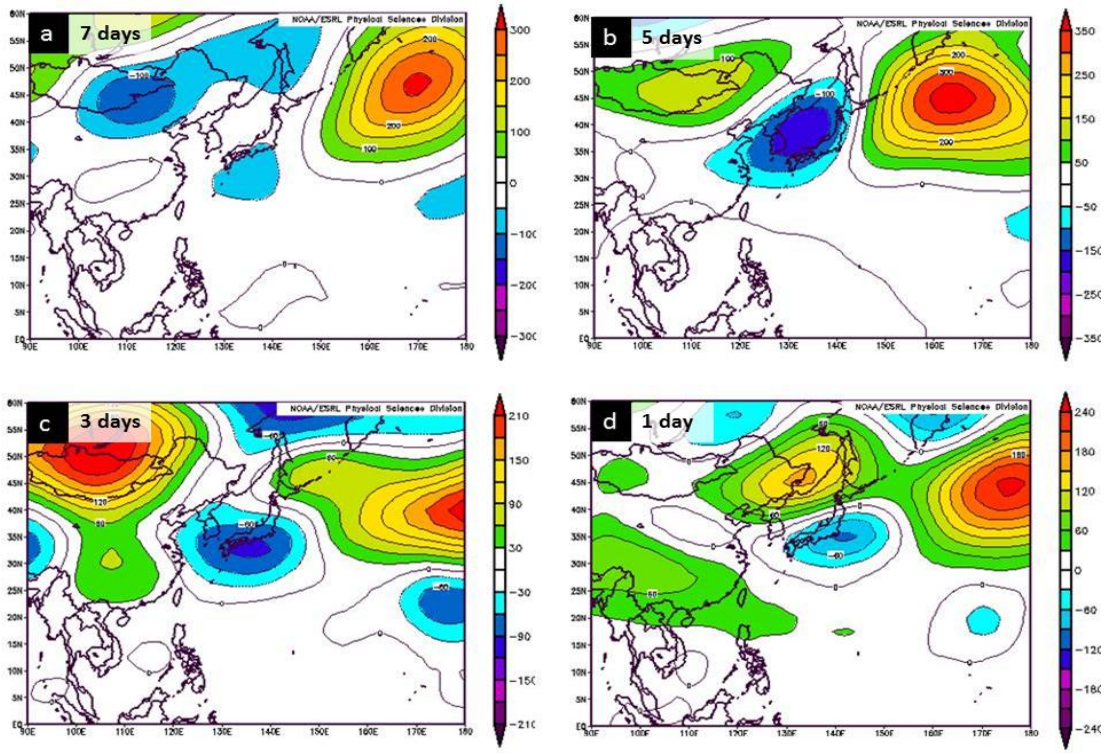

Figure 4.23. 200-hPa Geopotential Height Anomaly evolution through time for the 11-11-2001 Vietnam landfall. a) 7 days before landfall b) 5 days before landfall c) 3 days before landfall d) 1 day before landfall

This next set of figures was created to analyze the evolution of circulation features with regards to changes in typhoon intensity using a case study with a Taiwan-landfalling typhoon. Figures 4.24a through 4.24c shows a strengthening geopotential height anomaly ridge over the area in between Japan and China, along with a strengthening anomaly trough over Mongolia and northern China. During this time period the typhoon strengthened from a Category 1 at 75 knots to a Category 5 at 140 knots. Figures 4.24d through 4.24f show a weakening of both the positive and negative anomaly features, and during this time period the typhoon weakened back to a Category 1status at 65 knots. It brushed the northern tip of Taiwan on August 8, 1994, and eventually made a second landfall in China as tropical depression. A positive relationship exists between the positive height anomalies over Japan and typhoon intensity, but further research and a greater sample size is required to draw that conclusion.

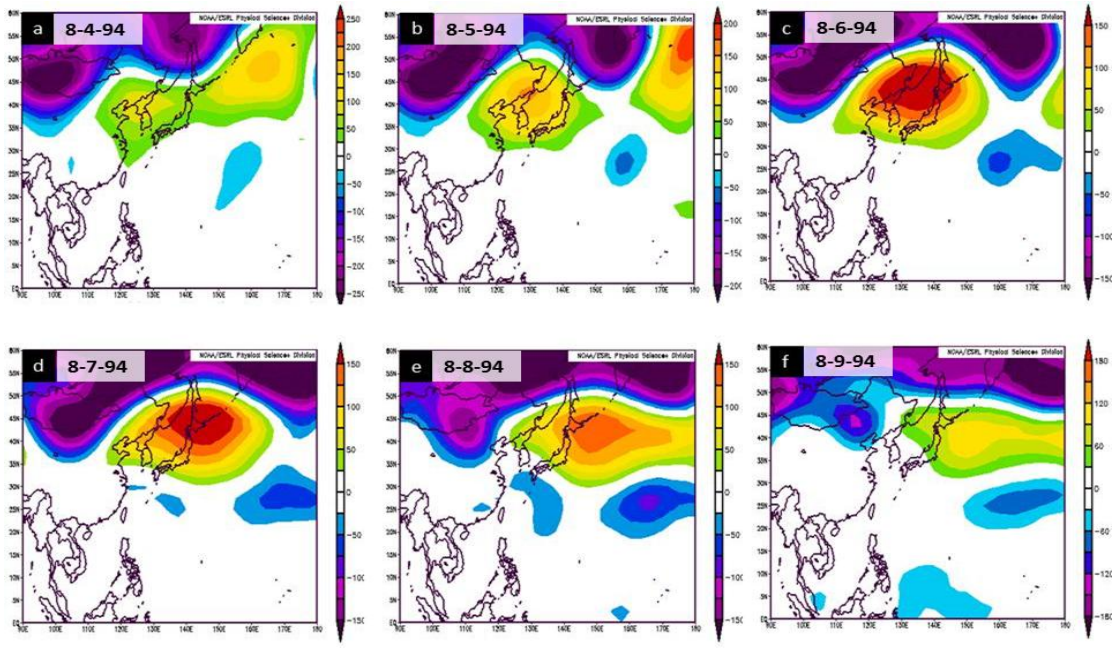

Figure 4.24. 200-hPa Geopotential Height Anomaly Composites throughout the daily progression of Super Typhoon #17 which made landfall in Taiwan on August 8, 1994. a) 8-4-1994 b) 8-5-1994 c) 8-6-1994 d) 8-7-1994 e) 8-8-1994 f) 8-9-1994

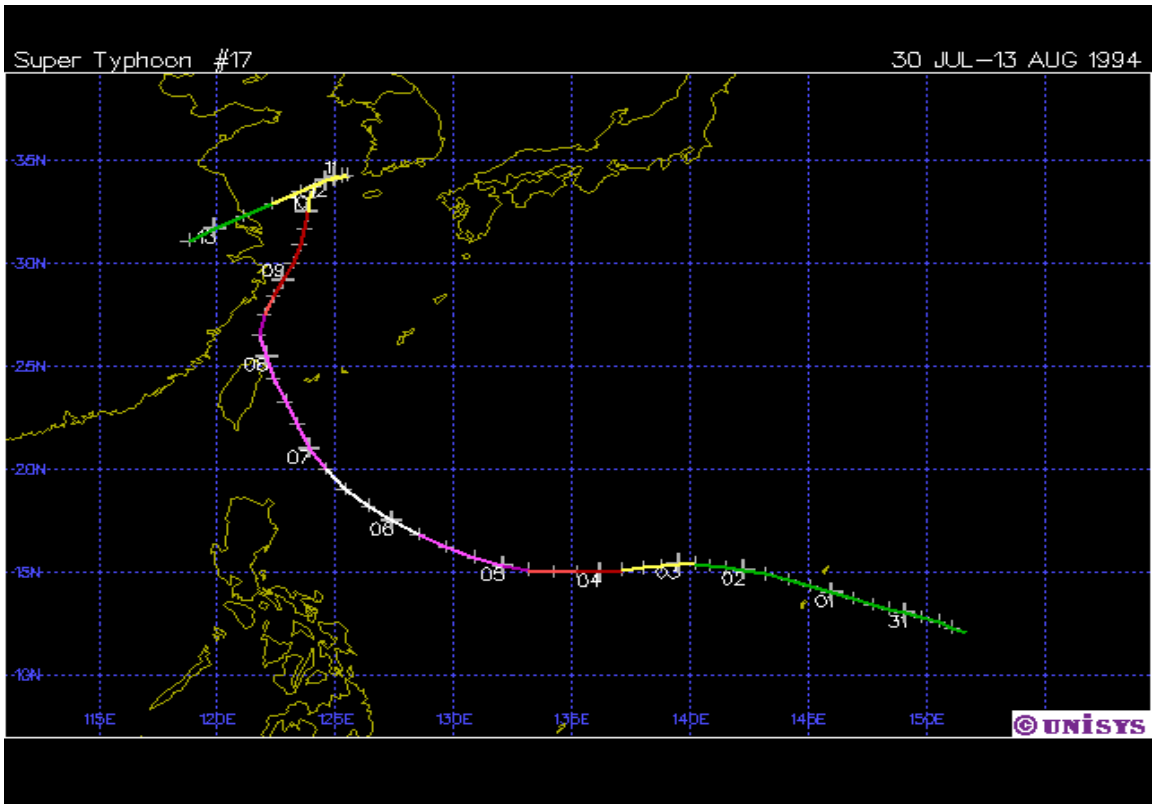

Figure 4.25. Track of Super Typhoon #17 in 1994 (Image source: Unisys, from JTWC Best Track Data)

4.2 Teleconnection Analysis

4.2 a) *Tropical Cyclones and ENSO*

Three El Nino (1997, 1982 and 1987) and three La Nina seasons (1988, 1999, 2007) were broken down into six categories, all for the months of August through December: total number of TCs, number of TCs ≥ 65 knots, percentage of TCs ≥ 65 knots (out of total TCs), number of TCs ≥ 100 knots, percentage of TCs ≥100 knots (out of TCs ≥ 65 knots), number of TC days ≥ 100 knots and average number of days ≥ 100 knots per TC. Table 4.1 shows that the difference in TC count between the El Nino and La Nina seasons sampled increases as we filter out storms with increasing intensity. The total TC count for both El Nino and La Nina is identical, at 53 per phase. El Nino seasons had ~15 more TCs ≥ 65 knots and 16 more TCs ≥ 100 knots. The number of TC days ≥ 100 knots were also counted to determine if the longevity of typhoons ≥ 100 knots increases during an El Nino event. Since TCs have a greater expanse of warm water to travel across during an El Nino, there is a good possibility that they can maintain sustained winds of at least 100 knots longer than during a La Nina, when the primary formation region shifts westward. Results show that in an El Nino, the 29 typhoons that reached wind speeds of ≥ 100 knots, remained at 100 knots or greater for 90.25 days. During La Nina conditions, the 13 typhoons that reached at least 100 knots remained at 100 knots or greater for a total of 28 days. This means that for this case, the average number of days ≥ 100 knots per storm during El Nino is 3.11 and during a La Nina is 2.15.

After running the PROC GLIMMIX model described in the methods, the only category where the value difference between the two ENSO phases was found to be

statistically significant is TC days ≥ 100 knots. For La Nina seasons, the mean number of TC days was calculated to be 9.33 and for El Nino seasons, the mean number of TC days was 30.08. The point estimate is 3.22, indicating that in El Nino years, we can expect the number of TC days ≥ 100 knots to increase by a factor of 3.22 over La Nina years. To determine the accuracy of the point estimate, the 95% confidence interval of the t-distribution is applied ($t_{0.025}$=3.182). The t-distribution critical values are applied to situations where the sample size is small (n<30) and the population standard deviation is unknown. It is useful for determining the statistical significance of the difference between sample means, creation of confidence intervals for the difference between two population means, and in linear regression analysis. In this analysis, the 95% confidence bounds on the rate are ($e^{1.858}$, $e^{0.483}$), which yields an increase of 1.62 to 6.41 times the number of TC days ≥ 100 knots in an El Nino versus a La Nina.

From Table 4.1, it can interpreted that while the total number of TCs during El Nino and La Nina is about the same, a higher percentage of tropical storms intensify to typhoon strengthen in a El Nino. Also, out of those that do become typhoons, a greater number develops further into super typhoons in an El Nino versus a La Nina. In addition, typhoons with winds greater than or equal to 100 knots last about an average of one day longer during an El Nino period and the longevity of total number of TC days of at least 100 knots increases threefold. Although the range of usable data for this analysis was limited, further research using a larger sample size should investigate these claims and evaluate other typhoon parameters with respect to various ENSO phases. It would be interesting to analyze different stage of typhoon development and how the environmental conditions during various stages of ENSO affect the size and forward speed of the storms

and vice versa. Furthermore, components of typhoon motion and direction can also be impacted by smaller scale factors and should be incorporated in combination with large-scale atmospheric controls.

Table 4.1 - Tropical cyclone frequency during selected El Nino and La Nina events (JTWC best track data)

ENSO event	Total number of TCs	Number of TCs ≥65 kts	% of TCs ≥65 kts (out of total)	Number of TCs ≥100 kts	% ≥100 kts (out of ≥65 kts)	Number of TC days ≥100 kts	Average number of days ≥100 kts per storm
	El Nino						
1997 ASOND	21	17	81%	9	53%	42	
1982 ASOND	16	14	88%	9	64%	19.25	
1987 ASOND	16	13	81%	11	85%	29	
Total	**53**	**44**		**29**		**90.25**	**3.11**
Mean	**17.7**	**14.7**	**83.3%**	**9.7**	**67.3%**	**30.1**	
	La Nina						
1988 ASOND	19	9	47%	5	56%	11.75	
1999 ASOND	16	8	50%	2	25%	3.75	
2007 ASOND	18	13	72%	6	46%	12.5	
Total	**53**	**30**		**13**		**28**	**2.15**
Mean	**17.7**	**10**	**56.3%**	**4.3**	**42.3%**	**9.3**	

4.2 b) *Tropical Cyclones and MJO*

Table 4.2 shows five various three-month MJO events that were analyzed based on total number of TCs, number of TCs ≥65 knots, percentage of TCs ≥65 knots, number of TCs ≥100 knots, percentage of TCs ≥100 knots (out of ≥65 knots), number of TC days ≥100 knots and average number of days ≥100 knots per storm. This proved to be challenging using the data provided because due to low temporal resolution, this analysis technique makes it too difficult to pinpoint which storms occurred during the positive (enhanced) and which storms occurred during the negative (suppressed) phases of the MJO, and during which time span the MJO event occurred. With these hindrances in mind, the obtained results show that WNP TC activity (frequency and intensity) during

the MJO is quite similar to the scenario when a La Nina is present. Even though the MJO events selected are over a three-month period rather than the five-month period selected for ENSO events, the total for each type of event (La Nina, El Nino and MJO) is 15 months, making Table 4.2 comparable to Table 4.1. In a side-by-side comparison, the totals in all categories for the MJO are very similar to those for La Nina. The two percentage categories are slightly higher in Table 4.2, but with the low sample size, it is hard to tell if it is significant without proper further statistical analysis. There is greater variability in total number of TCs among these particular MJO events than there was in the selected El Nino/La Nina events, but that may be due to the wide range in months used. For example, the April-May-June period is clearly going to have less total storms than the August-September-October period, but due to data limitations the three-month periods could not be homogenized. Therefore, in the case of the MJO, it is more advantageous to look at the means and percentages instead of the raw totals. Future work should investigate other sources of MJO data, with higher spatial and temporal resolution, and examine the effect the two MJO phases may have on storm track and intensification. Recent studies have shown that the enhanced MJO phase does make a region more favorable for cyclogenesis, but little is known about its effects on existing storms.

Table 4.2 - Tropical cyclone frequency during different MJO events (counts from JTWC best track data)

MJO event	Total number of TCs	Number of TCs ≥65 kts	% of TCs ≥65 kts (out of total)	Number of TCs ≥100 kts	% ≥100 kts (out of ≥65 kts)	Number of TC days ≥100 kts	Average number of days ≥100 kts per storm
1996 OND	11	6	55%	4	67%	5	
2000 ASO	17	11	65%	5	45%	12	
1979 JAS	12	7	58%	3	43%	6.75	
2002 AMJ	3	2	67%	1	50%	2	
2002 OND	6	4	67%	1	25%	3	
Total	**49**	**30**		**14**		**28.75**	
Mean	**9.8**	**6**	**62.4%**	**2.8**	**46%**	**5.75**	**2.05**

4.2 c) *Box Plots*

Figure 4.26 shows a box-and-whiskers plot of TC days greater than or equal to 65 knots for 11 different ENSO or MJO episodes (3 El Nino, 3 La Nina and 5 MJO), the same ones in Tables 4.1 and 4.2. Unlike the TC day counts in the tables that were listed per event, the ones in the boxplots were calculated per storm and then plotted as a single data point for that event. For example, if one MJO episode produced 3 typhoons where Typhoon #1 had 2 days ≥ 65 knots, Typhoon #2 had 3.5 days and Typhoon #3 had 4.5 days, three points would be plotted on the y-axis for that event – one at 2, one at 3.5 and one at 4.5.

From this plot we can see that El Nino events have more TC days greater than 65 knots, but also have a larger data range than La Nina or MJO events. This means that on a storm-by-storm basis during El Nino, you see a mixture of high and low numbers of TC days per storm. The MJO of 1996 was further investigated to determine if it also coincided with an El Nino or La Nina period due to its larger values, and for the entire duration of that MJO event (October, November and December 1996) the Multivariate

ENSO Index (MEI) was in the neutral phase (between -0.5 and 0.5). The biggest noticeable difference is between the El Nino and La Nina events, with El Nino events containing significantly more TC days ≥ 65 knots.

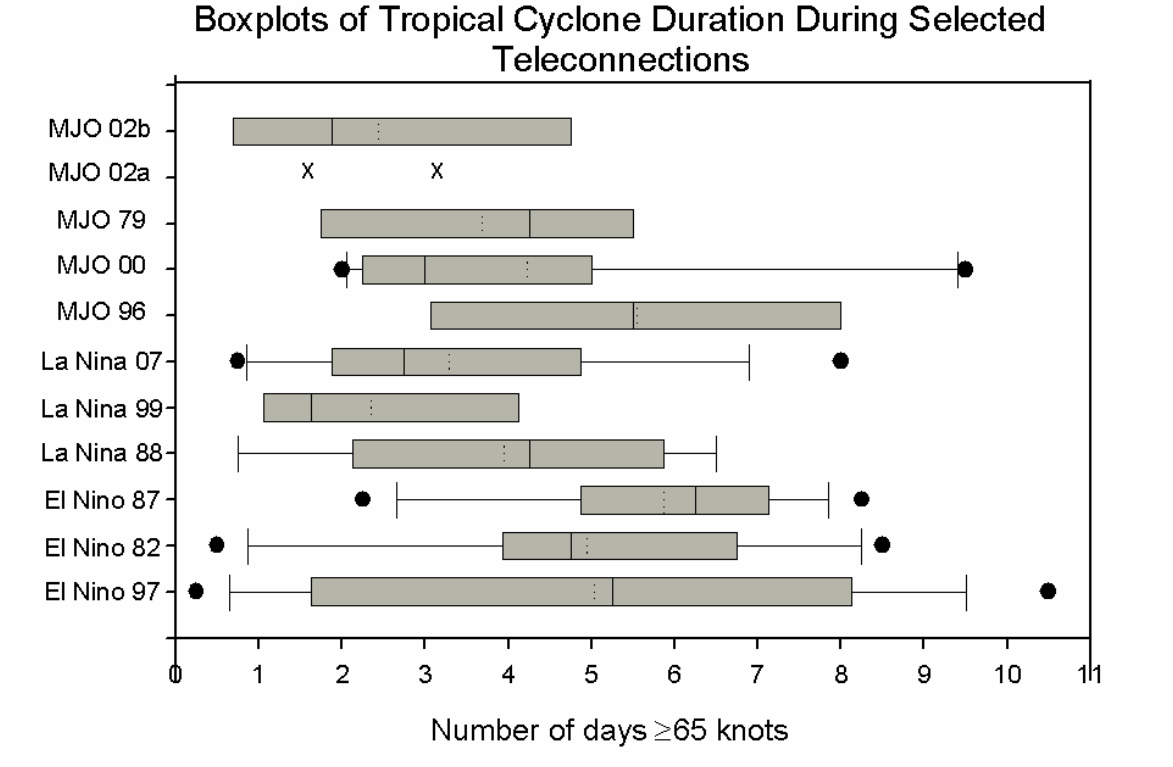

Figure 4.26 Boxplots of typhoon days greater than 65 knots during various El Nino, La Nina and MJO events showing data range (whiskers), first and third quartiles (Q1 and Q3, depicted by edges of the box), median (solid line in box), mean (dotted line in box) and outliers (black dots). Single data values denoted by "X".

Figure 4.27 shows a box-and-whiskers plot of TC days greater than or equal to 100 knots for the same ENSO and MJO events in Figure 4.26. There is a slightly greater number of TC days ≥ 100 knots in El Nino events, but even in the strongest 1997 El Nino, most of the data lies in between two and seven 100 knot days per storm. This is still very substantial when you consider the indication that one typhoon could have sustained

winds of at least 100 knots for a week straight. La Nina events seem to have a similar effect on typhoon days as MJO events, but further research is required to verify this assumption.

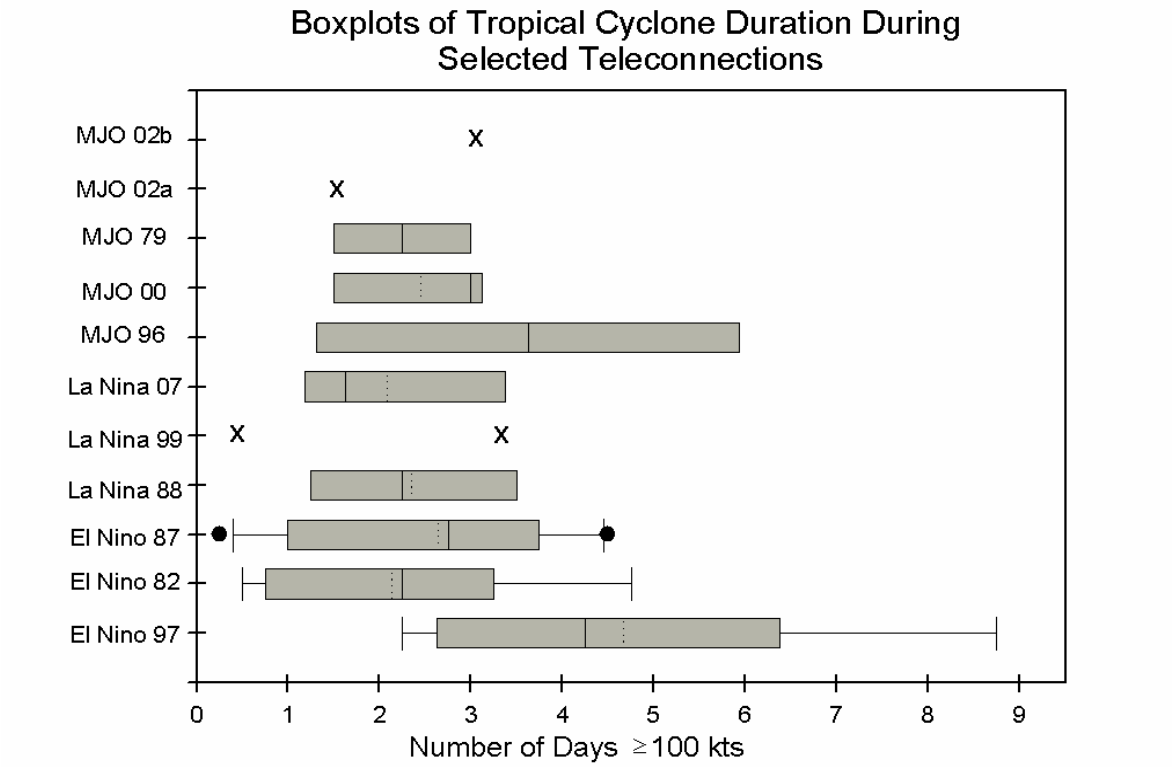

Figure 4.27 Boxplots of typhoon days greater than 100 knots during various El Nino, La Nina and MJO events showing data range (whiskers), first and third quartiles (Q1 and Q3, depicted by edges of the box), median (solid line in box), mean (dotted line in box) and outliers (black dots). Single data values denoted by "X".

CHAPTER 5

CONCLUSION AND SUMMARY

5.1 Synoptic Analysis

The tendency of a certain region to experience a typhoon landfall appears to be influenced by a combination of prevailing atmospheric patterns, teleconnections and how far into the tropical season we are. The likelihood of Taiwan landfalls occurs earlier in the season, around August, whereas more Japan landfalls occur in the month of September. Vietnam landfalls are more common later in the season around October and November because it is further south. TCs that form in the latter part of the season are restricted by the more southerly jet stream and cooler SST to the north so they generally travel westward in the direction of the Philippines and Vietnam. In addition, the genesis locations of all three landfall regions discussed here also differ. From the aforementioned sample of storms, Japan TCs formed further east than TCs that hit Taiwan and Vietnam. Taiwan TCs formed slightly further north and west than those that hit Japan, and TCs that made landfall in Vietnam formed the furthest west and south of the three landfall areas. If ENSO phase is factored in, since we know it also affects formation region (Chan, 1985; Wang and Chan, 2002), we can determine the probability of a specific region being targeted by tropical activity. For example, if most developing TCs in November are likely to affect Southeast Asia and it is also a La Nina year, where storms form further west and track further south, we could assume that there is an increased chance of a typhoon impact to Vietnam.

The upper-level composite pattern for the range of typhoons in this study (July through December 1964-2007) shows slightly below normal geopotential heights for the study area with the center of negative geopotential height anomalies located over the Bohai Sea in northern China (Fig. 4.8). This signifies that more often than not during the typhoon season, the atmospheric scenario that sets up contains an upper-level trough over northeast China, or pressure that is lower than normal. Breaking this down into various landfall dates, a different pattern becomes apparent. After analyzing 200 hPa geopotential height anomaly composites and identifying the dominant anomalous cyclones (areas of negative height anomalies) and anticyclones (areas of positive height anomalies), the typhoon tracks seem to follow the periphery of the anticyclones in both Taiwan and Vietnam landfalls (Fig. 4.10 and 4.11). In the case of Japan, the typhoons track right up the middle of the anomalous ridge (Fig. 4.9). Although the means and anomalies are spatially offset, and the anomalies do not reflect actual conditions, the 200 hPa height anomalies seemed to best indicator for locating steering currents among all the variables examined in this research.

Vector wind composites helped reinforce the findings brought forth by the geopotential height analysis. Mean vector wind composite analysis at various atmospheric levels showed little to no wind shear in the vicinity of Japan-bound typhoon tracks, maintaining a favorable environment for tropical cyclones (Fig 4.12). The anticyclonic flow also evident in the vector wind composites is what helped guide the storms toward Japan. Figure 4.14c, depicting mean vector winds for the 850 to 200 hPa layer for Taiwan landfalls, shows areas of higher wind shear north of the 35° latitude line, as well as south and southeast of Taiwan. Any typhoons that might have entered this area

of high shear would have probably fallen apart. On the contrary, the typhoons that made landfall in Taiwan did not penetrate this area and tracked along the northeast edge of this high-shear zone where they were able to preserve their structure and intensity. The 200 hPa vector wind anomaly composite for Taiwan landfalls (Fig 4.15a) shows that after storms made landfall, they were pulled inland by the anticyclone over China, where they likely sped up over land due to the anomalous area of strong winds. During Vietnam landfalls (Fig. 4.16), strong zonal winds extended all the way down to the 25° latitude parallel, containing storm tracks further south as a result.

Looking at the spatiotemporal evolution for specific typhoons, we can see the progression of geopotential height anomalies and synoptic features as we approach the landfall date. For the Japan case study (Fig. 4.21), the anomalous upper-level trough over the landfall location is significantly strongest at 3 days before landfall. For the Taiwan-landfalling typhoon (Fig. 4.22), pressure over eastern China increases steadily until landfall. An anomalous ridge also builds over Mongolia and northern China. In the Vietnam example (Fig. 4.23), an anomalous ridge builds over southern China and Southeast Asia as landfall nears. After conducting a case study for a quick assessment of intensity in relation to spatiotemporal propagation, in the case of Super Typhoon #17 in Figure 4.24 that made landfall in Taiwan, the strength of the anomalous ridge over Japan corresponded to the intensity of the typhoon and the relationship seemed to be directly proportional. Clearly this is only one example, so further conclusions cannot be made without additional examination.

5.2 Teleconnection Analysis

Analyzing the impact of atmospheric teleconnections has substantially increased our understanding of the climate system and the role of climate variability. Synoptic climatology has allowed us to transcend simple correlations between teleconnection indices and temperature/precipitation, into providing insight on the spatiotemporal manifestation of teleconnection anomalies, as well as further understanding these anomalies in circulation pattern frequencies (Sheridan and Lee, 2012). Although in this analysis the total number of TCs during the three El Nino events was equal to the total number of TCs during La Nina events, the similarities ended there. 44 out of 53 TCs during El Nino conditions, or 83%, went on to achieve typhoon strength at 65 knots. About 66% of those typhoons intensified even further to 100 knots, or super typhoon classification. This is in comparison to around 57% of TCs reaching wind speeds of 65 knots in a La Nina, and 43% of those becoming super typhoons of at least 100 knots. In addition to the number of storms, the number of TC days with winds of at least 100 knots was 3 times higher in the three-year period of El Nino events vs. the three-year period of La Nina events. Taking the average per storm, you could expect to see roughly one extra day of 100 knot winds or greater during an El Nino typhoon than a La Nina typhoon. After performing a statistical analysis on the date, despite the small sample size, it was discovered that the difference in number of TC days of at least 100 knots is statistically significant and that in El Nino years, we can expect the number of TC days with at least 100 knot winds to increase by a factor of 3.22 over La Nina years. When applying 95% confidence intervals, that rate ranges from 1.62 to 6.41 times. This tells us that the greater number of TC days of at least super typhoon strength is as a result of more

typhoons intensifying and not because there is a higher frequency of TCs during El Nino events. This makes sense climatologically because El Nino conditions provide a greater expanse of warm water for the TCs to travel across.

The same analysis conducted on TC counts during MJO events was less conclusive. One thing that stands out is the resemblance to the La Nina scenario, as the MJO values were very comparable to La Nina values in all categories. A greater sample size should eventually be tested to evaluate these claims further. Although the MJO events were grouped differently, they also consisted of a total 15-month period just like the El Nino and La Nina samples.

5.3 Implications and Future Research

Millions of people are affected by WNP typhoons every year and the more we learn about how to predict them, the more loss can be prevented. These results have many broad implications, ranging from forecast modeling to short-term planning strategies for emergency managers. Future studies should continue to expand on the topics brought forth in this thesis. A larger sample size is necessary to gather more significant conclusions regarding teleconnections and future reanalysis efforts may help increase the sample size.

Liebmann et al. (1994) showed that there is an increase in TC frequency during the enhanced phase of the MJO. However, there are very few studies regarding the relationship between MJO activity and TC track. Nakazawa (2006) stated that the monsoon trough over the WNP was enhanced during the convective phase of the MJO and generated most of the typhoons over that region. Due to the extended duration of this

convective phase, the steering flow anomaly persisted and storms tracked WNW from their origin locations providing a favorable environment for the unsurpassed quantity of Japan landfalls in 2004. Accessible and high resolution MJO data would lead to more studies like these that would help identify how intraseasonal oscillations such as the MJO affect typhoon activity.

A system to parameterize upper-level synoptic features as well as anomalous features would be extremely helpful. Not only must indices be incorporated as a way to quantify the magnitude of these atmospheric patterns, but spatial parameters must also be assimilated into the analysis. Wu et al. (2005) utilized two subtropical high indices in their study, one measuring the intensity of the high, as the sum of the geopotential heights on the 5880 meter contour between 110°E and 180°, and one measuring the extension of the subtropical high, defined by the westernmost longitude of the same contour. Gong and He (2002) constructed a similar index based on the mean value of the 500 hPa geopotential height level. In the Atlantic basin, the Bermuda High Index is developed using pressure differences between two points, in this case, Bermuda and New Orleans. These techniques could be used to quantify the anticyclonic features described in this thesis to be able to incorporate them into other models and track their progression.

Unlike in the mid-latitudes, where internal variability of both the atmosphere and the ocean is substantial, in the tropics, the ocean and the atmosphere are strongly controlled by the boundary conditions imposed by the other. The upper ocean circulation is largely determined by factors such as wind stress with little internal variability and tropical atmospheric circulation features are influenced by the SST. Differential atmospheric forcing by the SST boundary condition thermodynamically drives

circulation cells and convection tends to organize over the warmest SST, producing regions of strong surface convergence (Neelin et al., 1994). In addition, the largest driver of interannual climate variability, ENSO, is a result of ocean-atmosphere interaction.

SST feedback, the negative feedback on a TC's intensity after a passing storm, plays an important role in tropical climate variability. In slow-moving storms, the SST decrease is greater than in fast-moving storms over deep oceanic mixed layers. SST cooling decreases evaporation, which shuts off the storm's energy source. Not only does the evolution of SST have a significant impact on a typhoon itself, but the subtropical high index used by Gong and He (2002) showed a strong correlation with SST and that SST changes are mainly responsible for the high's interdecadal variability. Future work should incorporate SST data into investigations of dominant forcing mechanisms.

To determine the role SST plays in typhoon interaction, as well as other ocean-atmosphere fluxes, high resolution regional coupled ocean-atmosphere models must be used. Coupled models are beneficial to the skill of intensity forecasts, and ensembles or a combination of models are more accurate than individual models, and generally yield reduced forecast error (Goerss, 2000). In addition, coupled statistical-dynamical baroclinic models are capable of simulating three-dimensional atmospheric motion that lead to better track forecasting.

Multi-scale interactions pose difficulties in modeling tropical cyclones because of the requirement of massive computer resources and accurate representation of physical processes over a wide range of scales. Because many models can't incorporate these multi-scale interactions, various approximations have to be made, and only certain aspects of processes can be examined (Liu et al., 1997). The complexities revealed by

observations indicate a need for higher resolutions and advanced microphysics parameterizations to accurately model the structures of tropical systems. The measurements also provide ground truthing for verifying the performance of numerical models (Liu et al., 1997).

Aside from changes in SST, there are many ways the ocean is affected by TC landfalls. Typhoons play a substantial role in coastal processes, which downscaled data can be used to analyze. Typhoon-induced swells can create extensive sediment erosion and cause dramatic changes in coastal geomorphology. Fan et al. (2006) found that even without a direct impact, TC landfalling in China can induce waves significantly higher than the mean wave height, depending on local bathymetry and interaction with tides and other physical processes. Fluctuations in the bed level of intertidal mudflats have a strong association with wave heights. Erosion occurs when waves exceed a certain height even in non-typhoon conditions and serious erosion occurs during the presence of typhoons. These erosion zones quickly turn into accretion sites after the typhoon has passed or dissipated. Even distant typhoons can potentially produce large swells in the coastal parts of the WNP resulting in sediment transport and major morphological changes (Fan et al, 2006). Tropical cyclones are also among the most energetic forcing mechanisms near the coast. Long waves, such as large-scale edge waves, are generated by TC landfalls. These waves can become trapped on the continental shelf and propagate parallel to the coastline causing sea level fluctuations outside of the storm surge area (Yankovsky, 2009). This research can also help analyze paleotempestology records, such as intraseasonal proxies, on a smaller scale.

Coastal ocean responses are also evident in biological changes. Typhoons can induce large phytoplankton blooms and affect primary production. Zhao et al. (2008) discovered that the response of phytoplankton to typhoon forcing depends on its translation speed and intensity. Particularly during the period of strongest winds and lowest translation speeds, strong upwelling and vertical mixing occurred in the wake of typhoons. This lead to elevated nutrient levels in surface waters which stimulated phytoplankton blooms. Slower moving typhoons had a longer lasting mixing effect inducing a stronger bloom while a strong fast-moving typhoon resulted in a bloom over a larger area.

Although the steering flow, the vertically integrated mean flow in the middle to lower troposphere, is the primary factor that governs typhoon motion, it is still not clear how smaller-scale features affect TC tracks. Harr and Elsberry (1995) discussed the effect of the large-scale atmospheric circulation on TC tracks over the WNP, and showed that TCs tends to move westward when there is a negative geopotential height anomaly along 15°N and a positive anomaly along 30°N, just south of Japan. It is also hypothesized that the presence and location of a weakness in the ridge is critical when trying to predict a situation where the storm may recurve.

Generally, a TC tends to be small if a strong subtropical ridge dominates the low- and mid-level environment. In contrast, a TC may expand as it breaks through the subtropical ridge or the westerly flow north of the ridge. A case study of Typhoon Bart demonstrated the temporal evolution of the synoptic pattern and its relationship with the TC size change. Bart exhibited a distinct transition from the dominant ridge/ monsoon-

gyre synoptic pattern (which is associated with small TCs) to the southwesterly surge late-season pattern (which typically results in large TCs) and its size increased substantially (Liu and Chan, 2002). Many studies have claimed that the size of a TC may have a significant effect in modifying its movement. Although they are largely steered by their environmental flow, an extensive TC circulation may cause the motion of the TC to depart significantly from its expected path. A large TC may also alter its own environmental flow; therefore, it is necessary to conduct further studies on TC size, data that is currently not easily obtainable for the Western Pacific basin.

Besides the external environmental forces, the internal dynamics of the storm's structure also affect its track, and scientists are still uncertain regarding the processes that occur within. We are just starting to understand how TC structure affects its track, and a better prediction of TC dynamics is crucial for disaster mitigation strategy. Chen et al. (2012) showed that internal dynamics are more important to the development of compact typhoons, ones with a small radius of maximum wind and large rate of wind speed decrease outside the core, while the role of low-level external forcing is more important in the development of incompact TCs, which are large in size and typically move with larger deviations from the steering flow, especially during recurvature. Incompact TCs tend to interact with midlatitude troughs, which typically increases their wind speeds.

Understanding intensity, forward speed and the interaction the storm has with its surrounding atmosphere, as well as the influence of the larger-scale synoptic features on the TC's speed and intensity, is also very important in understanding typhoon dynamics. Some of these analyses were attempted during the preliminary research for this thesis, but data availability was an issue. Future work should also focus on developing higher

resolution, better quality, standardized, robust and readily-available data to support and allow for more extensive research. For synoptic analysis, other variables and atmospheric levels should be analyzed. Studying TC tracks in other locations along with the interannual variability of principal atmospheric patterns will help get us one step closer to identifying what drives these enigmatic global phenomena. Given enough time and resources, we will hopefully be able to grasp what we need to implement more skillful forecasting for the future.

REFERENCES

Aiyyer, A. R. and J. Molinari (2003): Evolution of mixed Rossby gravity waves in idealized MJO environments, *J. Atmos. Sci.,* **60**, 2837–2855

Atkinson, G. D., (1974): Investigation of gust factors in tropical cyclones. FLEWEACEN Tech Note: JTWC 74-1, Fleet Weather Center, Guam. 9 pp.

Avila, L. A., (1998): Forecasting tropical cyclone intensity changes: An operational challenge. Preprints, *Symp. on Tropical Cyclone Intensity Change,* Phoenix, AZ, Amer. Meteor. Soc., 1–3.

Barry, R. G. and A. H. Perry (1973): *Synoptic Climatology; Methods and Applications*, Methuen, London, pp. 161-165.

Bergman, J. W., H. H. Hendon, and K. M. Weickmann (2001): Intraseasonal air-sea interactions at the onset of El Nino, *J. Clim.*,**14**, 1702–1719.

Bessafi, M., and M. C. Wheeler, (2006): Modulation of south Indian Ocean tropical cyclones by the Madden–Julian oscillation and convectively coupled equatorial waves. *Mon. Wea. Rev.*, **134**, 638–656.

Birkeland K.W. and Mock C.J. (1996): Atmospheric circulation patterns associated with heavy snowfall events, Bridger Bowl, Montana, U.S.A. *Mountain Research and Development,* **16**, 281–286.

Briegel**,** L. M**.**, and W. M. Frank, (1997): Large- scale forcing of tropical cyclogenesis in the western North Pacific. *Mon. Weather. Rev*., 125, 1397-1413.

Camargo, S. J. and A. H. Sobel, (2005): Western North Pacific tropical cyclone intensity and ENSO. *J. Clim.*, **18**, 2996–3006.

Camargo, S.J., A.W. Robertson, S.J. Gaffney, P. Smyth and M. Ghil (2007b): Cluster analysis of typhoon tracks. Part II: Large-scale circulation and ENSO. *J. Clim.*, **20**, 3654–3676.

Camargo, S.J., M. C. Wheeler, and A. H. Sobel, (2009): Diagnosis of the MJO modulation of tropical cyclogenesis using an empirical index. *J. Atmos. Sci*., **66**, 3061–3074.

Chan, J.C.L (1985): Tropical cyclone activity in the Northwest Pacific in relation to the El Nino/Southern Oscillation phenomenon. *Mon. Weather Rev.,* **113**:599-606.

Chan, J. C. L. (2000): Tropical cyclone activity over the Western North Pacific associated with El Nino and La Nina events, *J. Clim.*, **13,** 2960-2972.

Chan, J. C. L. (2006): Comment on "Changes in tropical cyclone number, duration, and intensity in a warming environment". *Science,* **311**(5768): 1713b.

Chand, S. S., K. J. E. Walsh, (2010): The influence of the Madden–Julian Oscillation on tropical cyclone activity in the Fiji region. *J. Clim.*, **23**, 868–886.

Chang-Hoi H., J-J Baik, J-H Kim, D-Y Gong, C-H Sui. (2004): Interdecadal changes in summertime typhoon tracks. *J. Clim*., **17**:9, 1767-1776.

Chen, T.-C., and S.-P. Weng (1998): Interannual variation of the summer synoptic-scale disturbance activity in the western tropical Pacific. *Mon. Wea. Rev*., **126**, 1725-1733.

Chen, T.-C., S.-P. Weng, N. Yamazaki, and S. Kiehne, (1998): Interannual variation in the tropical cyclone formation over the western North Pacific. *Mon. Wea. Rev.*, **126,** 1080–1090.

Chen, D. Y. C., K. K. W. Cheung and C. S. Lee (2012): A study on the synoptic-dynamical characteristics of compact tropical cyclones in the Western North Pacific. *Mon. Wea. Rev*., **140**, 4046-4065.

Chia, H.-H., and C. F. Ropelewski, (2002): The interannual variability in the genesis location of tropical cyclones in the northwest Pacific. *J. Clim.*, **15,** 2934–2944.

Chin, P. C., (1972): Tropical cyclone climatology for the China Sea and Western Pacific from 1884 to 1970. Volume 1: Basic Data. Royal Observatory, Hong Kong. R.O. Technical Memoir No. 11, 55515.2, **265**, (265.6) 1961-70.

Chu, J.-H., C. R. Sampson, A. S. Levine, and E. Fukada (2002): The Joint Typhoon Warning Center tropical cyclone best-tracks, 1945–2000, Ref. NRL/MR/7540-02-16, Nav. Res. Lab., Washington, D. C.

Dvorak, V. F., (1975): Tropical cyclone intensity analysis and forecasting from satellite imagery. *Mon. Wea. Rev.*, **103**, 420-430.

Dvorak, V. F., (1984): Tropical cyclone intensity analysis using satellite data. *NOAA Tech. Rep.* NESDIS 11, 46.

Dvorak, V. F. (1995): Tropical clouds and cloud systems observed in satellite imagery: tropical cyclones. Workbook Vol. 2, 359.

Elsberry, R. L., G. J. Holland, H. Gerrish, M. DeMaria, C. P. Guard, and K. Emanuel, (1992): Is there any hope for tropical cyclone intensity prediction?—A panel discussion. *Bull. Amer. Meteor. Soc.*, **73,** 264–275.

Elsner, J. B. and K. B. Liu, (2003): Examining the ENSO-typhoon hypothesis. *Climate Res*., **25**:43–54.

Emanuel, K. A., and D. S. Nolan, (2004): Tropical cyclone activity and global climate. Preprints, *26th Conf. on Hurricanes and Tropical Meteorology*, Miami, FL, Amer. Meteor. Soc., 240–241 pp.

Emanuel, K.A., (2005): Increasing destructiveness of tropical cyclones over the past 30 years. *Nature*, **436,** 686–688.

Englebretson, R. E., (1992): Final Report - Joint Typhoon Warning Center (JTWC92) Model. Science Applications International Corporation. 92-29955, 90 pp. [Available online at http://www.dtic.mil/dtic/tr/fulltext/u2/a258646.pdf.]

Fan, D., Y. Guo, P. Wang and J.Z. Shi (2006): Cross-shore variations in morphodynamic processes of an open-coast mudflat in the Changjiang Delta, China: With an emphasis on storm impacts, *Continental Shelf Research*, **26**, 517–538.

Ferreira, R. N., and W. H. Schubert, (1999): The role of tropical cyclones in the formation of tropical upper-tropospheric troughs. *J. Atmos. Sci.,* **56,** 2891–2907.

Fink, A., and P. Speth (1997): Some potential forcing mechanisms of the year-to-year variability of the tropical convection and its intraseasonal (25 ± 70-day) variability, *Int. J. Climatol*., **17**, 1513–1534.

Folland, C. K., T. R. Karl and M. J. Salinger (2002): Observed climate variability and change. *Weather*, **57**: 269–278.

Franklin, J. L., M. L. Black and K. Valde (2003): GPS dropwindsonde wind profiles in hurricanes and their operational implications. *Weather Forecast.,* **18**, 32–44.

Gershunov, A. and T. Barnett, (1998): Inter-decadal modulation of ENSO teleconnections. *Bull. Amer. Meteor. Soc.,* **79**, 2715-2725.

Gong, D.-Y., and C.-H. Ho, (2002): Shift in the summer rainfall over the Yangtze River valley in the late 1970s. *Geophys. Res. Lett.,* **29**, 1436.

Gong D-Y., and X-Z He (2002): Interdecadal change in Western Pacific subtropical high and climatic effects, *Acta Geographica Sinica*, **57**(2): 185-193.

Gottschalck, J. and W. Higgins (2008): Madden Julian Oscillation impacts. NOAA Climate Prediction Center. [Available online at http://www.cpc.ncep.noaa.gov/products/precip/CWlink/MJO/MJO_1page_factsheet.pdf.]

Goerss, J. S., (2000): Tropical cyclone track forecasts using an ensemble of dynamical models, *Mon. Wea. Rev.*, 1187-1193.

Gray, W.M., (1979): Hurricanes: Their formation, structure, and likely role in the tropical circulation. In: *Meteorology over Tropical Oceans*, D. B. Shaw, Ed., *Roy. Meteor. Soc.*, Bracknell, Britain, 155–218.

Guard, C.P., L. E. Carr, F. H. Wells, R.A. Jeffries, N.D. Gural, and D.K. Edson (1992): Joint Typhoon Warning Center and the challenges of multibasin tropical cyclone forecasting. *Wea. and Forecasting*, **7**, 328-352.

Haight, F. A. (1967): *Handbook of the Poisson Distribution*. New York: John Wiley & Sons.

Hall, J. D., A. J. Matthews, and D. J. Karoly, (2001): The modulation of tropical cyclone activity in the Australian region by the Madden–Julian oscillation. *Mon. Wea. Rev.,* **129,** 2970–2982.

Hanley, D., J. Molinari, and D. Keyser, (2001): A composite study of the interaction between tropical cyclones and upper-tropospheric troughs. *Mon. Wea. Rev.,* **129,** 2570–2584.

Harr, P. A., and J. C. L. Chan (2004): Monsoon impacts on tropical cyclone variability. *The third international workshop on monsoons (IWM-III)*, Hangzhou, China, Secretariat of the World Meteorological Organization, 512-542.

Harr, P. A. and R. L. Elsberry, (1991): Tropical cyclone track characteristics as a function of large scale circulation anomalies. *Mon. Wea. Rev.*, **119**, 1448-1468.

Harr, P. A. and R. L. Elsberry, (1995): Large-scale circulation variability over the tropical Western North Pacific. Part I: spatial patterns and tropical cyclone characteristics. *Mon. Wea. Rev.*, **123**, 1225–1246.

Hayashi, Y., and A. Sumi (1986): The 30–40 day oscillations simulated in an ‘‘Aqua-planet’’ model, *J. Meteorol. Soc. Jpn*., **64**, 451–467.

Hayashi, Y., and D. G. Golder (1986): Tropical intraseasonal oscillation appearing in the GFDL general circulation model and FGGE data. Part I: Phase propagation, *J. Atmos. Sci*., **43**, 3058–3067.

Hendon, H.H., and M. L. Salby, (1994): The life cycle of the Madden–Julian oscillation. *J. Atmos. Sci.,* **51,** 2225–2237.

Hendon, H. H., C. Zhang, and J. D. Glick (1999): Interannual variation of the Madden-Julian Oscillation during Austral summer, *J. Clim*., **12**, 2538–2550.

Hirschboeck, K.K. Ni, Fenbiao, Wood, M.L. and Woodhouse, C.A. (1996): Synoptic dendroclimatology: overview and outlook in Dean, J.S., Meko. D.M. and Swetnam, T.W., eds. *Tree Rings, Environment, and Humanity: Radiocarbon*, 205-223.

Hong, X., C. H. Bishop, T. Holt and L. O'Neill (2011): Impacts of sea surface temperature uncertainty on the Western North Pacific subtropical high (WNPSH) and rainfall. *Wea. Forecasting*, **26**, 371–387.

Kalnay, E., M. Kanamitsu, R. Kistler, W. Collins, D. Deaven, L. Gandin, M. Iredell, S. Saha, G. White, J. Woollen, Y. Zhu, M. Chelliah, W. Ebisuzaki, W. Higgins, J. Janowiak, K. C. Mo, C. Ropelewski, J. Wang, A. Leetmaa, R. Reynolds, R. Jenne, and D. Joseph, 1996: The NCEP/NCAR 40-Year reanalysis project. *Bull. Amer. Meteor. Soc.*, **77**, 437-471.

Kessler, W. S., and R. Kleeman (2000): Rectification of the Madden-Julian oscillation into the ENSO cycle, *J. Clim.*, **15**, 3560–3575.

Kim, J.-H., C.-H. Ho, and C.-H. Sui (2005): Circulation features associated with the record-breaking typhoon landfall on Japan in 2004, *Geophys. Res. Lett.*, **32**, L14713.

Kim, J-H, C-H Ho, H-S Kim, C-H Sui, S. K. Park (2008): Systematic variation of summertime tropical cyclone activity in the Western North Pacific in relation to the Madden–Julian oscillation. *J. Clim.*, **21**, 1171–1191.

Klotzbach, P. J. (2006), Trends in global tropical cyclone activity over the past twenty years (1986–2005), *Geophys. Res. Lett.*, **33**, L10805

Knaff, J. A., and R. M. Zehr, (2007): Reexamination of tropical cyclone wind–pressure relationships. *Wea. Forecasting*, **22,** 71–88.

Knapp, K. R., M. C. Kruk, D. H. Levinson, H. J. Diamond, and C. J. Neumann, (2010): The International Best Track Archive for Climate Stewardship (IBTrACS): Unifying tropical cyclone best track data. *Bull. Amer. Meteor. Soc.*, **91**, 363-376.

Kossin, J. P., K. R. Knapp, D. J. Vimont, R. J. Murnane and B. A. Harper (2007): A globally consistent reanalysis of hurricane variability and trends, *Geophys. Res. Lett.*, **34**, L04815

Kruk, M. C., K. R. Knapp, and D. H. Levinson, (2010): A technique for combining global tropical cyclone best track data. *J. Atmos. Oceanic Technol.*, **27,** 680–692.

Kubota, H. & J.C.L Chan, (2009): Interdecadal variability of tropical cyclone landfall in the Philippines from 1902 to 2005.*Geophys Res. Lett.*, **36**, L12802.

Lackmann, G. M., (2011): Midlatitude synoptic meteorology: dynamics, analysis, and forecasting. *Amer. Met. Soc*., ISBN 978-1-878220-10-3, 345.

Landsea, C.W. (2005): Meteorology: hurricanes and global warming. *Nature*, **438**: E11–E12.

Landsea, C. W., B. A. Harper, K. Hoarau, and J. A. Knaff, (2006): Can we detect trends in extreme tropical cyclones? *Science*, **313**, 452–454.

Lau, N. C., and K.-M. Lau (1986): Structure and propagation of intraseasonal oscillations appearing in a GFDL GCM, *J. Atmos. Sci.,* **43**, 2023–2047.

Lazear, R., (2007): The effects of diabatic heating on upper-tropospheric anticyclogenesis. M.S. thesis, Department of Atmospheric and Oceanic Sciences, University of Winsconsin – Madison, 78 pp.

Liebmann, B., H. H. Hendon, J. D. Glick, (1994): The relationship between tropical cyclones of the western Pacific and Indian Oceans and the phase of the MJO. *J. Meteor. Soc. Jpn.,* **72,** 401–412.

Lin I. I., C. C. Wu, I. F. Pun and D. S. Ko (2008): Upper-ocean thermal structure and the western North Pacific category 5 typhoons. Part I: ocean features and the category 5 typhoons' intensification *Mon. Wea. Rev.,* **136** 3288–306.

Liu K-b, C. Shen, and K. Louie (2001): A 1000-year history of typhoon landfalls in Guangdong, southern China, reconstructed from Chinese historical documentary records. *Ann. Assoc. Am. Geogr.,* **91**:453–464.

Liu, K.S. and J. C. L. Chan (2002): Synoptic flow patterns associated with small and large tropical cyclones over the Western North Pacific. *Mon. Wea. Rev.*, **130**, 2134–2142.

Liu, K.S., and J. C. L. Chan. (2008): Interdecadal variability of Western North Pacific tropical cyclone tracks. *J. Clim.,* **21**:17, 4464-4476.

Liu, Y., D.-L. Zhang, and M. K. Yau, (1997): A multiscale numerical study of Hurricane Andrew (1992). Part I: Explicit simulation and verification. *Mon. Wea. Rev.*, **125,** 3073–3093.

Liu Y.M., G.X. Wu, (2000): Reviews on the study of the subtropical anticyclone and new insights on some fundamental problems. *Acta Meteorologica Sinica*, **58**(4), 500-512.

Lo, F., and H. H. Hendon (2000): Empirical extended-range forecasting of the Madden-Julian oscillation, *Mon. Wea. Rev*., **128**, 2528–2543.

Lynn K. S., J. K. Brewster. (2010): Oceanic heat content variability in the Eastern Pacific Ocean for hurricane intensity forecasting. *Mon. Wea. Rev.,* **138**:6, 2110-2131.

Madden, R. A., and P. R. Julian (1971): Detection of a 40–50 day oscillation in the zonal wind in the tropical Pacific, *J. Atmos. Sci*., **28**, 702–708.

Madden, R. A., and P. R. Julian (1972): Description of global-scale circulation cells in the tropics with a 40–50 day period, *J. Atmos. Sci.,* **29**, 1109–1123.

Maloney, E. D. and D. L. Hartmann (2001): The Madden–Julian oscillation, barotropic dynamics, and North Pacific tropical cyclone formation. Part I: observations. *J. Atmos. Sci*., **58**, 2545–2558.

Mantua, N. J., and S. R. Hare, (2002): The Pacific Decadal Oscillation. *J. Oceanogr.,* **58,** 35–44.

Mock C.J., P.J. Bartlein and P.M.Anderson (1998): Atmospheric circulation patterns and spatial climatic variations in Beringia. *International Journal of Climatology,* **18,** 1085–1104.

Nakazawa, T. (2006): Madden-Julian oscillation activity and typhoon landfall on Japan in 2004. *SOLA*, **2**(0), 136-139.

National Weather Service Southern Region, cited 2006: An Overview of NHC Prediction Models. [Available online at http://www.srh.noaa.gov/ssd/nwpmodel/html/nhcmodel.htm.]

Neelin, J. D., M. Latif, and F. F. Jin (1994): Dynamics of coupled ocean-atmosphere models: The tropical problem. *Annual review of fluid mechanics*, **26**(1), 617-659.

Neumann, C. J., (1987): The national hurricane center risk analysis program (HURISK). NOAA Tech. Memo. NWS NHC 39, 56.

Neumann, C. J., (1999): The HURISK model: An adaptation for the Southern Hemisphere (a user's manual). Science Applications International Corporation, 31.

Picaut, J., M. Ioualalen, C. Menkes, T. Delcroix and M. J. McPhaden (1996): Mechanism of the zonal displacements of the Pacific warm pool: Implications for ENSO, *Science*, **274**, 1486–1489.

Pielke, R. A. (2005): Meteorology: Are there trends in hurricane destruction? *Nature,* **438**: E13.

Rappin, E., M. C. Morgan and G. J. Tripoli (2011): The Impact of outflow environment on tropical cyclone intensification and structure. *J. Atmos. Sci.*, **68**, 177–194.

Ren, F., J. Liang, G. Wu, W. Dong and X. Yang (2011): Reliability analysis of climate change of tropical cyclone activity over the Western North Pacific. *J. Clim.*, **24**, 5887–5898.

Sadler, J.C. (1976): A role of the tropical upper tropospheric trough in early season typhoon development. *Mon. Wea. Rev.*, **104** (10): 1266–1278.

Salby, M. L. and H. H. Hendon (1994): Intraseasonal behavior of clouds, temperature, and motion in the tropics. *J. Atmos. Sci.*, **51,** 2207–2224.

Schreck, C. J., III and J. Molinari (2011): Tropical cyclogenesis associated with Kelvin waves and the Madden–Julian oscillation. *Mon. Wea. Rev.*, **139**, 2723–2734.

Sheridan, S.C. and C.C. Lee (2012): Synoptic climatology and the analysis of atmospheric teleconnections. *Prog. Phys. Geogr.,* **36**(4) 548-557.

Sinclair, M. R. (2002): Extratropical transition of southwest Pacific tropical cyclones. Part I: Climatology and mean structure changes. *Mon. Wea. Rev.*, **130**, 590–609.

Slingo J. M., K. R. Sperber, J. S. Boyle, J. –P. Ceron, M. Dix, B. Dugas…N. Renno (1996): Intraseasonal oscillations in 15 atmospheric general circulation models: Results from an AMIP diagnostic subproject, *Clim. Dyn.*, **12**, 325–357.

Slingo, J. M., D. P. Rowell, K. R. Sperber and F. Nortley (1999): On the predictability of the interannual behavior of the Madden-Julian Oscillation and its relationship with El Nino, *Q. J. R. Meteorol. Soc*., **125**, 583–610.

Sobel, A. H., and E. D. Maloney (2000): Effect of ENSO and MJO on the western North Pacific tropical cyclones. *Geophys. Res. Lett*., **27**, 1739–1742.

Song J-J, Y. Wang, and L. Wu (2010): Trend discrepancies among three best track data sets of western North Pacific tropical cyclones. *J. Geophys. Res.,* **115**: D12128.

Spencer, R.W., W. D. Braswell, J. R. Christy and J. Hnilo (2007): Cloud and radiation budget changes associated with tropical intraseasonal oscillations, *Geophys. Res. Lett.,* **34**, L15707.

Sperber, K. R., J. M. Slingo, P. M. Inness and K. M. Lau (1997): On the maintenance and initiation of the intraseasonal oscillation in the NCEP/NCAR reanalysis and the GLA and UKMO AMIP simulations, *Clim. Dyn*., **13**, 769–795.

Stidd, C.K. (1954): The use of correlation fields in relating precipitation to circulation. *Journal of Meteorology*, **11**, 202-213.

Sui, C.-H., P.-H. Chung and T. Li (2007): Interannual and interdecadal variability of the summertime western North Pacific subtropical high. *Geophys. Res. Lett.*, **34**, L11701.

Terry, J.P. and C.C. Feng (2010): On quantifying the sinuosity of typhoon tracks in the western North Pacific basin. *Appl. Geogr.*, **30**:678–686.

Thompson, C. S., S. Ready and X. Zheng (1992): Tropical cyclones in the southwest Pacific: November 1979 to May 1989. *New Zealand Meteorological Service*, 35.

Tian H. and C-Y Li (2010): Further study of typhoon tracks and the low-frequency (30-60 Days) wind-field pattern at 850 hPa, *J. Atmos. and Oceanic Sci. Letters*, **3**(6), 319-324.

Tu, J.Y., C. Chou, P. Huang and R.H. Huang (2011): An abrupt increase of intense typhoons over the western North Pacific in early summer. *Environ. Res. Lett*., **6**, 034013.

Waliser, D. E., C. Jones, J.-K. Schemm and N. E. Graham (1999a): A statistical extended-range tropical forecast model based on the slow evolution of the Madden-Julian Oscillation, *J. Clim*., **12**, 1918–1939.

Waliser, D. E., K. M. Lau, W. Stern and C. Jones (2003): Potential predictability of the Madden-Julian Oscillation, *Bull. Amer. Meteor. Soc.*, **84**, 33-50.

Wang, B. and J. C. L. Chan (2002): How strong ENSO events affect tropical storm activity over the western North Pacific. *J. Clim.*, **15,** 1643–1658.

Weatherford, C. L. and W. M. Gray (1988): Typhoon structure as revealed by aircraft reconnaissance. Part I: Data analysis and climatology. *Mon. Wea. Rev.*, **116**, 1032–1043.

Webster, P. J., G. J. Holland, J. A. Curry and H. R. Chang (2005): Changes in tropical cyclone number, duration, and intensity in a warming environment. *Science*, **309**: 1844–1846.

Weyman, J. C. and L. J. Anderson-Berry (2002): Societal impact of tropical cyclones. *Fifth International Workshop on Tropical Cyclones*. Miami, FL, Atlantic Oceanographic and Meteorological Laboratory.
[Available online at http://www.aoml.noaa.gov/hrd/iwtc/AndersonBerry5-1.html.]

Winkler, J.A. (1988): Climatological characteristics of summertime extreme rainstorms in Minnesota, *Annals of the Association of American Geographers*,**78**, 57-73.

World Meteorological Organization, (2009): Typhoon Committee Operational Manual: Meteorological Component, Tropical Cyclone Programme (TCP) 23. (WMO/TD No. 196).

Wu, M.-C., K.-H. Yeung and W.-L. Chang (2006): Trends in western North Pacific tropical cyclone intensity, *Eos Trans. AGU*, **87**(48), 537.

Wu, C.C. and Kuo, Y.H. (1999): Typhoons affecting Taiwan: Current understanding and future challenges, *Bull. Amer. Meteor. Soc.*, **80**, 67-80.

Wu, M. C., W. L. Chang and W. M. Leung (2004): Impacts of El Niño–Southern Oscillation events on tropical cyclone landfalling activity in the Western North Pacific. *J. Clim.*, **17 (6)**: 1419–1428.

Wu, L., B. Wang and S. Geng (2005): Growing typhoon influence on East Asia, *Geophys. Res. Lett*., **32**, L18703.

Xie, L. and T. Yan (2007): West North Pacific typhoon track patterns and their potential connection to Tibetan Plateau snow cover. *Nat. Hazards*, **42**:2, 317-333.

Xue, Y., W. Higgins and V. Kousky (2002): Influences of the Madden Julian Oscillations on temperature and precipitation in North America during ENSO-neutral and weak ENSO winters, *A Workshop on Prospects for Improved Forecasts of Weather and Short-term Climate Variability on Subseasonal (2 week to 2 month) Time Scales*, Greenbelt, MD, NASA/Goddard Space Flight Center, April 16-18, 2002.

Xue-zhao H. and G Dao-yi (2002): Interdecadal change in Western Pacific Subtropical High and climatic effects. *Journal of Geographical Sciences*, **12**(2): 202-209.

Yankovsky, A (2009): Large-scale edge waves generated by hurricane landfall, *J. Geophys. Res*., **114**, C03014.

Yano, J., R. Blender, C. Zhang and K. Fraedrich (2004): 1/f noise and pulse-like events in the tropical atmospheric surface variabilities, *Quart. J. Roy. Meteor. Soc*., **130**, 1697– 1721.

Yarnal B. (1993): Synoptic Climatology in Environmental Analysis. Belhaven Press: London, 195 pp.

Zhang, C. and J. Gottschalck (2002): SST Anomalies of ENSO and the Madden-Julian Oscillation in the Equatorial Pacific, *J. Clim*., **15**, 2429-2445.

Zhang, C. (2005): Madden-Julian Oscillation, *Rev. Geophys*., **43**, RG2003.

Zhao, H., D. L. Tang and Y. Wang (2008): Comparison of phytoplankton blooms triggered by two typhoons with different intensities and translation speeds in the South China Sea, *Mar. Ecol. Prog. Ser.*, **365**, 57–65.

Zhou, T., R. Yu, J. Zhang, J. Li, X. Xin, H. Drange, C. Cassou, E. Sanchez-Gomez, C. Deser, Y. Okumura, D.L.R. Hodson and N. Keenlyside (2009): Why the Western Pacific Subtropical High has extended westward since the late 1970, *J. Clim.*, **22**, 2199-2215.